Title
STOPPING POWER AND RANGE FOR ANY NUCLEUS IN THE SPECIFIC ENERGY INTERVAL 0.01-TO 500-MeV/amu IN ANY NONGASEOUS MATERIAL

Author
Steward, Palmer G.

Publication Date
1968-05-01

UCRL-18127

Cy. 2

R

University of California

Ernest O. Lawrence Radiation Laboratory

STOPPING POWER AND RANGE FOR ANY NUCLEUS IN THE SPECIFIC ENERGY INTERVAL 0.01- TO 500-MeV/amu IN ANY NONGASEOUS MATERIAL

Palmer G. Steward

(Ph. D. thesis)

May 1968

Berkeley, California

DISCLAIMER

UCRL-18127

UNIVERSITY OF CALIFORNIA

Lawrence Radiation Laboratory
Berkeley, California

AEC Contract No. W-7405-eng-48

STOPPING POWER AND RANGE FOR ANY NUCLEUS IN THE SPECIFIC ENERGY INTERVAL 0.01- TO 500-MeV/amu IN ANY NONGASEOUS MATERIAL

Palmer G. Steward

(Ph. D. thesis)

May 1968

STOPPING POWER AND RANGE FOR ANY NUCLEUS IN THE SPECIFIC ENERGY INTERVAL 0.01-TO 500-MeV/amu IN ANY NONGASEOUS MATERIAL

Contents

STOPPING POWER AND RANGE FOR ANY NUCLEUS IN THE SPECIFIC ENERGY INTERVAL 0.01- TO 500-MeV/amu IN ANY NONGASEOUS MATERIAL

Palmer G. Steward

Lawrence Radiation Laboratory
University of California
Berkeley, California

May 1968

ABSTRACT

A method is presented for calculating range and stopping-power data for any heavy ion with $0.01 \leq \varepsilon \leq 500$ MeV/amu incident upon any nongaseous stopping medium. The method is incorporated into a FORTRAN IV computer program. Results for H, ^{4}He, ^{12}C, ^{20}Ne, ^{40}Ar, ^{84}Kr, ^{131}Xe, and ^{222}Rn ions each incident upon H_2O, Al, Cu, Ag, Pb, and U are presented.

For ions at low energy with $Z \leq 10$, the program uses experimental data. For ions with $Z > 10$, the nuclear and electronic stopping-power theory developed by Lindhard et al. is adjusted to fission-product range data at low energy; for intermediate-energies, charge-state data developed from experimental Ar range-energy data in Al is extended to other ions and stopping media. Bethe's theory is used for all ions at high energy.

Bloch's theory is discussed, although it is not used in the method.

The particle ranges calculated by the method are pathlength ranges and do not include the effects of multiple scattering. A method for calculating projected range at low energies is presented as an appendix.

The following table is presented as an example of the results.

Ion	Stopping Medium	Maximum Stopping Power MeV gm/cm^2	Specific Energy at Maximum Stopping Power (MeV/amu)	Range at 500 MeV/amu (gm/cm^2)
H	H_2O	940	0.08	115
H	U	78	3.0	239
Rn	H_2O	140000	0.2	3.6
Rn	U	45000	9.5	7.6

NOTATION

Symbol	Page of First Appearance	Description of Symbol
ε	1	The specific energy of the ion in units of MeV per atomic mass unit of the ion
Z_1	6	The atomic number of the ion (projectile).
Z_2	6	The atomic number of the stopping medium (target).
β	6	The ratio of the velocity of the ion to that of light in a vacuum.
A_1	6	Atomic weight of the ion.
V	6	The velocity of the ion
E	6	Energy of the ion in units of MeV.
r	10	The ratio of the root mean square of the ion Z_1 to that of its nucleus.
m	10	The mass of the ion.
$\frac{dE}{dR}$	12	Stopping power in units of MeV/(g/cm^2).
B	12	The stopping number (dimensionless).
A_2	12	Atomic weight of the stopping medium
Re	12	Real part of a complex number.
e	12	The charge on an electron.
m_e	12	The rest mass of an electron

Symbol	Page of First Appearance	Description of Symbol
c	12	The velocity of light.
I	12	Average atomic excitation potential of the stopping medium.
ζ	13	The dimensionless unit corresponding to range due to Lindhard et al.
ϵ	14	The dimensionless unit corresponding to energy due to Lindhard et al.
k	14	Electronic stopping-power constant from Lindhard et al. (see Eq.(16) and Ref. (18).
S	22	Identical to dE/dR above. This symbol is used where a less cumbersome notation is desirable.
f	22	The ratio of the stopping power of an ion Z_1, at a particular velocity, in a given medium Z_2, to the stopping power of the same ion Z_1 at the same velocity in Al, $Z = 13$. This is called "relative stopping power" in the text.
$\left(\frac{dE}{dR}\right)_p$	28	Stopping power (MeV/(g/cm^2)) for protons.
λ	28	Proton range (g/cm^2).
A_p	29	Mass of a proton in atomic mass units.

Symbol	Page of First Appearance	Description of Symbol
I_{adj}	28	Average atomic excitation energy of the stopping medium adjusted so that the shell corrections can go to zero in the relativistic limit.
ε_p	28	$\varepsilon_p = A_p \varepsilon$.
ρ	32	Density of the stopping medium.
R	35	Ion range (g/cm^2).
$\left(\frac{dE}{dR}\right)_e$	37	Electronic stopping power ($MeV/(g/cm^2)$).
$\left(\frac{dE}{dR}\right)_n$	38	Nuclear coulomb stopping power ($MeV/(g/cm^2)$).
$Z_{1_{eff}}$	40	$r Z_1$
$\frac{v_e}{v_i}$	40	The ratio of the velocity of an electron in an ion's electron cloud to the velocity of the ion at which this electron's capture and loss cross sections are equal.

I. INTRODUCTION

A. Purpose for the Research

The purpose for the research reported here is to provide estimates of the stopping power and ranges of all charged particles which will be accelerated by the Omnitron. The Omnitron[1] is a proposed synchrotron which will accelerate any nucleus from hydrogen through uranium to any specific energy up to four to five hundred MeV/amu.

Throughout this paper we refer to MeV/amu, represented by the symbol ε, as a unit of specific energy. It is a unit intermediate between velocity and energy. The relationship to velocity is given by:

$$\varepsilon = 931 \left[(1 - \beta^2)^{-1/2} - 1 \right] , \text{ or}$$

$$\beta = \frac{\frac{\varepsilon}{931} \left(\frac{\varepsilon}{931} + 2 \right)^{1/2}}{\frac{\varepsilon}{931} + 1} ;$$

and the relationship to energy is given by:

$$\varepsilon = \frac{E}{A_1} .$$

The slowing-down mechanism of a charged particle in matter is similar throughout any plane of constant velocity in (V, Z_1, Z_2) space. Since ε is a function of velocity only, the same statement can be made regarding any plane of constant specific energy in (ε, Z_1, Z_2) space. This statement cannot be made for a plane of constant energy in (E, Z_1, Z_2) space. In this paper, we use specific energy as the independent variable rather than velocity or energy. Thus we use a unit which is a natural variable of the stopping-power process in the

same sense that velocity is, while at the same time we have a simple relationship between this unit and a common unit of energy.

We will find it convenient in this report to discuss information in terms of (ε, Z_1, Z_2) space. For instance in Fig. 1 the slabs covering the bottom and part of the back of the box represent the volume of this space for which present accelerators can provide heavy particles. Alpha particles, as indicated in the figure, can be accelerated by the 184-Inch Synchrocyclotron to 230 MeV/amu. Protons, represented by the bottom slab, can be accelerated above 500 MeV/amu. The AGS at Brookhaven and the comparable accelerator at CERN can accelerate protons to about 30 000 MeV/amu. The accelerator at Serpukhov can accelerate protons to 70 000 MeV/amu. The computational method incorporated into the computer program of Appendix A can supply stopping-power and range data for Z_1 and Z_2 greater than 92 and for ε up to 1200 MeV/amu. In this paper, however, the boundaries of the space we consider are given by: $0.01 \leq \varepsilon \leq 500$, $1 \leq Z_1 \leq 92$, $1 \leq Z_2 \leq 92$, because it is this region of (ε, Z_1, Z_2) space which describes the capabilities of the Omnitron. The slab along the back of the box describes the capabilities of the Hilac at Berkeley and the comparable accelerator at Kharkov. These two accelerators can give ions with $Z_1 \lesssim 20$ a specific energy of up to 10.4 MeV/amu.

Using this (ε, Z_1, Z_2) space as a device for restating the purpose of this research, we may say that it is our aim in this report, to provide a computational method for filling the box in Fig. 1 with range and stopping-power data.

We wish to state here at the outset that the range we calculate is the total path-length mean range and does not take into consideration the shortening of the projected range due to coulomb multiple scattering. This is discussed further in section III B 1.

A second purpose of this research is to provide the basic stopping-power data which are needed to calculate the beam properties

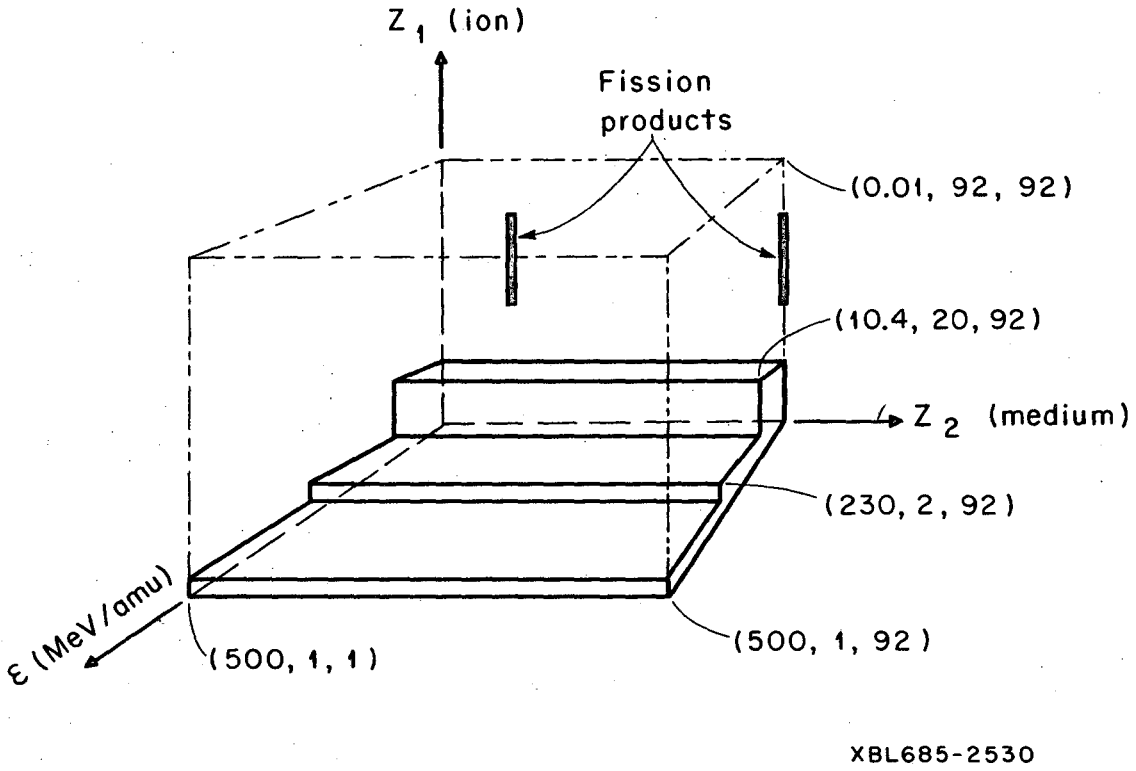

Fig. 1. A geometric view of that part of (ε, Z_1, Z_2) space for which $0.01 \leq \varepsilon \leq 500$, $1 \leq Z_1 \leq 92$, and $1 \leq Z_2 \leq 92$. The regions of this subspace for which experimental stopping power is available are indicated by the slabs covering the bottom and part of the back of the box (accelerated particle data) and the two lines on the back of the box (fission product range data).

of the Omnitron particles. For example, relative dose, particle energy spectrum, LET spectrum, and beam width all as a function of depth have been calculated by Litton[2, 3] by means of introducing the effects of straggling, removal of particles due to nuclear collisions, and multiple coulomb scattering. Litton's calculations have been carried out in such a way that the characteristics of the Bragg peak are carefully determined.

A third purpose of this research is to provide the radiobiologist with early information about the energy deposition or LET distribution of the Omnitron particles. This information is useful in anticipating radiobiological effects, suggesting experiments, and designing the facilities associated with the Omnitron.

B. Guidelines for the Research

The approximate limits of the only useful experimental stopping-power or range data available are illustrated in Fig. 1. The three slabs of (ε, Z_1, Z_2) space in which experimental stopping power has been accumulated by means of presently accelerated particles are shown. The two lines on the back of the box in Fig. 1 represent experimental fission product range values in aluminum and uranium respectively. Since the experimental data from these small regions must be extrapolated throughout the entire volume of the box, it is clear that the first guideline must be to include enough physical theory in order to make this extrapolation effective.

The theory that we normalize to the experimental data must be general enough to allow extrapolation to remote regions of (ε, Z_1, Z_2) space. Were we to have limited our study to a smaller region of this space, we could have considered, in more detail specific inadequacies in the present theories such as those found by Aras, et al.[4] and Fastrup, et al.[5] We could have used, more directly, isolated experimental data and empirical range formulas. However, for our

purposes here, we are willing to sacrifice some accuracy in specific cases in order to retain the generality of our theory.

The final guideline is that our method of computing range and stopping power must be conveniently programmed requiring a minimum of computer time and core space.

C. Historical Background

1. Theory

The interactions of energetic heavy charged particles with matter has been of great interest for over half a century. Bohr developed the semi-classical stopping-power theory using impact parameters in 1913.[6, 7] Bethe published his purely quantum mechanical theory in 1930.[8, 9]

Each of those theories is valid in only part of the (ε, Z_1, Z_2) space. Bohr's theory is valid only when the following inequalities are satisfied.[10]

$$Z_2 \ll 137\beta, \tag{1}$$

$$(Z_2^2 \, r \, Z_1)^{1/3} \ll 137\beta, \tag{2}$$

$$\frac{\hbar}{mV} \ll \text{screening distance of scattering atom, and} \tag{3}$$

$$r Z_1 \gg 137\beta, \tag{4}$$

where $\hbar$ is Plank's constant divided by 2π, m is the mass of the ion, V is its velocity, and the screening distance of an atom is the distance from its nucleus to the radius where the screening by its electron cloud has reduced the effective nuclear charge to 1/e of its true value.

The expression 137β appears many times throughout this paper. This expression is the ion velocity in units of the Bohr orbital K shell velocity of the hydrogen atom. When discussing the interactions of charged particles with matter, this is a very convenient unit of velocity. Since the K shell electron velocity of the one-electron atom is proportional to the charge of the nucleus, inequality (1) can be restated:

"In order for Bohr's theory to be valid, the velocity of the ion must be greater than the K shell electron velocity of the stopping medium." Similarly, inequality (4) limits the ion velocity to less than its own K shell electron velocity. Therefore Bohr's theory is limited to that region of (ε, Z_1, Z_2) space where the ion carries along with it its own electron cloud. This limits the usefulness of Bohr's theory to the few cases for which adequate charge-state data is available.

Bethe's theory, because use was made of the Born approximation, is limited to the region where

$$r Z_1 \ll 137\beta. \tag{5}$$

However, it was shown later by Mott[11] that the less restrictive of inequality (5) or

$$r Z_1 \ll Z_2 \tag{6}$$

is sufficient. Thus, since the K shell velocity of the ion is approximately $\beta = Z_1/137$ the use of Bethe's theory is essentially restricted to the region of (ε, Z_1, Z_2) space where the ion is completely ionized; although for very low energy when $r \sim 0$ the theory is again valid. Bethe originally also required inequality (1). However, he later showed with Livingston[12] how the inclusion of shell corrections could eliminate the need for this inequality. These shell corrections, in effect, subtract from Bethe's formula the contribution to the stopping power of those most tightly bound electrons in the stopping medium which at low ion velocities, are rarely excited. Walske[13] made a detailed derivation of the K shell correction. He later made an estimate for the L shell.[14] Recently Bichsel[15] has estimated corrections for all higher shells of the stopping atom.

In 1933 Bloch[16] developed his theory which, in addition to inequality (1), is restricted by

$$(Z_2 r Z_1)^{1/2} \ll 137\beta \tag{7}$$

Bloch's theory provides a bridge between Bethe's and Bohr's theories in the sense that Bloch's theory agrees with Bohr's theory in the limit of inequality (4) and with Bethe's theory in the limit of inequality (5).

Each of these theories gives the stopping power in the form

$$\frac{dE}{dR}\left(\frac{MeV}{g/cm^2}\right) = 0.3072 \frac{(r Z_1)^2}{\beta^2 A_2} B. \tag{8}$$

Bohr found

$$B = Z_2 \left[\ln \frac{1.123\ m_e V^3}{r Z_1 e^2 \omega} - \ln (1 - \beta^2) - \beta^2 \right] \tag{9}$$

where ω may be regarded as an effective oscillation frequency of the electrons in the scattering atom. For Bethe's theory, including shell corrections,

$$B = Z_2 \left[\ln \frac{2m_e c^2 \beta^2}{I} - \ln (1 - \beta^2) - \beta^2 - \frac{\sum_i C_i}{Z_2} - \delta \right]. \tag{10}$$

Here I is the average excitation potential of the stopping medium, and $\sum_i C_i$ are the shell corrections summed over the electronic shells of the stopping medium (i. e. i = K, L, M, ...), and δ is the correction due to polarization of the stopping medium. For our purposes we may neglect δ since it makes a significant contribution only for ion specific energies above 500 MeV/amu. For Bloch's theory

$$B = Z_2 \left[\ln \frac{2m_e c^2 \beta^2}{I} + \psi [1] - \mathrm{Re}\, \psi \left[1 + i \frac{r Z_1}{137 \beta} \right] - \ln (1 - \beta^2) - \beta^2 \right] \tag{11}$$

where ψ is the logarithmic derivative of the gamma function.

The usefulness of any of these theories is limited for $137\beta \leq Z_1$ because for these low velocities the ion carries along its own electron cloud, implying that r is less than one and usually unknown. As stated above this makes Bohr's theory not generally useful because his theory is valid only when this inequality holds. It also mades Bloch's theory not very useful except in the region of (ε, Z_1, Z_2) space where Bethe's theory is also valid. Lindhard, et al.[17,18] have recently developed the only generally useful theory valid at low ion velocities. Lindhard has made use of the Thomas-Fermi description of the electron clouds of the ion and stopping atom to give a formula for the stopping power due not only to excitation and ionization of the stopping atoms, but also to the elastic coulomb collisions of ion and nucleus of the stopping atom.

The contribution of the former to the stopping power (i.e. the excitation and ionization of atoms in the stopping medium) is the only effect included by Bohr, Bethe, and Bloch in their three theories discussed above. For specific energies above 1.0 MeV/amu we may neglect all other contributions to the slowing down of the ion because this electronic stopping power is usually more than two orders of magnitude greater than any other contribution. However, as discussed by Bohr[10], in that region of (ε, Z_1, Z_2) space defined by small ε and especially for large Z_1 and large Z_2, the slowing down of the ion due to elastic coulomb collisions between the ion and the nuclei of the stopping medium (i.e. nuclear coulomb stopping power*) will afford the major contribution to the stopping power.

Lindhard has found it convenient to express his theory in dimensionless units. His unit corresponding to distance is

$$\zeta = 4\pi a^2 N_a \frac{A_1}{(A_1 + A_2)^2} R \qquad (12)$$

---

*This is usually called nuclear stopping power in the literature.

where N_a is Avogardro's number and

$$a = 0.8853\, a_0 \left(Z_1^{2/3} + Z_2^{2/3}\right)^{-1/2} \tag{13}$$

where a_0 is $0.529 \quad 10^{-8}$ cm, the first Bohr radius for hydrogen. The unit corresponding to energy is

$$\epsilon = 1.602 \times 10^{-6} \frac{a}{e^2} \frac{A_1 \quad A_2}{A_1 + A_2} \quad \frac{\varepsilon}{Z_1 \, Z_2} \tag{14}$$

where a is given by Eq. (13) and e is $4.803 \quad 10^{-10}$, the electronic charge in esu. Now Lindhard's expression for the electronic stopping power is

$$\left(\frac{d\epsilon}{d\zeta}\right)_e = k\, \epsilon^{1/2} \tag{15}$$

where k is a constant given by

$$k = \xi\, 0.0793 \quad \frac{Z_1^{1/2} \, Z_2^{1/2}}{\left(Z_1^{2/3} + Z_2^{2/3}\right)^{3/4}} \frac{(A_1 + A_2)^{3/2}}{A_1^{3/2} \quad A_2^{1/2}} \tag{16}$$

where ξ is of the order of $Z_1^{1/6}$. The volume of (ε, Z_1, Z_2) space for which Eq. (15) is valid is given by

$$Z_1 \text{ and } Z_2 >> 1 \text{ and} \tag{17}$$

$$Z_1^{1/3} \geq 137\beta. \tag{18}$$

(Lindhard suggests $Z_1^{2/3} \geq 137\,\beta$ instead of inequality (18), but we find this to be an inadequate restriction.)

The stopping power due to nuclear coulomb collisions is not expressed in closed form by Lindhard because the Thomas-Fermi scattering cross section cannot be expressed in closed form. It is graphically presented in Fig. 2 in the dimensionless units of Eqs. (12) and (14). The validity of this formulation is restricted by inequality (17). The contribution of this elastic component of the total stopping power is significant only in the region identified by inequality (18).

In Fig. 3 we illustrate the volume of (ε , Z_1, Z_2) space in which each of the above four theories is valid. The boundaries separating each of the regions are somewhat arbitrarily placed. Lindhards theory is valid over a plane across most of the back of the box. (It is actually a slab of thickness given by $0.01 \lesssim \varepsilon \lesssim 0.5$ MeV/amu.) Bethe's theory with shell corrections is valid throughout perhaps a third of the box. It is valid over essentially all of the box for which r is unity. There is a small region in which Bloch's or Bohr's theory is valid and Bethe's theory is not valid. However, in this region r is less than one and uncertain. Thus the advantage of Bloch's or Bohr's theory over Bethe's in any region of the box is questionable. It is clear, at any rate, that over a large portion of the box there is no valid theory (see Fig. 3) and no experimental data (see Fig. 1).

We refer the reader to the literature for other surveys of stopping-power theory. For a development from first principles of the form of Bethe's theory used today, see Fano.[19] For a brief overview of the development of Bohr's and Bethe's theories see Turner.[20] For more comprehensive reviews of the same nature as is presented here, see Bethe and Ashkin[21] and Northcliffe.[22] For a general theoretical treatise on the interactions between heavy energetic charged particles and matter, including charge exchange and the relationship between the classical and quantum mechanical approaches, see Bohr[10]. For a

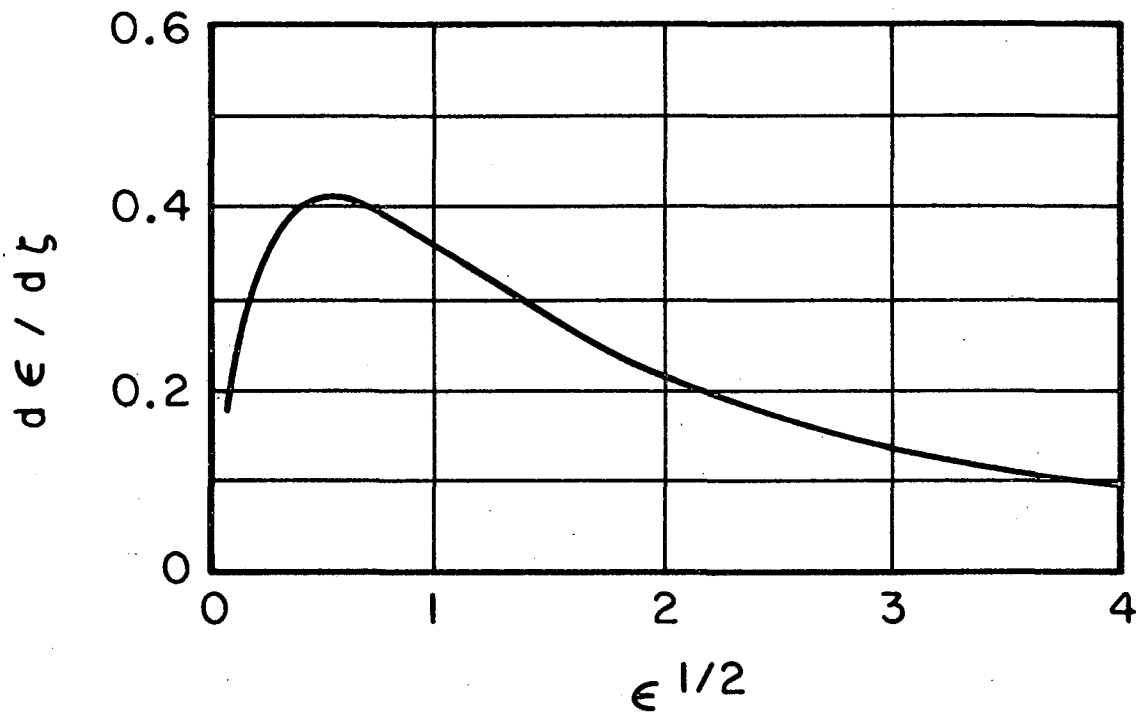

Fig. 2. The nuclear coulomb stopping power for heavy ions at low velocities. The ζ - ϵ units used in this figure (see text) allow one curve to provide this stopping power for any ion in any medium.

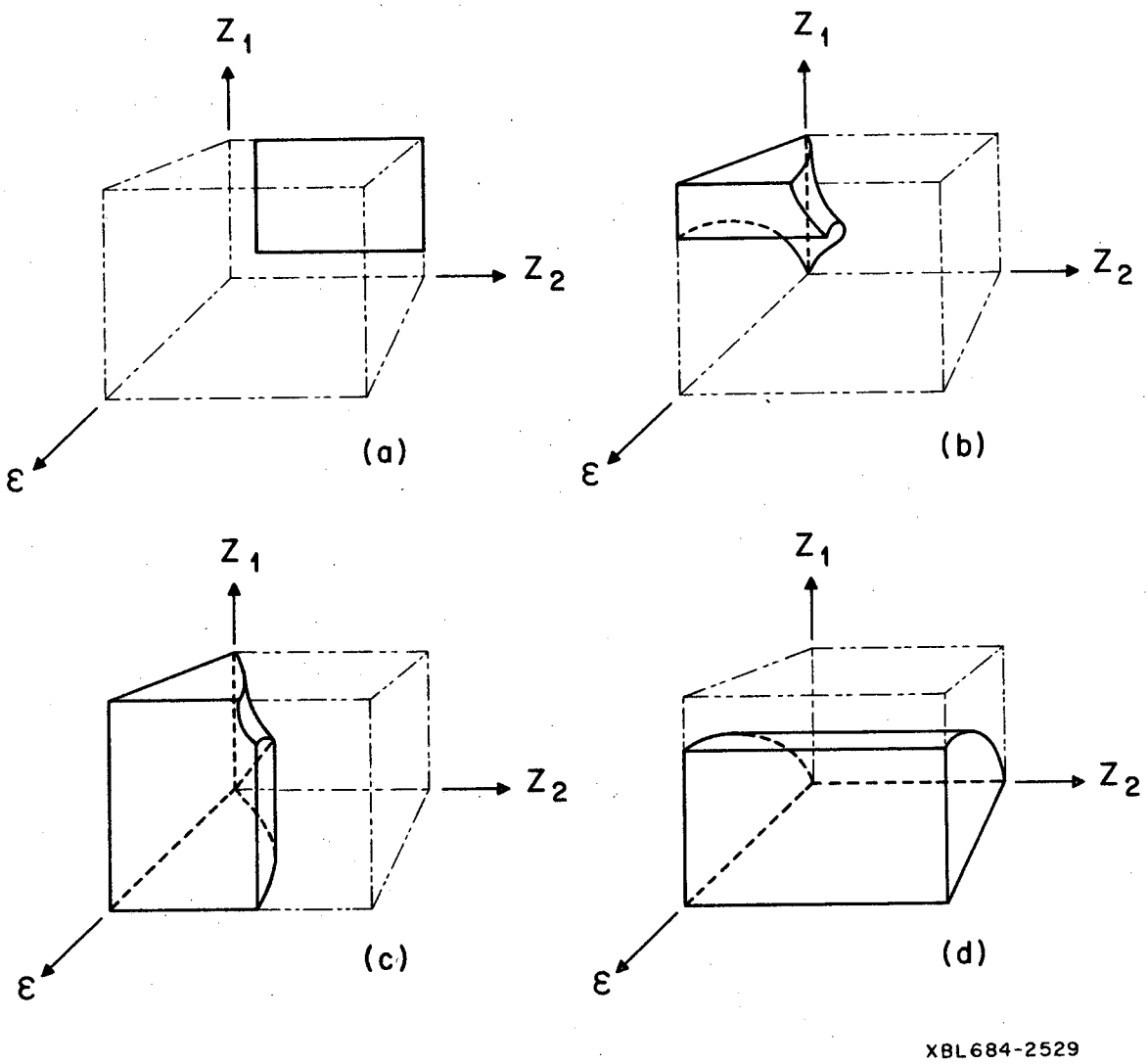

Fig. 3. In these four views of (ε, Z_1, Z_2) space we depict the regions of validity of four different theories. The theories are: (a) Lindhard et al.[18]; (b) Bohr[6,7]; (c) Bloch[16]; and (d) Bethe[8,9].

a recent and useful tabulation using Bethe's theory of stopping power and range of protons and mesons, see Barkas and Berger.[23] For an up-to-date discussion of several topics on the penetration of charged particles in matter, see NAS-NRC publication 1133.[24]

2. Experiment

The availability of experimental stopping power or range values is limited to that portion of (ε, Z_1, Z_2) space illustrated in Fig. 1. Northcliffe[22] has produced the most useful summary of the experimental data in the slab against the back of the box (see Fig. 1). Whaling[25] has summarized experimental data in this slab extensively for protons and alpha particles and also for heavier ions in gases. The researchers who originally obtained this data are referenced in either of these two sources.

The fission product range data represented by the two lines on the back of the box (see Fig. 1) is summarized by Hyde.[26] Since the printing of this reference, Aras[4] has published a summary of his Ph. D. research with fission product range values in aluminum and uranium and some comments on the use of Lindhard's theory for predicting those ranges.

Extensive experimental data filling the slab on the bottom of the box in Fig. 1 is not available. A few isolated experimental points in this slab have been obtained in a variety of stopping media for the purpose of finding empirical values of I, the average excitation energy of the medium, for use in Bethe's theory. Bethe's theory is considered very accurate in this region of (ε, Z_1, Z_2) space so that extensive experimental data is neither necessary nor useful. Both tables of and formulas for range and stopping power in this region are given by Barkas and Berger.[23]

D. Scope and Structure

The unique aspect of the research reported here is that nowhere else has stopping power and range been generated for such a large

continuous volume of (ε, Z_1, Z_2) space where active charge exchange between ion and stopping medium occur. We have generated stopping power and ranges for all ions from hydrogen through uranium in any nongaseous stopping medium over the velocity interval from 0.01 to 500 MeV/amu continuously. Over this velocity interval the charge on the ion varies from less than 10% to 100% of its nuclear charge. The dE/dR maximum is contained in this interval for all ions. The generation of accurate stopping power for the very heavy ions in the region of dE/dR maximum is at this time a difficult undertaking. The techniques developed here is a first order attempt to supply this data. We expect and solicit critical appraisal. It is expected that the Omnitron, upon completion, will allow experimental evaluation of our techniques.

There have been several efforts to produce stopping power tables for use by researchers, but these tables usually do not give values which are valid for that difficult and large region of (ε, Z_1, Z_2) space in which active charge exchange occurs (see eg. Refs. (23) and (27) through (30)). Bichsel[31], however, has developed a procedure for obtaining good stopping power in the region $1 \leq Z_1 \leq 12$, $1 \leq Z_2 \leq 92$, and $0.5 \leq \varepsilon \leq 1000$. Bichsel uses Bethe's theory paying careful attention to the shell corrections. He estimates charge-state corrections for the ions at low velocity. Benton[32] is working towards a method which will provide stopping power for at least some of this region of (ε, Z_1, Z_2) space which is so difficult to treat. He is generalizing experimental data obtained from track segments of heavy ions in polymers by fitting these data with polynomials of the type suggested by Barkas and Berger (see Eqs. (22) and (23) for examples).

The availability of experimental stopping power and the validity of the various theories are each restricted to its own region of (ε, Z_1, Z_2) space as discussed in the previous section. Thus in developing our method for generating stopping power, it is convenient for us to

divide (ε, Z_1, Z_2) space into corresponding regions. We develop for each region its own technique and strive for continuity in stopping power at the boundaries. The first boundary is the plane $Z_1 = 10$. For $Z_1 \leq 10$ experimental data are generally available where active charge exchange occurs. It is important to utilize these data, because it is not possible to treat this region well theoretically. Experimental data for $Z_1 > 10$ is very incomplete.

We subdivide the region defined by $Z_1 \leq 10$ into two subregions. For $\varepsilon < 10$ MeV/amu and $Z_1 \leq 10$ we make maximum use of experimental data from the Hilac and similar accelerators. We devise a technique in this subregion for generating stopping power which is not theoretically rigorous, but which does accurately duplicate available experimental data. For $\varepsilon \geq 10$ MeV/amu and $Z_1 \leq 10$, the ion is completely stripped of electrons and the application of Bethe's theory is straighfforward.

We subdivide the region defined by $Z_1 > 10$ into four subregions. In the low-specific-energy region defined by $137\,\beta \leq Z_1^{1/3}$, we generate stopping power using Lindhard's theories which are very slightly modified to conform to experimental fission product range data. Into the narrow medium-low-specific-energy region defined by $Z_1^{1/3} < 137\,\beta \leq 9$ we merely extend the data generated in the adjacent regions by means of a polynomial function. In the medium-high-specific-energy region defined by $9 < 137\,\beta \leq 3\,Z_1$ we develop a technique for estimating the charge state of the heavy ions as a function of velocity, $r(\beta)$. We then obtain the stopping power using this charge state with Bethe's theory. In the high-specific-energy region, defined by $137\beta > 3\,Z_1$, the ion is again completely stripped of its electrons and Bethe's theory is used.

The division of (ε, Z_1, Z_2) space is roughly illustrated in Fig. 4. The depths of the low- and medium-low-specific-energy regions have been exaggerated in order to make them visible. The depth of the region for which $Z_1 \leq 10$ and $\varepsilon < 10$ has also been exaggerated.

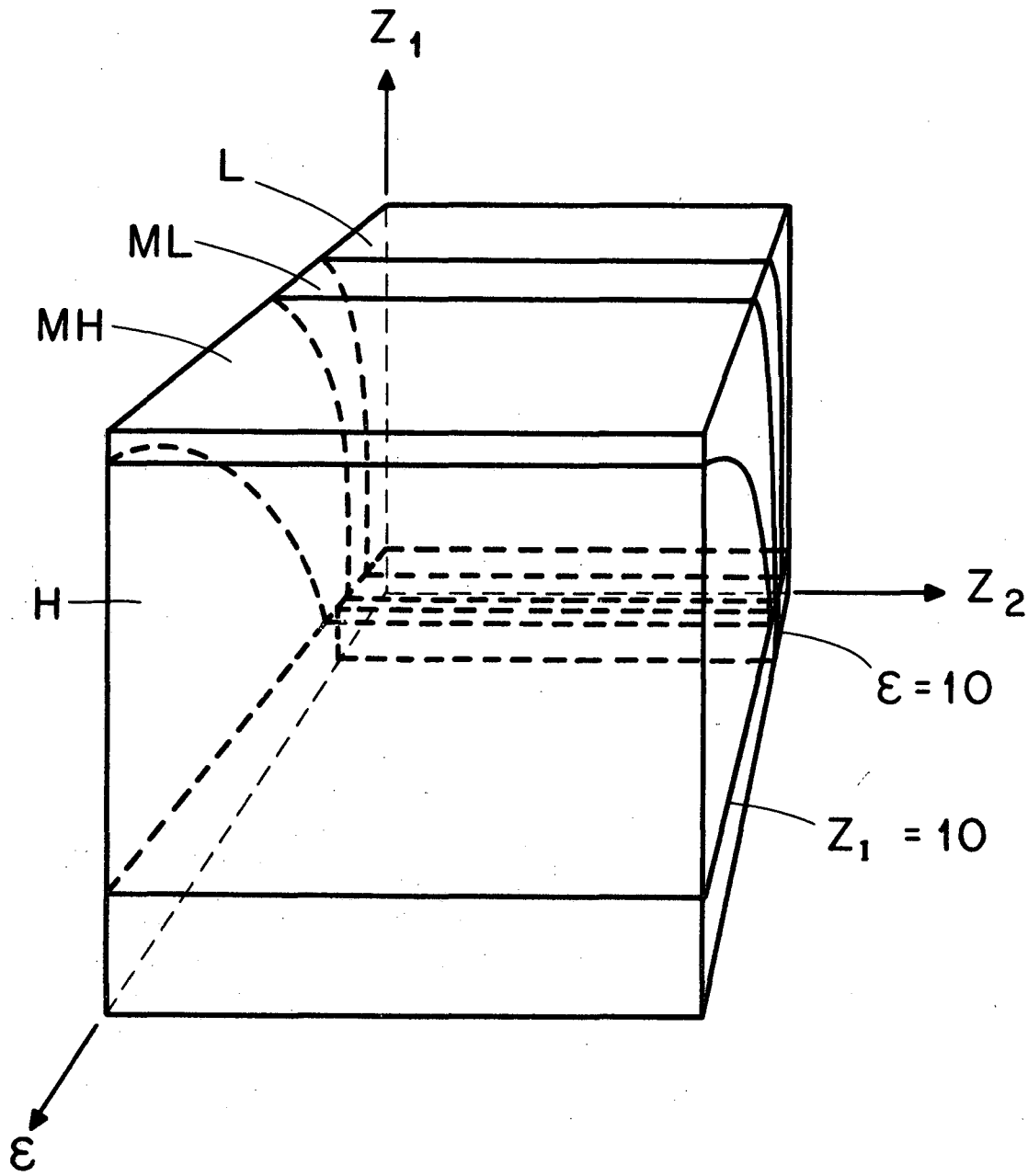

XBL684-2528

Fig. 4. In this view of (ε, Z_1, Z_2) space we illustrate the regions into which we divide this space. In the high-specific-energy region (H) and the region for which $Z_1 < 10$ and $\varepsilon \geq 10$ we use Bethe's theory directly. In the medium-high-specific-energy region (MH) we use Bethe's theory with charge-state data. In the medium-low-specific-energy region (ML) we use a cubic polynomial (see text). In the low-specific-energy region (L) we use Lindhard's theories. In the region for which $Z_1 \leq 10$ and $\varepsilon < 10$ we use experimental data.

II. METHOD

A. Method for Z_1 Less Than Eleven

1. Specific Energy Less Than 10 MeV/amu

In this region of (ε, Z_1, Z_2) space some experimental data are available. Active charge exchange occurs making theoretical treatment difficult. Thus we make maximum use of the experimental data. To do this we have modified a method proposed by Northcliffe[22] for generating smooth stopping-power curves through experimental points.

We wish to summarize the method in order to orient the reader before beginning on the detailed description of the method. First we calculate the relative stopping power of the ion in two different stopping media. One medium is the medium in which we want the stopping power, the other medium is Al. That is to say, we calculate

$$f_{Z_2}^{Z_1}(\varepsilon) = \frac{S_{Z_2}^{Z_1}}{S_{13}^{Z_1}} \tag{19}$$

where f is the relative stopping power, S is stopping power (i.e. an alternative symbol for dE/dR used to make the notation less cumbersome), the superscript represents the ion, Z_1, and the subscript represents the stopping medium, Z_2. This relative stopping power is obtained for $\varepsilon > 2$ MeV/amu by assuming that $f_{Z_2}^{1}(\varepsilon) = f_{Z_2}^{Z_1}(\varepsilon)$, i.e. this relative stopping power for protons is the same as that for any other ion for which $Z_1 \leq 10$. This is consistent with Bethe's theory if we assume that the charge state of the ion

is independent of the stopping medium. This is probably a fairly good assumption since, for $\varepsilon \sim 2$, the ion velocity is comparable to the velocity of its K shell electron for Ne and F ions; and the ion velocity is greater than the K shell electron velocity for all the other possible ions, implying that $r \sim 1$ for most of the ions most of the time. For $\varepsilon < 2$ MeV/amu the relative stopping power is taken from purely experimental data for certain ions, certain stopping media, and certain velocities. For any specific case, the relative stopping power is then found essentially by interpolation.

Finally, we obtain the desired stopping power by multiplying this relative stopping power by the accurately measured experimental stopping power of the ion in Al, that is

$$S_{Z_2}^{Z_1} = f_{Z_2}^{Z_1} \, S_{13}^{Z_1} .$$

We divide our more detailed description of this method into two main steps. In the first step we obtain and store for later use the relative stopping power for certain ions in certain stopping media for $\varepsilon < 2$ MeV/amu. In the second step we use this stored information to obtain the relative stopping power of our specific ion in our specific stopping medium, and then use this to get the actual stopping power.

a. <u>First step</u>. For $\varepsilon < 2$ we fit cubic polynomials of the form

$$\ln f(\varepsilon) = \sum_{n=0}^{3} C_n (\ln\varepsilon)^n \qquad (20)$$

for each possible combination of H, He, C, and Ne ions in the stopping media H_2, C, Al, Ni, Ag, and Au. That is to say we have 4 ions in 6 stopping media or 24 polynomials of the form of Eq. (20).

As we will discuss in the second step, we let the relative stopping power for $\varepsilon > 2$ be of the form $f(\varepsilon) = p\varepsilon^q$ where the constants p and q will also be discussed later. We now determine two of the constants of Eq. (20) by requiring that Eq. (20) give the same slope and magnitude of the relative stopping power at $\varepsilon = 2$ as $f(\varepsilon) = p\varepsilon^q$.

$$\ln[f(\varepsilon)] = \sum_{n=0}^{1} \left\{ C_n [\ln\varepsilon - \ln 2]^2 [2 \ln 2 \ln\varepsilon]^n \right\} + \ln[p\varepsilon^q]. \qquad (21)$$

The remaining two constants are determined by a least squares fit to experimental data at 0.01, 0.04, 0.1, 0.4, and 1.0 MeV/amu. Therefore by storing only 48 constants we have available 24 cubic polynomials of the form of Eq. (21). When new and better experimental data become available in this region of (ε, Z_1, Z_2) space, we can up-date our method by merely changing the two constants corresponding to the ion and stopping medium for which the experimental data are available.

The experimental data which we have used for the numerator of the relative stopping power (see Eq. (19)) are tabulated in Table I. The denominators are taken from Table V (to be discussed later). The data for stopping media other than H_2 come from Northcliffe.[22] The data for H_2 as stopping medium are inferred from the data of Teplova et al.,[33] Weyl,[34] and Allison and Littlejohn.[35]

b. Second step. Figure 5 shows a plane of (ε, Z_1, Z_2) space taken for any constant specific energy, say ε_0. Illustrated in the figure are 24 points for which we have stored (see paragraph (a) above) the relative stopping power. When $\varepsilon < 2$ we obtain the relative stopping power at any desired point (Z_1, Z_2) by a double

Table IA. Stopping Power for H Ions ($Z_1 = 1$) in Various Stopping Media

	MeV/(g/cm^2)					
ε	$H_2(Z_2 = 1)$	$C(Z_2 = 6)$	$Al(Z_2 = 13)$	$Ni(Z_2 = 28)$	$Ag(Z_2 = 47)$	$Au(Z_2 = 79)$
0.01	2170	260	190	103	80	40
0.04	3790	510	370	200	160	79
0.1	3380	610	430	250	200	110
0.4	1310	404	300	195	150	91
1.0	655	235	175	125	98	62.5

Table IB. Stopping Power for He Ions ($Z_1 = 2$) in Various Stopping Media

	MeV/(g/cm^2)					
ε	$H_2(Z_2 = 1)$	$C(Z_2 = 6)$	$Al(Z_2 = 13)$	$Ni(Z_2 = 28)$	$Ag(Z_2 = 47)$	$Au(Z_2 = 79)$
0.01	2660	640	480	252	200	100
0.04	5340	1260	940	520	396	200
0.1	7310	1720	1240	740	560	308
0.4	5140	1480	1080	720	560	336
1.0	2620	920	680	500	388	246

Table IC. Stopping Power for C Ions ($Z_1 = 6$) in Various Stopping Media

	MeV/(g/cm^2)					
ε	$H_2(Z_2 = 1)$	$C(Z_2 = 6)$	$Al(Z_2 = 13)$	$Ni(Z_2 = 28)$	$Ag(Z_2 = 47)$	$Au(Z_2 = 79)$
0.01	7200	1870	1400	775	595	296
0.04	14400	3960	2780	1480	1150	596
0.1	22300	5760	4320	2270	1820	990
0.4	27200	6480	4860	3200	2480	1480
1.0	18300	6120	4500	3170	2450	1550

Table ID. Stopping Power for Ne Ions ($Z_1 = 10$) in Various Stopping Media

	MeV/(g/cm^2)					
ε	$H_2(Z_2 = 1)$	$C(Z_2 = 6)$	$Al(Z_2 = 13)$	$Ni(Z_2 = 28)$	$Ag(Z_2 = 47)$	$Au(Z_2 = 79)$
0.01	4380	2600	1950	1060	810	400
0.04	8730	5150	3900	2100	1650	820
0.1	13850	8200	6000	3300	2700	1450
0.4	26500	10500	9200	6100	4900	2900
1.0	29300	10000	9100	6800	5150	3300

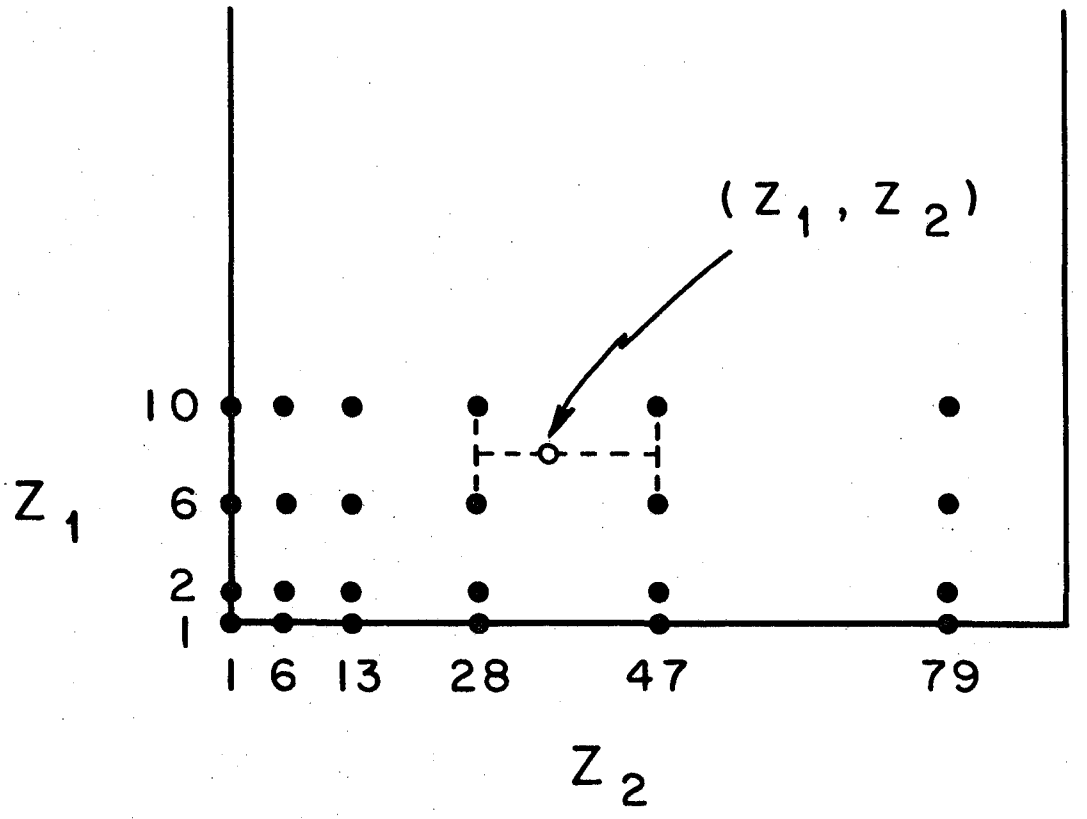

Fig. 5. A plane from (ε, Z_1, Z_2) space taken for any constant specific energy, say ε_o. Illustrated are the 24 points for which we can calculate the relative stopping power, each with one of 24 polynomials. We do a double linear interpolation in Z_1 and Z_2 to get the relative stopping power at the desired point (Z_1, Z_2) (see text).

linear interpolation in Z_1 and Z_2 between the four relative stopping powers at the four points of the grid which bracket (Z_1, Z_2).

To obtain the relative stopping power when $\varepsilon > 2$ we first calculate the relative stopping power for a proton in the stopping medium at the two specific energies $\varepsilon = 2$ and $\varepsilon = 10$ MeV/amu. We then assume that the relative stopping power has a functional form

$$f(\varepsilon) = p\varepsilon^{q}$$

where the constants p and q are determined by the two points, one at 2 and the other at 10 MeV/amu. (Actually the relative stopping power at 2 MeV/amu is multiplied by 0.97 before determining p and q. This is done only because it has been found that this slightly modified slope gives results which more closely duplicate experimental data.) Finally we assume, as discussed above, that for $\varepsilon > 2$ this proton relative stopping power in a given stopping medium is the same for all ions for which $Z_1 \leq 10$.

We obtain the 2 MeV/amu stopping power for protons in the given stopping medium and also in Al from Barkas and Berger's[23] polynomial fit to experiment data

$$\left(\frac{dE}{dR}\right)_p = \frac{\varepsilon_p}{\lambda}\left\{\sum_{n=1}^{2}\sum_{m=0}^{2} n\, a_{mn}\,(\log I_{adj})^m(\log \varepsilon_p)^{n-1}\right\}^{-1} \qquad (22A)$$

for $1 \leq \varepsilon_p \leq 7$ where

$$\log \lambda = \log \frac{A_2}{Z_2} + \sum_{n=0}^{2}\sum_{m=0}^{2} a_{mn}(\log I_{adj})^m(\log \varepsilon_p)^n - 3 \log 10. \qquad (22B)$$

Similarly at 10 MeV/amu we use Barkas and Berger's polynomial fit to Bethe's theory

$$\left(\frac{dE}{dR}\right)_p = \frac{\varepsilon_p}{\lambda}\left\{\sum_{n=1}^{3}\sum_{m=0}^{3} n\, a_{mn} (\log I_{adj})^m (\log \varepsilon_p)^{n-1}\right\}^{-1} \qquad (23A)$$

for $7 \leq \varepsilon_p \leq 1200$ where

$$\log \lambda = \log \frac{A_2}{Z_2} + \sum_{n=0}^{3}\sum_{m=0}^{3} a_{mn} (\log I_{adj})^m (\log \varepsilon_p)^n. \qquad (23B)$$

Several comments should be made explaining Eqs. (22) and (23). The symbol ε_p represents specific energy in units of MeV per number of proton masses. That is $\varepsilon_p = A_p \varepsilon$ where A_p is the mass of a proton in amu. The coefficients a_{mn} and α_{mn} are tabulated in Tables II and III respectively. Shell corrections are included in Eq. (23) by means of a polynomial expression which Barkas and Berger[23] fit to data by Walske[13, 14] and Bichsel.[36] These shell correction data approach zero in the limit of relativistic ion velocity. Since this is theoretically incorrect (see Fano[19]), an average excitation energy, I_{adj}, must be used which is adjusted for heavy stopping atoms to compensate for this error. The I_{adj} which we use for $Z_2 \leq 10$ are inferred from data presented by Turner[37] and given in Table IV. For $Z_2 > 10$ we use the formula communicated to Barkas and Berger[23] by Sternheimer,

$$\frac{I_{adj}}{Z_2}\,(\text{eV}) = 9.76 + 58.8\, Z_2^{-1.19}. \qquad (24)$$

Table II. Coefficients a_{mn} for Eq. 22.

m	n = 0	n = 1	n = 2
0	-7.5265×10^{-1}	2.5398	-2.4598×10^{-1}
1	7.3736×10^{-2}	-3.12×10^{-1}	1.1548×10^{-1}
2	4.0556×10^{-2}	1.8664×10^{-2}	-9.9661×10^{-3}

Table III. Coefficients a_{mn} for Eq. 23.

m	n = 0	n = 1	n = 2	n = 3
0	-8.0155	1.8371	4.5233×10^{-2}	-5.9898×10^{-3}
1	3.6916×10^{-1}	-1.452×10^{-2}	-9.5873×10^{-4}	-5.2315×10^{-4}
2	-1.04307×10^{-2}	-3.0142×10^{-2}	7.1303×10^{-3}	-3.3802×10^{-4}
3	3.4718×10^{-3}	2.3603×10^{-3}	-6.8538×10^{-4}	3.9405×10^{-5}

Table IV. Adjusted Average Excitation Energies for $Z_2 \leq 10$ from Turner.[37]

Z_2	I_{adj} (eV)
1	18.7
2	42
3	38
4	60
5	70
6	78
7	84.5
8	88.5
9	108
10	131

Now that we have the relative stopping power defined by Eq. (19) for any $\varepsilon < 10$ MeV/amu, we obtain the desired stopping power by multiplying the relative stopping power by the accurately measured experimental stopping powers of ions in Al. Through this stopping-power data in Al, Northcliffe[22] has placed smooth curves which are presented in Fig. 6. The specific values we use are given in Table V.

When there is more than one atomic component to the stopping medium as in mixtures and compounds, we assume that the stopping power of each component acts independently and is thus additive to the others. This is Bragg's rule which can be expressed

$$\frac{dE}{dR} = \frac{1}{\rho} \sum_i \rho_i \left(\frac{dE}{dR}\right)_i \tag{25}$$

where $(dE/dR)_i$ is the stopping power of the ith component in density independent units such as MeV/(g/cm^2), ρ_i and ρ are the partial density of the ith component and the overall density of the medium respectively ($\rho = \sum_i \rho_i$).

The validity of Bragg's rule is discussed in section IIIA1.

2. Specific Energy Greater Than 10 MeV/amu.

In this region of (ε, Z_1, Z_2) space ($Z_1 \leq 10$, $\varepsilon \geq 10$ MeV/amu), the ions are completely stripped of orbital electrons so that we may extend to all ions the proton stopping power of Eq. (23) by the formula

$$\frac{dE}{dR} = Z_1^2 \left(\frac{dE}{dR}\right)_p \tag{26}$$

where dE/dR is the stopping power of the ion of charge Z_1 at the

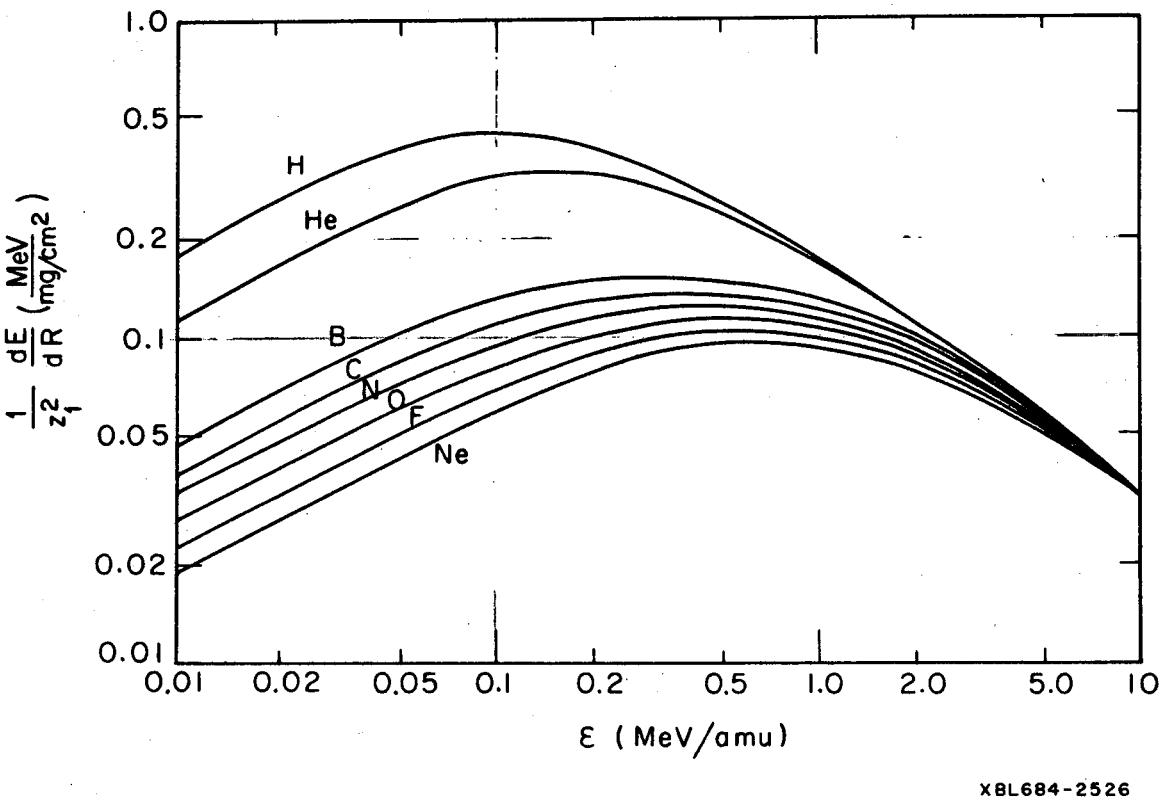

Fig. 6. Smoothed stopping-power curves for various ions in Al. These data from Northcliffe,[22] which are tabulated in Table IV, are the basis of the stopping-power calculation for $Z_1 \leq 10$ and $\varepsilon < 10$ MeV/amu.

Table V. Stopping Power of Ions in Al for Which $Z_1 \leq 10$ from Northcliffe.[22]

	$\frac{1}{Z_1^2}\frac{dE}{dR}$ (MeV/g/cm^2)									
(MeV/amu)	H	He	Li	Be	B	C	N	O	F	Ne
.010	183	118	95	71	48	39 38.9	34	28	23	19
.015	230	141	114	86	58	47	40	33	27	23
.020	265	164	132	99	66	54	47	38	32	27
.030	320	205	164	122	80	65	56	47	39	32
.040	360	235	187	140	93	75 77.2	64	54	46	38
.050	390	260	208	155	103	83	71	60	51	43
.070	430	285	230	175	120	97	82	69	59	50
.100	440	315	254	193	132	111 120	94	80	69	60
.150	410	325	264	203	142	123	108	92	80	70
.200	380	320	263	206	149	130	112	100	87	77
.300	330	290	243	196	150	133	121	109	96	87
.400	290	270	230	189	149	133 135	122	110	100	91
.500	265	250	216	181	147	131	122	111	101	93
.700	220	215	193	166	140	128	120	110	101	94
1.000	172	170	156	142	129	120 125	111	107	98	90
1.500	131	131	124	117	111	107	100	95	90	84
2.000	109	109	105	101	98	94	90	86	81	76
3.000	83	83	81	80	79	78	75	73	70	67
4.000	69	69	68	67	67	66	64	62	60	58
5.000	58	58	58	57	57	57	56	55	54	52
7.000	45	45	45	45	45	45	44	43	42	42
10.000	34	34	34	34	34	34	34	34	34	34

same velocity and in the same stopping material as that of the proton whose stopping power is $(dE/dR)_p$. This transformation is consistent with Bethe's theory.

When the stopping medium is a mixture or a compound, we use Bragg's rule as before. This implies that in Eq. (23) we make the two substitutions

$$\left\langle \frac{A_2}{Z_2} \right\rangle = \left[\frac{1}{\rho} \sum_i \rho_i \frac{Z_{2_i}}{A_{2_i}} \right]^{-1}, \tag{27}$$

and

$$I_{adj} = \exp\left\{ \left\langle \frac{A_2}{Z_2} \right\rangle \frac{1}{\rho} \sum_i \frac{Z_{2_i}}{A_{2_i}} \rho_i \ln(I_{adj})_i \right\}. \tag{28}$$

Here Z_{2_i}, A_{2_i}, ρ_i, and $(I_{adj})_i$ are the atomic number, atomic weight, partial density, and average adjusted excitation potential respectively of the ith component of the stopping medium.

3. Ion Mean Ranges for $Z_1 \leq 10$

The mean range of these ions in units of g/cm^2 is obtained for $\varepsilon \leq 10$ MeV/amu from the expression

$$R(\varepsilon) = 2\left(\frac{0.01\, A_1}{S(\varepsilon=0.01)}\right) + A_1 \int_{0.01}^{\varepsilon} \frac{d\varepsilon'}{S(\varepsilon')} \tag{29}$$

where $S(\varepsilon)$ is the stopping power of the ion at specific energy ε. The

first term of this expression is an estimate of the range of a 0.01 MeV/amu ion. This assumes that the stopping power is proportional to $\varepsilon^{1/2}$ below 0.01 MeV/amu. The effect of this assumption is discussed in section IIIA3. The integration indicated in the second term is performed by means of the trapezoidal rule where in each energy interval the integrand is here assumed to map a straight line on a log-log scale rather than a straight line on a linear scale which is normally the case. The energy intervals are those indicated in Table V.

The mean range for the case when $\varepsilon > 10$ MeV/amu is obtained from

$$R(\varepsilon)=2\left(\frac{0.01\,A_1}{S(\varepsilon=0.01)}\right)+A_1\int_{0.01}^{10.0}\frac{d\varepsilon'}{S(\varepsilon')}+\frac{A_1}{A_p Z_1^2}\left[\lambda(A_p\varepsilon)-\lambda(10\,A_p)\right], \quad (30)$$

where the above comments on the first and second terms of Eq. (29) also apply to the first and second terms here. In the third term A_p is the atomic weight of a proton, and λ is taken from Eq. (23B).

B. Method for Z_1 Greater Than Ten

1. Low-Specific-Energy Region ($137\beta \leq Z_1^{1/3}$)

In this region the ions are rapidly capturing electrons, thus losing effective charge. The stopping power or linear energy transfer (LET) is decreasing with decreasing velocity. In units of MeV/amu, the lower limit in this specific-energy region is 0.01 and the upper limit varies from 0.1 to 0.5 as Z_1 varies from 10 to 92. The LET of the ions is not large compared with that in the other regions. The average velocity of the ions at the Bragg peak of a beam of ions is normally well above this region. Thus the stopping power of these ions is of relatively minor important to the radio-

biologist.

There are several reasons, however, to expend considerable effort to provide valid stopping power in this region. To the nuclear chemist or physicist, this is the region of the recoil nucleus or nuclear reaction products. Stopping power in this region determines the range of these particles. Stopping power in this region may also be used to determine the energy of particles causing nuclear coulomb excitation. Charged particles in this region may be of more concern to the radiobiologist than indicated above because the radiation damage is qualitatively different from the damage for higher energy particles (see for example Kistemaker et al.[38] and Jung[39]). A final reason for developing good stopping-power data in this region is that we rely heavily on this data for the generation of stopping power in the medium-low- and medium-high-specific-energy regions as discussed in sections IIB2 and IIB3.

Lindhard et al.[17,18] have developed a theory for this velocity region (see section IC1). Their theory for the electronic stopping power is given in Eq. (15). By modifying the constant k (Eq. (16)) very slightly we obtained better agreement with experimental fission product range data in Al and U and stopping-power data for Ne and Ar ions in Al. We increased the contant by 1.5% and changed ξ from $Z_1^{1/6}$ to $Z_1^{0.207}$. Making these modifications, along with a change of units, we obtain for the electronic stopping power

$$\left(\frac{dE}{dR}\right)_e \quad \frac{MeV}{g/cm^2} = C_e \, \varepsilon^{1/2}, \tag{31}$$

where

$$C_e = 7.39 \times 10^4 \frac{Z_1^{1.207} Z_2}{A_2 (Z_1^{2/3} + Z_2^{2/3})^{3/2}} , \quad (32)$$

The theory developed by Lindhard et al. for the nuclear coulomb stopping power is represented by the curve in Fig. 2. By fitting a function to this curve and changing units again we get

$$\left(\frac{dE}{dR}\right)_n \frac{MeV}{g/cm^2} = C_n' \varepsilon^{1/2} \exp\left[-45.2(C_n' \varepsilon)^{0.277}\right] \quad (33)$$

where

$$C_n = 4.14 \times 10^6 \left(\frac{A_1}{A_1+A_2}\right)^{3/2} \left(\frac{Z_1 Z_2}{A_2}\right)^{1/2} \left(Z_1^{2/3}+Z_2^{2/3}\right)^{-3/4} , \quad (34)$$

and

$$C_n' = \frac{A_1 A_2}{Z_1 Z_2} \frac{1}{A_1+A_2} \left(Z_1^{2/3}+ Z_2^{2/3}\right)^{-1/2} . \quad (35)$$

Thus, for the low-specific-energy region, the total stopping power is given by

$$\frac{dE}{dR} = \left(\frac{dE}{dR}\right)_e + \left(\frac{dE}{dR}\right)_n , \quad (36)$$

where $(dE/dR)_e$ and $(dE/dR)_n$ are given in Eqs. (31) and (33) respectively.

When the stopping medium is either a compound or a mixture, we use Bragg's rule (Eq. (25)) to calculate the stopping power. See section IIIA1 for a discussion of the validity of this rule for these low velocities.

2. Medium-Low-Specific-Energy Region ($Z_1^{1/3} < 137\,\beta \leq 9$)

This is a narrow region connecting the variable upper boundary of the low-specific-energy region with the fixed lower boundary of the medium-high-specific-energy region. There are no experimental data nor theories available for this region which are satisfactory for estimating the stopping power. However, since this region is so narrow, a simple cubic polynomial, matching the slope and magnitude of the stopping power at both boundaries, provides the stopping power relation within the region very adequately.

We know that the stopping power tends to depend upon energy in a logarithmic fashion. Thus it is to be expected that a polynomial fit of the stopping power should contain $\ln\varepsilon$ as the variable. Thus we choose a cubic of the form

$$\ln\left(\frac{dE}{dR}\right) = \sum_{n=0}^{3} C_n (\ln\varepsilon)^n \tag{37}$$

which is completely determined by the magnitude and first derivative of the stopping power at the upper and lower boundaries of this region.

When the stopping medium is a mixture or compound, we again make use of Eq. (25).

3. Medium-High-Specific-Energy Region ($9 < 137\,\beta \leq 3\,Z_1$)

This region is bounded on the high side by the velocity at which the ion can be considered to be completely stripped of electrons. It is bounded on the low side by velocities for which we believe the method described below cannot adequately provide stopping power.

Our method uses charge-state data derived from range-energy data available for Ar ions incident upon Al. These charge-state data are generalized to all ions for which $Z_1 > 10$ and all stopping media as follows.

Knipp and Teller,[40] on the basis of the Thomas-Fermi picture of the atom, derived a relationship between $Z_{1_{eff}}/Z_1$ and $(v_e/V_i)(137\,\beta/Z_1^{2/3})$, where $Z_{1_{eff}}/Z_1$ is the mean fractional ionization of the ion, and v_e/V_i is the ratio of the velocity of an electron in the ion's electron cloud to the velocity of the ion at which this electron's capture and loss cross sections are equal. For completeness we point out that $Z_{1_{eff}}$ is a function of ion velocity and it is the root mean square of the charge of a large number of randomly sampled ions all at the same velocity. The fact that Knipp and Teller used the mean charge instead of the root mean square charge is of little concern for two reasons. First, these two values have experimentally been found by Neufeld and Snyder[41] to be nearly identical for nitrogen and oxygen ions. This is due to the fact that the charge distribution at any velocity is very narrow. Second, the method by which we drive the value of r automatically gives the root mean square fractional ionization of the ion, which is exactly what we desire.

The factor (v_e/V_i) varies somewhat as a function of Z_1 and Z_2, but here we assume it is constant. (See section IIIB3 for a discussion of this assumption.) Then $Z_{1_{eff}}/Z_1$ should be a function

of only $137\beta/Z_1^{2/3}$ when the electron cloud of the ion is populated to such an extent that the statistical nature of the Thomas-Fermi picture is appropriate. As the electron cloud is depleted, $137\beta/Z_1^{2/3}$ will no longer be the appropriate variable. In fact the semi-classical Bohr picture of the atom leads us to expect that the charge ratio $Z_{1_{eff}}/Z_1$ varies according to the variable $137\beta/Z_1$ for the limiting case of the one-electron atom. Thus we look for a function

$$\frac{Z_{1_{eff}}}{Z_1} = r(X), \tag{38}$$

where

$$X = \frac{137\beta}{Z_1^{g}} \tag{39}$$

with

$$\left.\begin{aligned} g &= \frac{2}{3} && \text{for } 137\beta \leq Z_1^{2/3}, \\ g &= \frac{137\beta + 4Z_1 - 3Z_1^{2/3}}{6Z_1 - 3Z_1^{2/3}} && \text{for } Z_1^{2/3} < 137\beta < 2Z_1, \\ g &= 1 && \text{for } 2Z_1 \leq 137\beta \leq 3Z_1. \end{aligned}\right\} \tag{40}$$

We required that the function r(X) satisfy five criteria.

1. $r(0) = 0$.
2. $r(X)$ approaches 1 asymptotically.
3. For all Z_1 and Z_2, $Z_1^2 r^2(3) (dE/dR)_p$ and its first derivative are approximately continuous with the stopping power and

its first derivative respectively at the low-velocity boundary of the high-specific-energy region. (Note that $X = 3$ for $137\beta = 3\,Z_1$.)

4. For all Z_1 and Z_2, $Z_1^2\, r^2(9/Z^g)\,(dE/dR)_p$ and its first derivative are approximately continuous with the stopping power and its first derivative respectively at the high-velocity boundary of the low-specific-energy region. That is to say, the cubic polynomial of the previous section (Eq. (37)) must smoothly connect the low- to the medium-high-specific-energy regions without any unlikely curvature.

5. The function $r(X)$ must be such that

$$R(\varepsilon) = \frac{A_1}{Z_1^2} \int_0^{\varepsilon} \frac{d\varepsilon}{r^2(X)\,(dE/dR)_p}$$

fits closely the known range-energy data for Ar in Al. These range data are taken from estimates made by Northcliffe[42] which agree well with some experimental data of Sikkeland.[43]

There is some question about what formulation of the proton stopping power to use in steps 3, 4, and 5 above. Some of this medium-high-specific-energy region is outside the limits of validity for the Born approximation (see section IC1 for a discussion of these limits), so Bethe's theory is not rigorously valid. The velocity is too high to use Bohr's theory. When we use Bloch's theory the resulting stopping power for this region differs from the stopping power when using Bethe's theory by much less than the total uncertainty of our method (see section IIIB3 for a discussion of this comparison). Bethe's theory is the most commonly used and the most convenient to use. We therefore choose Bethe's theory realizing that the resulting $r(X)$ which satisfies the above criteria may not physically represent $Z_{1_{eff}}/Z_1$ at the low-velocity end of this region. However, due to the nature of the above criteria, the

error in r(X) will compliment to some extent the error in Bethe's theory for this low-velocity end of the region, so that the final stopping power may be fairly accurate.

A function which satisfies criteria one and two, and which can be adjusted to satisfy the other three as well is

$$r(X) = 1 - \frac{1}{a} \; e^{-f_1(X)} \; - \frac{1 - \frac{1}{a}}{f_2(X) + 1} \quad , \tag{41}$$

where a is a positive constant and $f_1(X)$ and $f_2(X)$ are functions which satisfy

$$\begin{aligned} & f_1(X) \text{ and } f_2(X) \geq 0 \text{ for } X \geq 0, \\ \lim_{X \to 0} \quad & f_1(X) \text{ and } f_2(X) = 0, \\ \lim_{X \to \infty} \quad & f_1(X) \text{ and } f_2(X) = \infty, \end{aligned} \tag{42}$$

and X is given by Eq. (39). By trial and error and the use of a minimization computer program called VARMIT[44] we have satisfied all 5 criteria with the combination

$$a = 1.848$$

$$f_1(X) = 0.413 \, X^{2.67}$$

$$f_2(X) = 10.48 \, X^{2.216}$$

which yields

$$r(X) = 1 - \frac{\exp(-0.413X^{2.67})}{1.848} - \frac{0.848}{1.848(10.48X^{2.216} + 1)}, \qquad (43)$$

where X is given by Eq. (39). A graph of Eq. (43) appears in Fig. 7. The stopping power in this medium-high-specific-energy region now becomes

$$\frac{dE}{dR}(\varepsilon) = Z_1^2 \; r^2 \left(\frac{dE}{dR}(\varepsilon)\right)_p , \qquad (44)$$

where the proton stopping power $(dE/dR)_p$ is given by Eq. (22) for $\varepsilon \leq 7$ MeV/amu and by Eq. (23) for $\varepsilon > 7$ MeV/amu.

Again, when the stopping medium is a compound or a mixture, we obtain its stopping power by using Bragg's rule, Eq. (25). Bragg's rule is implemented through the use of Eqs. (27) and (28).

4. High-Specific-Energy Region ($137\beta > 3Z_1$)

In this region the ion is assumed to be completely stripped of its orbital electrons and the conditions for the validity of the Born approximation are met. Thus Bethe's theory gives the stopping power

$$\frac{dE}{dR}(\varepsilon) = Z_1^2 \left(\frac{dE}{dR}(\varepsilon)\right)_p , \qquad (45)$$

where $(dE/dR)_p$ is given by Eq. (23).

When the stopping medium is a compound or a mixture, Bragg's rule, through the use of Eqs. (27) and (28), again yields the stopping power.

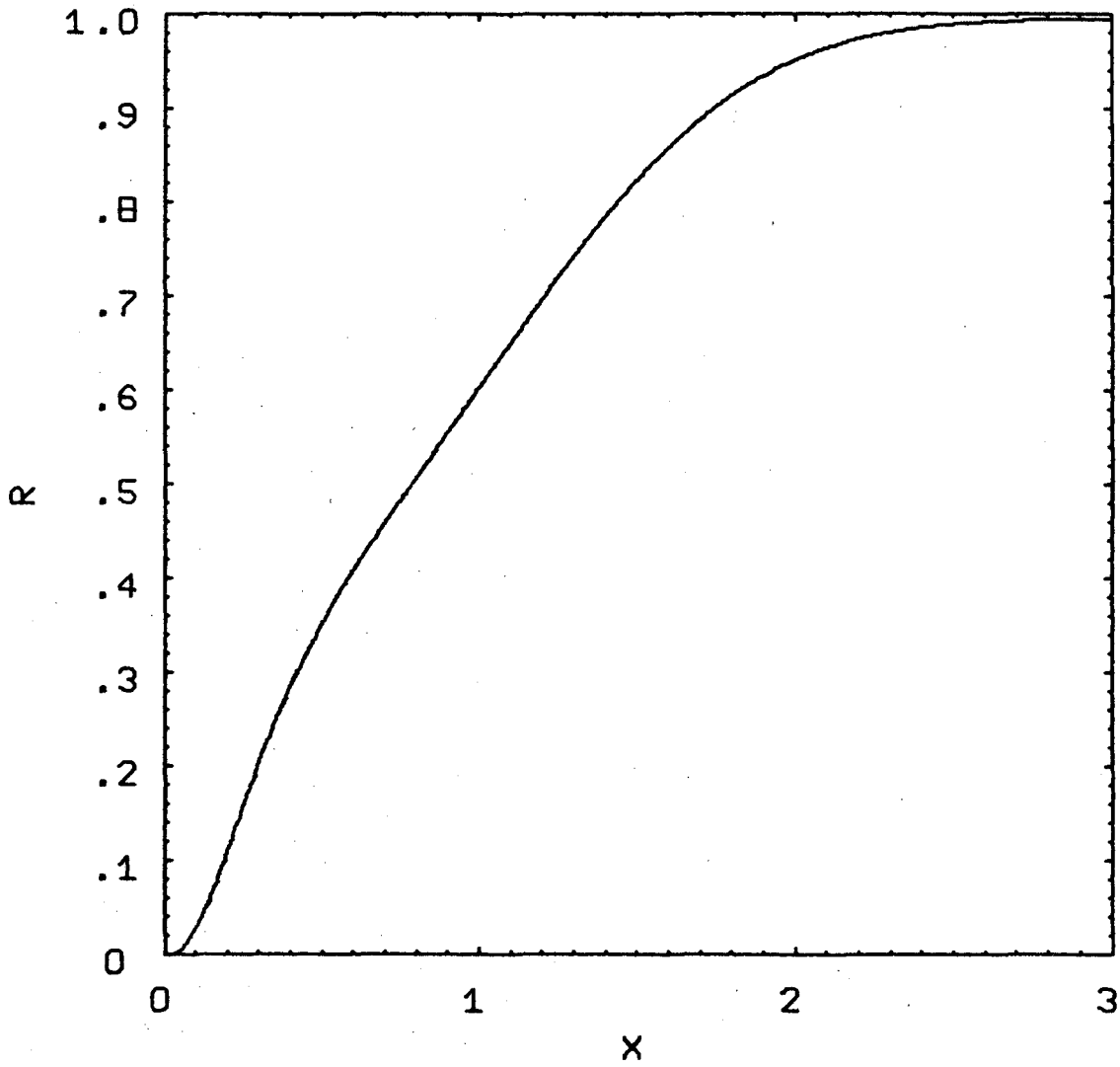

XBL 685-847

Fig. 7. A plot of Eq. (43). Here $X = 137\,\beta/Z_1^g$ where g is given by Eq. (40), r is the charge state $Z_{1_{eff}}/Z_1$ which, when used with Bethe's theory gives, for example, the results illustrated in Fig. 10.

5. Ion Mean Range for $Z_1 > 10$

The mean range of ions with a specific energy of ε in the high-specific-energy region is given by

$$R(\varepsilon) = A_1 \int_0^{\varepsilon_1} \frac{d\varepsilon}{(dE/dR)_L} + A_1 \int_{\varepsilon_1}^{\varepsilon_2} \frac{d\varepsilon}{(dE/dR)_{ML}} + A_1 \int_{\varepsilon_2}^{\varepsilon_3} \frac{d\varepsilon}{(dE/dR)_{MH}} + \frac{A_1}{Z_1^2 A_p} [\lambda(A_p \varepsilon) - \lambda(A_p \varepsilon_3)], \tag{46}$$

where $(dE/dR)_L$, $(dE/dR)_{ML}$, $(dE/dR)_{MH}$, and λ are given by Eqs. (36), (37), (44), and (23B) respectively, ε_1 and ε_2 are respectively the lower and upper boundaries of the medium-low-specific-energy region, and ε_3 is the lower boundary of the high-specific-energy region. For ε in the medium-high-specific-energy region, the last term of Eq. (46) is deleted and ε_3 is replaced by ε. If ε is in the medium-low-specific-energy region, the last two terms are deleted and ε_2 is replaced by ε. If ε is in the low-specific-energy region, only the first term is used and ε_1 is replaced by ε.

The integrals of Eq. (46) are evaluated iteratively by Simpson's rule. The number of points at which the integrand is evaluated doubles for each iteration. The integration process is terminated for each integral at the ith iteration when the result of the iteration, I_i, differs from the preceding iteration, I_{i-1}, by less than 0.05%. That is the integral is given the value I_i when

$$\left| I_{i-1} - I_i \right| < 0.0005.$$

III. DISCUSSION OF METHOD

A. Z_1 Less Than Eleven

1. Specific Energy Less Than 10 MeV/amu.

In this region of (ε, Z_1, Z_2) space considerable experimental stopping-power data are available. Northcliffe[22] has summarized the availability of these data and he has plotted them for the cases of H, He, B, C, N, O, F, and Ne ions each incident upon C, Al, Ni, Ag, and Au. Where there are data points from more than one investigator, a spread is greatest for the cases of Ne ions in the various stopping media. Here the two principle investigators, Porat et al.[45, 46], and Teplova et al.[33], often disagree by 50%. The total spread in uncertainty (i. e. twice the absolute uncertainty) for the data points quoted by the investigators commonly varies from 5 to 30%.

Northcliffe[22] has developed a graphical technique for generating smooth curves which first of all follow closely the data points he believes to be the most reliable, and second they show a uniform variation from ion to ion and stopping material to stopping material. We are reluctant to estimate error limits for these smooth curves by Northcliffe, but we have more confidence in them than we do in much of the raw experimental points. We expect the error limits are greatest for $\varepsilon < 0.1$ MeV/amu, smaller for $0.1 < \varepsilon < 5$ MeV/amu and quite small for $5 < \varepsilon < 10$ MeV/amu. Also we expect the error limit to increase with increasing Z_1. It is values taken from these smooth curves that appear in Table I for the stopping media C, Al, Ni, Ag, and Au.

As stated in section II A 1, the stopping power of H_2 which appears in Table I is inferred from data replotted from Teplova et al.[33], Weyl[34], and Allison and Littlejohn.[35] We plotted the data points on a scale of $(1/Z_2)$ (dE/dR) in MeV/(g/cm^2) as a function of specific energy in units of MeV/amu. We drew smooth curves through the

points requiring a consistent variation from ion to ion. We made no attempt, however, to force a consistent variation from H_2 to the other stopping media because we expect the variation to be very rapid as we go from $Z_2 = 6$ to $Z_2 = 1$. It is points taken from these curves that appear in Table I.

Again, we are reluctant to assign error limits to the stopping power in H_2 which appears in Table I. As before, the error limit will decrease with increasing ion velocity. We have more reason than before, however, to expect that the error limit will increase with increasing Z_1. Our method is designed to calculate stopping power of nongaseous media, but the data for H_2 in Table I was collected from experiments in gaseous hydrogen. This introduces an error due to the following effect. In condensed stopping media, the time interval between ion-electron collisions is shorter than in gases. Thus the electronic levels of the ion excited by one collision will have less opportunity to relax before the next collision. The probability of removing an electron from the ion is greater for these condensed media because the electrons are maintained in more highly excited states. Thus an ion which is not completely stripped of its electrons will have a larger mean charge and thus a greater stopping power in condensed media than in gaseous media. The error introduced by this effect should be small for protons and alpha particles because they are completely ionized much of the time over most of this region of (ε, Z_1, Z_2) space. However in the low-velocity part of this region, carbon and particularly Ne ions should have a larger stopping power in condensed hydrogen than we estimate by our method. We suspect therefore that for $Z_1 \leq 10$ and $\varepsilon < 1$ MeV/amu our method may underestimate somewhat the stopping power in condensed hydrogenous media such as water and tissue.

We have described our sources of the experimental data tabulated in Table I and we have expressed some reservation about their

applicability. Now we discuss how closely our method of section II A 1 reproduces these data. In Table VI we have tabulated the percentage deviation of stopping power calculated by our method from the values in Table I. The experimental stopping powers at $\varepsilon = 4$ MeV/amu were not listed in Table I because they were not used in determining the constants of Eq. (21), but the percentage deviation of the experimental stopping power from that calculated by our method is given in Table VI at $\varepsilon = 4$ in order for the reader to be able to evaluate our method at this velocity. Our method overestimates the experimental data for positive values in Table VI and underestimates for negative values. Table VI shows that our method usually reproduces Northcliffe's stopping power to within 5%. The glaring exception is the case of Ne ions in carbon. However, if we examine Northcliffe's estimate of this stopping power we see that it diverges from the experimental points by 20 to 30%, (see Fig. 7 of Ref. (22). We conclude that our method duplicates Northcliffe's stopping power to within the uncertainty of the magnitude of these values. Our method has some difficulty in reproducing our estimate of the stopping power of H_2 for helium and particularly carbon ions. But as we have just stated, the degree of applicability of these values to condensed stopping material is uncertain. We could obtain better reproduction of basic data by complicating the form of Eq. (21), but this seems hardly worthwhile until better basic data is available.

We use Bragg's rule in order to calculate the stopping power of compounds and mixtures throughout (ε , Z_1, Z_2) space. In the low-velocity portion of this space, e. g. $\varepsilon < 1$ MeV/amu, Bragg's rule is less valid than for the higher velocity regions. The main reason for this is that as the velocity of the ion decreases, the more tightly bound inner electronic shells of the stopping medium play a smaller role in the stopping process. Thus the most loosely bound shells, for example the valence shell, contribute a larger fraction of the stopping. Since it is primarily the valence shell whose energy

Table VI. Percentage Deviation of the Method of Section II A 1 From The Stopping-Power Values Of Table 1.

Table VI A. Hydrogen Ions ($Z_1 = 1$) in Various Stopping Media

ε	$H_2(Z_2 = 1)$	$C(Z_2 = 6)$	$Al(Z_2 = 13)$	$Ni(Z_2 = 28)$	$Ag(Z_2 = 47)$	$Au(Z_2 = 79)$
0.01	0.8	-0.5	0.05	0.05	-0.5	-0.3
0.04	-2.6	1.0	-1.2	-0.9	1.0	1.1
0.1	0.9	1.4	3.0	2.0	1.8	-1.2
0.4	4.9	-3.9	-3.2	-2.1	-4.1	-0.4
1.0	-3.5	-5.4	-1.7	-1.0	-6.8	1.6
4.0	0.5	0.4	1.5	1.9	0.6	2.0

Table VI B. Helium Ions ($Z_1 = 2$) in Various Stopping Media

ε	$H_2(Z_2 = 1)$	$C(Z_2 = 6)$	$Al(Z_2 = 13)$	$Ni(Z_2 = 28)$	$Ag(Z_2 = 47)$	$Au(Z_2 = 79)$
0.01	-2.6	-0.8	0.08	-0.05	-0.9	-0.3
0.04	9.4	2.3	-0.5	0.04	2.5	1.2
0.1	-3.3	-0.2	0.8	0.3	1.0	-1.3
0.4	-10.5	-3.4	-0.5	-0.2	-5.5	-0.4
1.0	-6.7	-4.7	-0.1	-1.9	-7.2	1.9
4.0	0.5	-0.2	0.	3.8	1.8	2.0

Table VI. (cont.)

Table VI C. Carbon Ions ($Z_1 = 6$) in Various Stopping Media

ε	$H_2(Z_2 = 1)$	$C(Z_2 = 6)$	$Al(Z_2 = 13)$	$Ni(Z_2 = 28)$	$Ag(Z_1 = 47)$	$Au(Z_2 = 79)$
0.01	-4.6	-0.04	-0.5	-0.02	-1.0	0.1
0.04	14.2	-0.3	2.4	-0.5	3.0	-0.2
0.1	1.0	0.8	-2.5	1.5	0.02	-0.6
0.4	-24.4	0.8	1.0	-1.6	-4.8	1.2
1.0	-14.9	-8.4	-3.4	-2.0	-6.5	3.0
4.0	-0.3	0.7	4.7	3.0	1.0	0.8

Table VI D. Neon Ions ($Z_1 = 10$) in Various Stopping Media

ε	$H_2(Z_2 = 1)$	$C(Z_2 = 6)$	$Al(Z_2 = 13)$	$Ni(Z_2 = 28)$	$Ag(Z_2 = 47)$	$Au(Z_2 = 79)$
0.01	1.5	1.4	0.1	0.2	-1.0	-0.2
0.04	-5.7	-2.4	-0.8	-2.0	2.3	0.4
0.1	4.2	-4.4	1.2	3.8	2.4	0.6
0.4	3.7	12.3	-0.7	-2.4	-7.9	-2.4
1.0	2.4	15.4	-1.0	-4.9	-7.2	0.6
4.0	0.5	-0.3	-1.7	-1.6	-4.0	-1.6

levels are modified by molecular binding, it is primarily the low velocity ions whose stopping rate will be affected by the chemical state of the atomic components of the stopping medium. As a corollary to this line of reasoning, we wish to point out that for all ion velocities one expects that compounds of the lighter atoms, such as H, C, N, and O will not follow Bragg's rule as well as compounds of heavier atoms. This is because a larger fraction of the total electron cloud of the lighter atoms are valence electrons. Thus, for $\varepsilon \ll 1$ MeV/amu, our calculation of stopping power in compounds may suffer from the use of Bragg's rule, particularly when the stopping medium is tissue, a hydrocarbon, water, or other hydrogenous compounds.

The error introduced by using Bragg's rule is not large in most cases. Thompson[47] has found that the use of Bragg's rule for calculating the stopping power of hydrocarbons for high-energy protons (200 to 340-MeV) introduces an error on the order of 1 to 2% or less. Aniansson[48] makes similar findings for 5.3 MeV alpha particles. Reynolds et al.[49] have found that Bragg's rule introduces an error in the calculation of stopping power of gaseous H, C, N, and O compounds which increases to more than a couple percent as the proton energy decreases below 0.15 MeV.

2. Specific Energy Greater Than 10 MeV/amu

In this region the ion is completely ionized and Bethe's theory, Eqs. (8) and (10), is valid. Therefore the stopping power calculated by our method should be as accurate as the polynomial of Barkas and Berger((Eq. (23)).

Bethe's theory with the shell corrections used by Barkas and Berger should be accurate to within about 1%. Barkas and Berger[23] have determined that the root-mean-square percentage deviation of Eq. (23) from 600 points calculated by this theory is 0.6% for λ and 1.3% for the stopping power. The maximum error for λ is 2.8%. Therefore the overall accuracy of our method in this region (i.e. of

Eq. (23)) should be about 1 to 3%.

3. The Mean Ion Range for $Z_1 \leq 10$

The range given by Eq. (30) should have an accuracy approximately comparable to the corresponding stopping-power calculation. There are two assumptions made in the evaluation of this equation which should introduce only a small uncertainty. First, the first term of Eq. (30) is correct only if the stopping power varies as $\varepsilon^{1/2}$ below 0.01 MeV/amu. This may introduce an error in the range for say $\varepsilon < 0.03$, but as the ion velocity increases, a smaller and smaller part of the total range is contributed by that specific-energy region below 0.01 MeV/amu. Thus the error introduced by this first assumption quickly becomes negligible as the initial ion specific-energy increases above 0.01 MeV/amu.

It is assumed in evaluating the second term of Eq. (30) that, between the specific energies indicated in Table V, the stopping power maps a straight line on a log-log scale. This is a very good assumption, but even if it were not good the error would be quickly lost as the initial specific energy increases above 10 MeV/amu, as discussed above.

B. Z_1 Greater Than Ten

1. Low-Specific-Energy Region ($137\beta \leq Z_1^{1/3}$)

In this region our method used the two theories developed by Lindhard et al.[17, 18] which are based upon the Thomas-Fermi model of the atom. These theories are described in Section I C (see Eqs. (12) through (16)). In developing their theories, Lindhard, et al. treat separately the effect of elastic collisions between the ion and the coulomb field of the nuclei in the stopping material, and the effect of inelastic collisions between the ion and the atomic electrons in the stopping material. The assumption that these two effects are

uncorrelated may result in systematic overestimation of the stopping power, according to Lindhard. Lindhard also warns that the validity of this theory is uncertain for $\varepsilon < 10^{-2}$ MeV/amu, since the Thomas-Fermi treatment of the atom is a crude approximation when the ion and atom do not come close to each other.

Others have been critical of these theories too, particularly of the theory for the stopping due to inelastic collisions (see Eqs. (15) and (16)). The variation of k(Eq. (16)) with Z_1 and Z_2 has been found to be imperfect, and the variation of stopping power with velocity has been found to differ somewhat from $\varepsilon^{1/2}$ (Eq. (15)).

Ormrod and Duckworth[50] and Ormrod, MacDonald and Duckworth[51] have subjected this theory to an experimental test for ions of $Z_1 \leq 18$ in carbon and aluminum films for specific energies of $\lesssim 0.01$ MeV/amu. There was generally fairly good agreement. However, for a constant velocity of $\varepsilon = 0.0004$ they found that as they varied Z_1 the experimental stopping power oscillated about the theoretical predictions of Lindhard. Gilat and Alexander[52] have studied the ranges of recoil Dy ions of specific energies $0.04 < \varepsilon < 0.14$ in various gases and Al. They find for Dy ions in Al that the dependence of the stopping power upon velocity is more pronounced than $\varepsilon^{1/2}$. They suggest that a velocity dependence of $\varepsilon^{0.67}$ would provide a better fit of their experimental data. Kaplan and Ewart[53] have studied the ranges of recoil Cl^{34m} nuclei in Al for $0.2 < \varepsilon < 0.9$ MeV/amu. They found that k was predicted by Lindhard's theory to be 10 to 15% too small. They also found that for this case the stopping power should be a weaker function of velocity than that predicted by Lindhard. Gilat and Alexander had found the opposite.

These findings have recently been put into perspective by Fastrup et al.[5] They have studied the stopping by carbon of ions with $6 \leq Z_1 \leq 20$ and $0.003 < \varepsilon < 0.03$. Ormrod and Duckworth studied the region below these velocities. Porat and Ramavataram[45, 46]

studied the region above these velocities. Fastrum et al. have combined the results of these researchers with their own to provide a systematic test of Lindhard's theory. They verified the findings of Ormrod and Duckworth that the value of k oscillates about the value predicted by Lindhard as Z_1 is varied. This oscillation exists when the specific energy is held constant at each of the four values ε = 0.0004, 0.01, 0.02, and 0.03. As the velocity increases, however, the amplitude of oscillation decreases and becomes less regular. This may imply that at low energies, where the electron clouds do not overlap to a great extent, atomic shell effects are important. The Thomas-Fermi atomic model is of course inadequate to deal with such effects.

Fastrum et al. also tested the energy dependence of Lindhard's theory. They modified Eq. (15) by letting $(d\epsilon/d\zeta)_e = k\epsilon^p$ be of the form where p was found from the experimental data and compared with the theoretically predicted value of 1/2. They found that, when plotted as a function of Z_1, p tended to oscillate about the value of 1/2. However, the behavior of the variation of p with Z_1 was dependent on the velocity interval over which p was determined.

It is clear that there are some inelastic interactions between low-velocity heavy ions and matter which are more complex than can be dealt with by a statistical atomic model such as the Thomas-Fermi model. However, until these interactions are better understood, we use the Thomas-Fermi model and Lindhard's theory (slightly modified as described below) expecting for certain cases 10 to 20% errors (perhaps more) in the stopping power.

Wherever we have direct comparison with experimental data available, the ranges calculated by our method are usually very close to the experimental values. We calculate ranges which are within 5 to 10% of the ranges measured for Cl ions in Al by Kaplan and Ewart.[53] This comparison is discussed in the next section because

we believe the velocities of the Cl ions measured are above the region of validity for Lindhard's theories. The fact that the ranges of these Cl ions were measured at such high velocities ($0.2 \leq \varepsilon \leq 0.9$ MeV/amu) may have contributed to the finding that the variation of stopping power with energy was less pronounced than $\varepsilon^{1/2}$.

We also calculate ranges which are usually within 5 to 10% of the ranges measured for Dy ions in Al by Gilat and Alexander.[52] This comparison is made in Fig. 8. Our value of k (see Eq. (32)) is clearly slightly large. Had we not increased ξ from $Z_1^{1/6}$ to $Z_1^{0.207}$ we would have closer agreement with the experimental points, but then we would have poorer agreement with the fission-product data discussed below. We do not attempt to compare ranges calculated by our method with those measured by Gilat and Alexander for Dy ions in various gases. For reasons stated in Sec. III A 1, stopping power can be more than a factor of two lower in gases than in condensed media. This can be seen from Fig. 12 of Lassen[54] where the charge state of fission products in gases and solids is illustrated. Alexander and Gilat have found errors of this magnitude in Lindhard's theory when comparing with the range data obtained in gases.

We have collected U^{235} fission-product ranges from several sources (Refs. (55) through (59)). The velocities of each of the fission products chosen were taken from Ref. (60). (These references are all summarized in Hyde (26).) By making the very slight modifications in k (see Section II B 1) which consist only of increasing k by a constant 1.5% and increasing ξ from $Z_1^{1/6}$ to $Z_1^{0.207}$, we have obtained the good agreement shown in Tables VII and VIII.

Since the experimental ranges are a measure of the distance the ion travels projected onto the initial direction of flight, we should compare the experimental ranges with a calculation of the mean projected range. The path-length range, obtained from Eq. (46), is the total mean distance the ion travels no matter how twisted its path

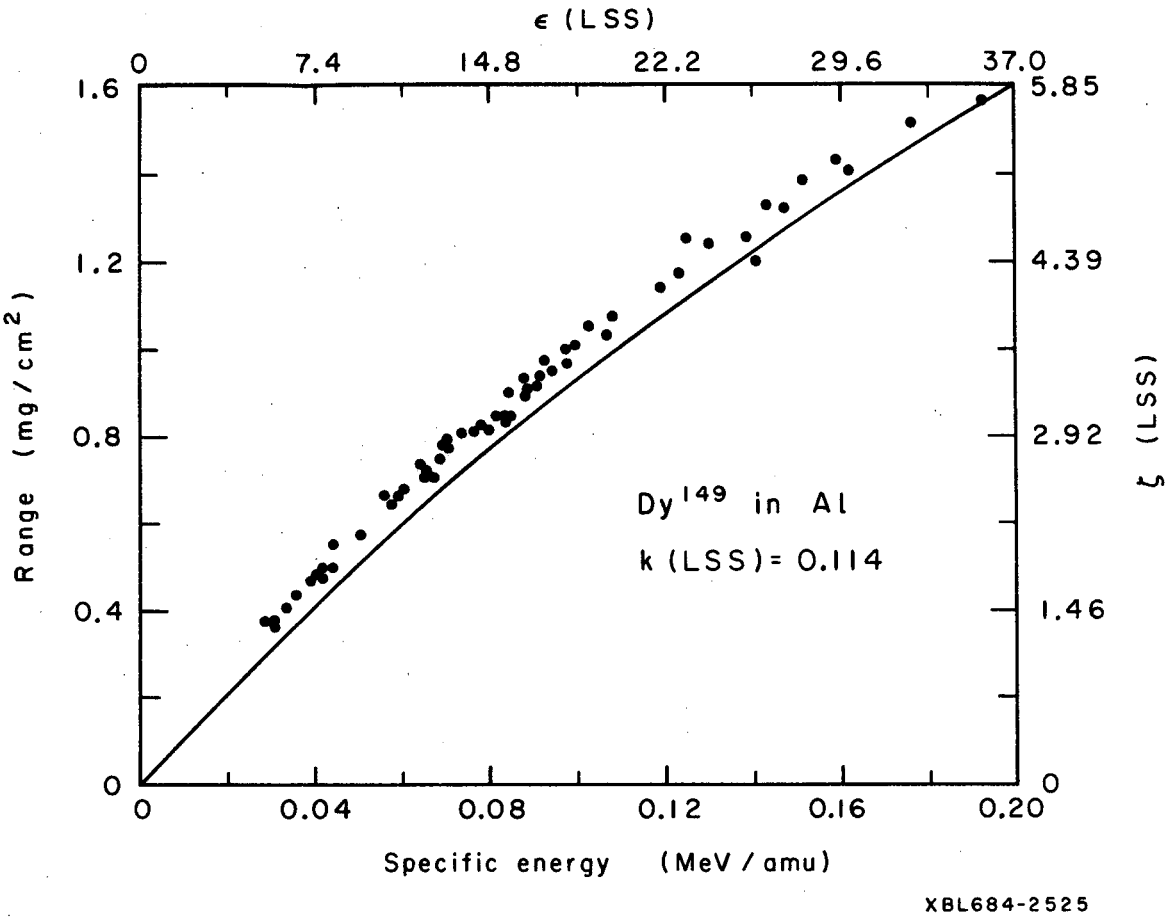

Fig. 8. The theory used in the low-specific-energy region (line) is compared with experimental range data (circules) obtained by Gilat and Alexander[52] for Dy^{149} ions in Al. The dimensionless range and velocity used by Lindhard, Scharff, and Schiott (designated LSS) are given at the right and upper axes respectively. The value of the constant k (see Eq. (16)) is also given.

Table VII. Ranges In Al Calculated By The Program Compared With The Experimental Fission-product Ranges.

Ion	Estimated specific energy (MeV/amu)	Range (mg/cm^2)		
			Calculated	
		Experimental	Projected	Path-length
$^{89}_{38}Sr$	1.12	4.09	4.12	4.15
$^{115}_{48}Cd$	0.613	3.32	3.14	3.18
$^{140}_{56}Ba$	0.489	2.98	3.03	3.07
$^{144}_{58}Ce$	0.437	2.76	2.84	2.87

Table VIII. Experimental Fission-product Ranges in U Compared With Ranges Calculated By The Program

Ion	Estimated specific energy (MeV/amu)	Range (mg/cm^2)		
			Calculated	
		Experimental	Projected	Path-length
$^{89}_{38}Sr$	1.12	11.55	11.76	12.82
$^{109}_{46}Pd$	0.816	10.14	9.91	10.87
$^{115}_{48}Cd$	0.613	9.52	8.35	9.27
$^{140}_{56}Ba$	0.489	8.74	7.64	8.48
$^{144}_{58}Ce$	0.437	8.37	7.04	7.85

may be. The difference between the projected and path-length ranges is due to multiple scattering of the ion by nuclei in the stopping material. As one would expect, this difference is the more significant the lighter the ion and the heavier the nuclei of the stopping medium. In order to calculate the projected range for these experimental comparisons, two computer programs were written. One calculates the mean projected range of the ions and the other calculates the difference between the mean projected range and the mean path-length range. The computer programs and the method used in each are discussed in Appendix B.

Table VII shows that there is good agreement between theory and experiment for fission products incident upon Al. The dependence upon Z_1 is approximately correct for this case. However, Table VIII shows that the agreement is not so good for the case of fission products incident upon uranium. Aras et al.[4] have also made this observation. The theory predicts in this case that the stopping power increases with increasing Z_1 faster than it does in reality (i.e. the range decreases too fast). We thought at first that, since the multiple scattering of the ion in uranium would be greater than in aluminum, a computation of the projected range might remove the discrepancy. But Table VIII shows that the discrepancy became worse. Another possibility is that, although increasing ξ from $Z_1^{1/6}$ to $Z_1^{0.207}$ is proper for Al as the stopping medium, we should decrease the dependency of ξ on Z_1 for uranium as the stopping medium. However, we choose not to make further changes in Lindhard's theory for three reasons. First, as mentioned above, the inelastic processes by which an ion in this low-velocity region can lose energy are numerous and not well understood. For example, the correlation between the elastic nuclear coulomb collisions and inelastic collisions are not known, so we here assume that they do not exist. Therefore, perhaps at this time we should not expect consistently good agreement here

between theory and experiment. Second, we are more anxious to have an accurate calculation for light stopping material than for very heavy stopping material, since the light stopping material are of greater radiobiological importance. Therefore the modification which gives good agreement in Al takes precedence over the corresponding modification in uranium. Finally, we cannot make modifications indiscriminately and still retain a sufficient amount of physics in the theory to give us confidence that our calculations are valid in regions of (ε, Z_1, Z_2) space where no experimental data are available.

When the stopping medium is either a compound or a mixture we always use Bragg's rule, Eq. (25), to calculate the stopping power. The limitations of this rule for low ion velocities were discussed at the end of Section III A 1. The use of Bragg's rule in the present region is subject to the same limitations. We refer the reader to the earlier discussion.

2. Medium-Low-Specific-Energy Region ($Z_1^{1/3} < 137\beta \leq 9$)

The upper limit of this region is 2 MeV/amu. The lower limit ranges from 0.1 to 0.5 MeV/amu as Z_1 ranges from 10 to 92 respectively. Thus the region is very narrow. By using Eq. (37) and matching the slope and magnitude of the stopping power at both boundaries we cannot expect the error within the region to differ significantly from that at the boundaries.

This observation is born out in Fig. 9 where we compare our method (range values calculated by Eq. (46)) with the measured values for Cl^{34} ions in Al obtained by Kaplan and Ewart[53] which were discussed in the previous section. The lower limit of this medium-low-specific-energy region for $Z_1 = 17$ (i.e. for Cl ions) is 0.2 MeV/amu. Note that the velocity dependence of the range calculated by our method is approximately correct. Also note that the $\varepsilon^{1/2}$

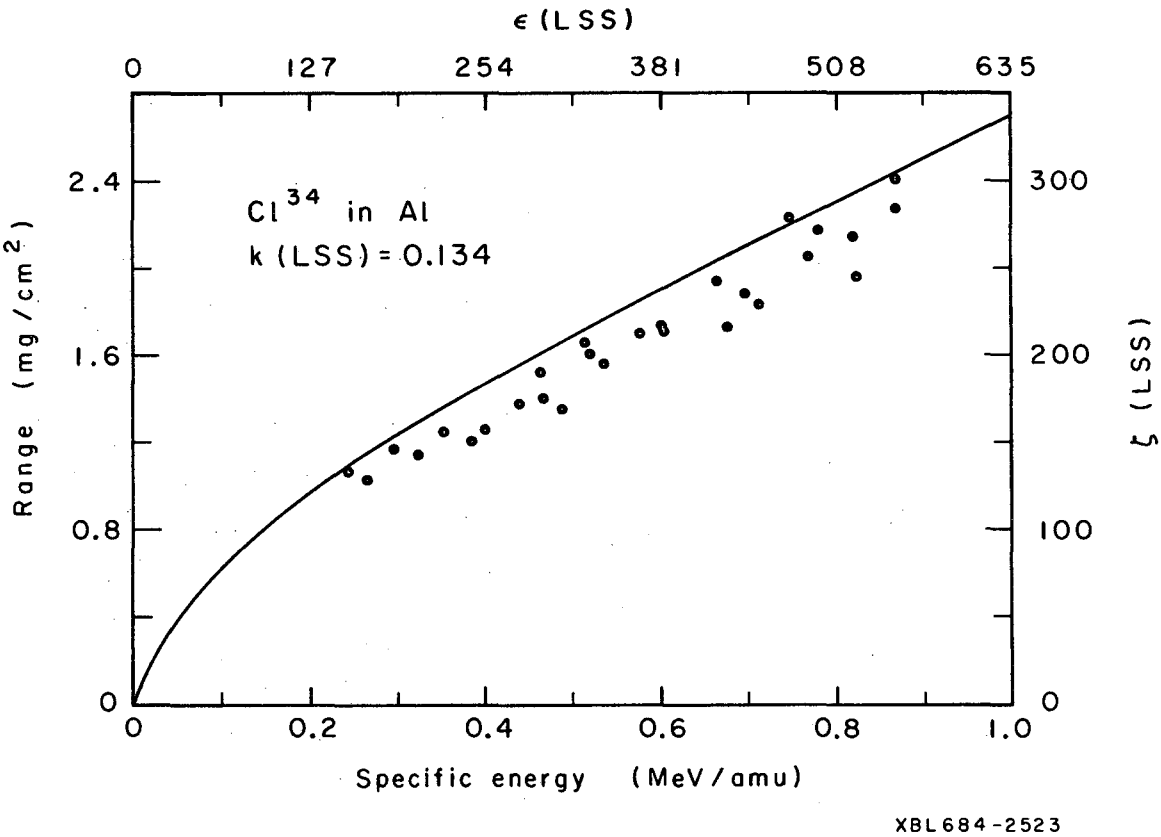

Fig. 9. The theory used in the medium-low-specific-energy (line) is compared with experimental range data (circles) obtained by Kaplan and Ewart[53] for Cl^{34m} ions in Al. The dimensionless range and velocity used by Lindhard, Scharff, and Schiott (designated LSS) are given at the right and upper axes respectively. The value of the constant k (see Eq. (16)) is also given.

dependence which is predicted by Lindhard's theory would not be correct as this would produce a curve which would pass from the point R = 0.97 mg/cm^2 and ε = 0.2 MeV/amu to R = 1.94 and ε = 0.8. We believe that this is evidence for our view that the application of Lindhard's theory here constitutes a misuse of the theory to the extent that it is generally no longer valid at velocities which are this large.

The ranges calculated by our method which are illustrated in Fig. 9 are about 5 to 10% large. Since we calculate the approximately correct velocity dependence, this implies that the magnitude of the stopping powers at the boundaries is of the order of 5 to 10% small. Other than this, it is difficult to say anything about the agreement of our method with this experiment at the upper boundary of this region (ε = 2) since Kaplan and Ewart give no experimental range values above ε = 1.

3. Medium-High-Specific-Energy Region ($9 < 137\beta \leq 3 Z_1$)

There are two major assumptions implicit in Eq. (44) which prevent our generating stopping power with theoretical rigor using this equation. One assumption is that Bethe's theory is valid in this region of (ε, Z_1, Z_2) space. This is not true since neither inequality (5) nor (6), one of which is required for use of the Born approximation, is always fulfilled. We will discuss this in more detail later in this section.

The second assumtion is that r, which is a function of $X = 137\beta/Z_1^g$ and which satisfies the five criteria of section II B 3, can successfully give the charge state of all ions in all stopping media throughout this region of (ε, Z_1, Z_2) space. We conclude from the work of Knipp and Teller[40] that the Thomas-Fermi model of the atom is compatible with this assumption for g = 2/3 if v_e/V_i is a constant. As in section II B 3, v_e/V_i is the ratio of the velocity of an electron in the ion's electron cloud to the velocity of the ion at which this

electron's capture and loss cross sections are equal. Brunnings, Knipp, and Teller[61] investigated this ratio. Using the Thomas-Fermi model they empirically found this ratio under two extreme assumptions. First, it is the energetically least tightly bound electron on the ion whose capture and loss cross sections are equal when the ion velocity is V_i. Second, it is the outermost electron on the ion whose capture and loss cross sections are equal when the ion velocity is V_i. Under the first assumption, the empirically indicated values of v_e/V_i are:

Z_1	v_e/V_i
10	1.2
55	1.8

Using the second assumption:

Z_1	v_e/V_i
6	0.6
10	0.45
37	0.37
55	0.35

These results show that the ratio of v_e/V_i is probably not constant. However, since the two extreme assumptions of Brunnings, Knipp, and Teller indicate opposite behaviors of this ratio with respect to Z_1, the assumption that v_e/V_i is constant may be as appropriate as any other.

We now look into the high-velocity end of this region of (ε, Z_1, Z_2) space where the Thomas-Fermi model is not valid since the electron cloud of the ion becomes depleted. For high velocities we apply a correction to the Thomas-Fermi model by allowing g to approach 1.0 at $137\beta = 2 Z_1$ (see Eq. (40)). Even if this correction does not describe the true deviation from reality of this statistical model, the error introduced into the stopping power, through

Eq. (44), is small because r approaches 1.0. Thus we conclude that we have corrected for some of the error introduced by using the Thomas-Fermi model near the high-velocity boundary of this region, but, since r is nearly 1.0 here, the stopping power is not very sensitive to the model used anyway.

In our development of the charge state of the ion, r(X), we have ignored any dependence upon the stopping medium. The charge exchange process between the ion and the medium is to some extent a function of the electron capture and loss properties of the medium. Also, the electron density of the medium may slightly affect the charge of the ion by the same mechanism discussed in section III A 1 where the ionic charge in gases was compared with that in condensed media. We here assume that the dependence of r upon Z_2 in negligible compared with its dependence upon ε and Z_1.

As mentioned above, the first major assumption implicit in Eq. (44) is that Bethe's theory is valid in the medium-high-specific-energy region. For the validity of the Born approximation, and thus also for the validity of Bethe's theory, either one or both of inequalities (5) and (6) must be fulfilled. For convenience to the reader we repeat these inequalities here:

$$r Z_1 \ll 137\beta, \text{ and} \qquad (5)$$

$$r Z_1 \ll Z_2. \qquad (6)$$

Inequality (5) is nowhere well satisfied since the high-velocity boundary of this region is $3 Z_1 = 137\beta$. Therefore we cannot be certain that Bethe's theory will generate correct stopping power unless inequality (6) is satisfied, that is to say unless the nuclei of the stopping medium are heavier than the ion. It is clear then that we cannot use Bethe's theory here with certainty whenever the stopping material is water, tissue, or any hydrocarbon.

Because these are very important stopping materials and

because inequality (7) for Bloch's theory is less restrictive than inequality (5) for Bethe's, we have investigated the use of Bloch's theory in that part of the medium-high-specific-energy region for which inequalities (5) or (6) are not satisfied. (The mechanics of the use of Bloch's theory, Eqs. (8) and (11) are discussed in Appendix C.) We found two functions for r(X), of the form indicated in Eq. (41), for use with Bloch's theory. Both of these functions satisfied all five criteria of section II B 3, where Bloch's theory was now used in criteria 3, 4, and 5. For each value of X, these functions differed from one another by less than the uncertainty of the magnitude of either one for that value of X. Our aim was to calculate the stopping powers of a variety of light stopping materials for a variety of ions using Bloch's theory with first one of these functions and then with the other. The difference in these two stopping powers would give an estimate of the minimum uncertainty of the method overall. If this difference was comparable to or greater than the difference between the stopping power calculated using Bloch's theory and that using Bethe's theory through Eq. (44), then we would conclude that the advantage of Bloch's theory over Bethe's was dwarfed by the uncertainty in the function r(X).

We found generally good agreement between Eq. (44) and our use of Bloch's theory for several ions in water and Al. Rarely did the two methods differ by more than 5%. When the disagreement was greatest, Bloch's theory, using r(X), calculated stopping powers 6 to 8% less than that calculated using Eq. (44). However, using Bloch's theory with the alternative function r(X) mentioned above, we calculated in these cases stopping powers which were only 1 to 3% less than that calculated by Eq. (44). In these cases of greatest disagreement, inequality (7) was satisfied; so Bloch's theory was valid.

We conclude that Eq. (44), using Bethe's theory with the r(X) function which was derived especially for use with Bethe's theory, gives stopping-power values which are within the accuracy of the

function r(X) throughout any part of this medium-high-specific-energy region in which Bloch's theory is valid.

To compare the method used in this velocity region with experimental data, we plot in Fig. 10 some range data points for Ar ions in Al obtained by Sikkeland[43] with the range calculated by Eq. (46). Note that this is primarily a measure of the success with which we executed criterion five of section II B 3. It is not a measure of the correctness of our method of extrapolating charge-state data, nor is it a measure of the correctness of the use of Bethe's theory where the Born approximation is not rigorously valid. For experimental data which would satisfactorily test this, we must await the completion of the Omnitron. The greatest deviation of the data points from our theory is about 5% and it occurs at the lower velocities.

4. High-Specific-Energy Region ($137\beta > 3 Z_1$)

For ions in this region, the stopping power is given in Eq. (45). The Barkas and Berger polynomial, Eq. (23), which is based upon Bethe's theory, is used to calculate the proton stopping power $(dE/dR)_p$. Bethe's theory should be perfectly valid in this velocity region since inequality (5) is satisfied and the shell corrections used by Barkas and Berger remove the necessity for inequality (1) being satisfied. The only feature of Eq. (45) left to be discussed is the accuracy of the polynomial fit to Bethe's theory, and this discussion is given in section III A 2.

5. Ion Mean Range for $Z_1 > 10$

The range is given by Eq. (46). The integrals are solved numerically by Simpson's rule. The number of intervals into which the domain of integration is divided is doubled for each successive trial, and the convergence criterion is set such that the value of the integral is given by the second of two consecutive trials that differ by less than 0.05%. Thus the range calculation is consistent with the stopping-power calculation discussed above. The accuracy of the

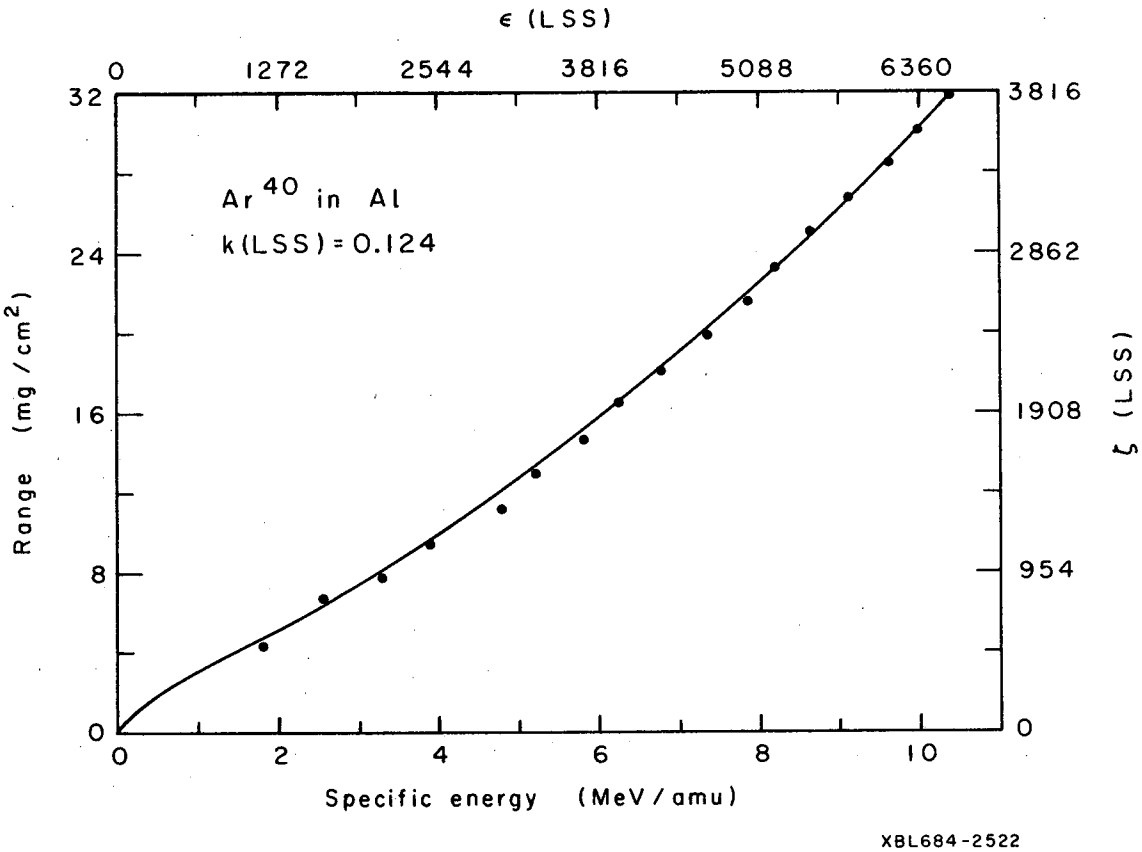

Fig. 10. The theory used in the medium-high-specific-energy region (line) is compared with experimental range data (circles) obtained by Sikkeland[43] for Ar^{40} ions in Al. The dimensionless range and velocity used by Lindhard, Scharff, and Schiott (designated LSS) are given at the right and upper axes respectively. The value of the constant k (see Eq. 16)) is also given.

range calculation is essentially the same as that of the stopping-power calculation.

The range calculated by Eq. (46) is the mean total pathlength that the ion travels. The range which is often measured experimentally is the mean distance the ion travels in the initial direction of flight. These two ranges differ because of multiple scattering of the ion in the stopping material. For specific energies above a few MeV/amu, this projected range is usually less than 1% shorter than the pathlength range. As one would expect, the percentage difference increases with decreasing ε, increases with decreasing Z_1, and increases with increasing Z_2. The ranges for various fission products in Al and U are tabulated in Tables VII and VIII. A method of estimating the projected range at low velocity is given by Lindhard et al.[18] A computer program which calculates the projected range is described in Appendix B. The method for calculating the projected range of high-velocity ions is given by Rossi[62] and by Litton.[2, 3]

IV. RESULTS

The computer program described in Appendix A has generated a sampling of ranges and stopping powers to be displayed in this section. The ions chosen are hydrogen, helium-4, carbon-12, neon-20, argon-40, krypton-84, xenon-131, and radon-222. Data are presented for each of these ions incident upon water, aluminum, copper, silver, lead, and uranium.

In Figs. 11 through 16, stopping power is plotted as a function of specific energy. One of the conspicious features of these curves is the difference in behavior in the low-specific-energy region between the ions for $Z_1 > 10$ and $Z_1 \leq 10$. This reflects the fact that a completely different method is used to calculate the stopping power in these two cases. For $Z_1 > 10$, Eq. (36) is used. The increasing contributions of the nuclear coulomb stopping-power term as Z_1 increases and ε decreases causes the slope of the curves to decrease under these conditions. According to Lindhard et al.[18], the assumption that the nuclear and electronic stopping powers are separable may lead to a systematic overestimation of the stopping power in this low-specific-energy region. The smoothed experimental stopping power which we try to duplicate with our method for $Z_1 \leq 10$ does not usually show a decreasing slope for decreasing velocity because the scatter of the experimental points is usually too great to permit the resolution of such fine detail. Thus the decreasing slope for decreasing velocity may be overestimated for Ar ions and underestimated for Ne ions, leading to a discontinuity in the systematic change of behavior across the $Z_1 = 10$ boundary.

It may be useful to examine this discontinuity in more detail in order to obtain a measure of the accuracy of our method for $Z_1 \sim 10$. In Fig. 17 the lower pair of curves are plots of the stopping power of Ne ions in Al by both methods. The agreement between

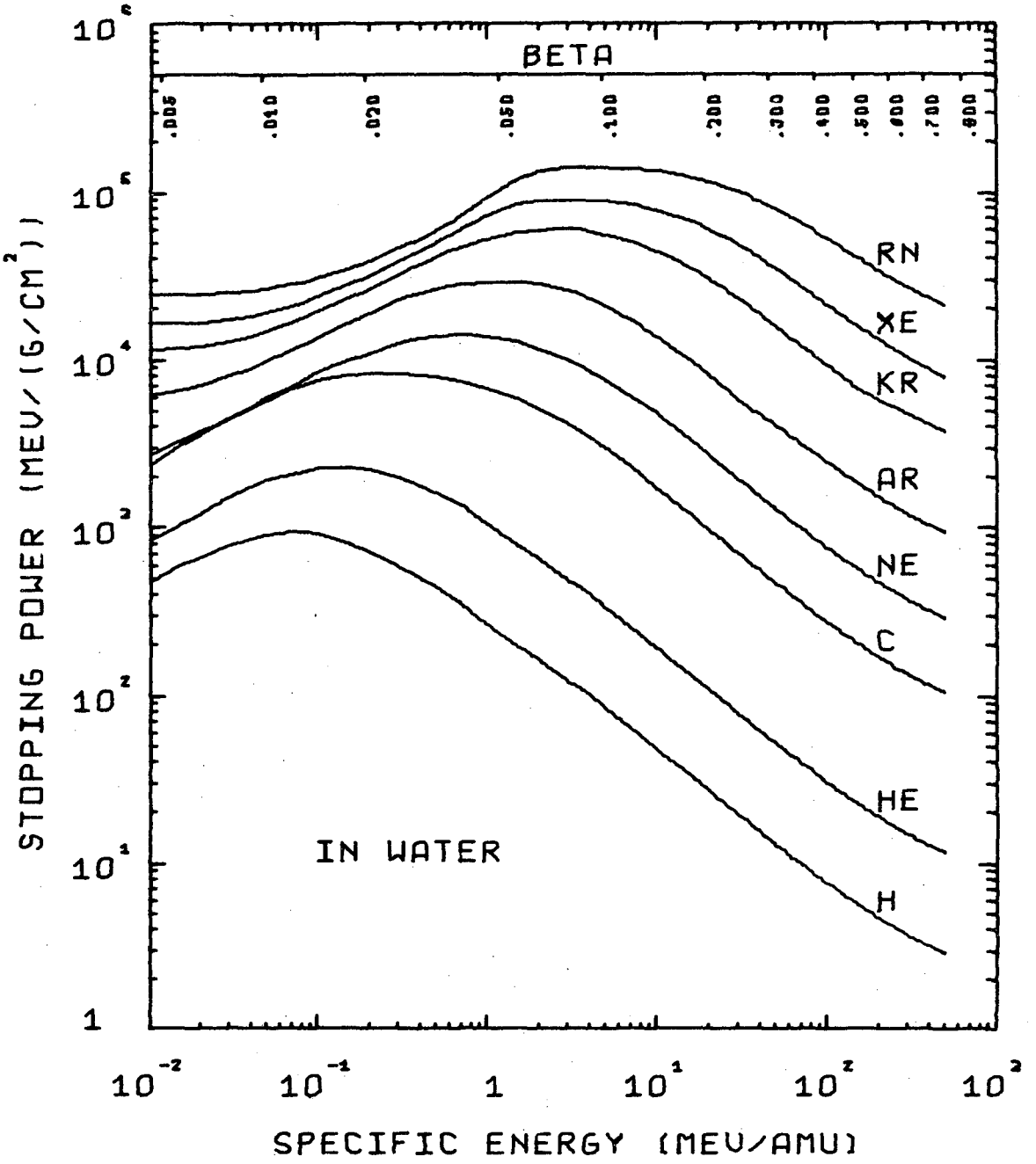

XBL 685-840

Fig. 11. Stopping-power curves as a function of specific energy for various ions in water as calculated by the computer program. At the top of the figure, values of $\beta = V/c$ are displayed. The Ne and C curves touch at about 0.04 MeV/amu due to an inaccuracy in the program which is apparent from Table VIC and D. Our method overestimates the experimental stopping power for carbon ions in hydrogen at 0.04 MeV/amu by 14% and underestimates it for Ne ions by 6%.

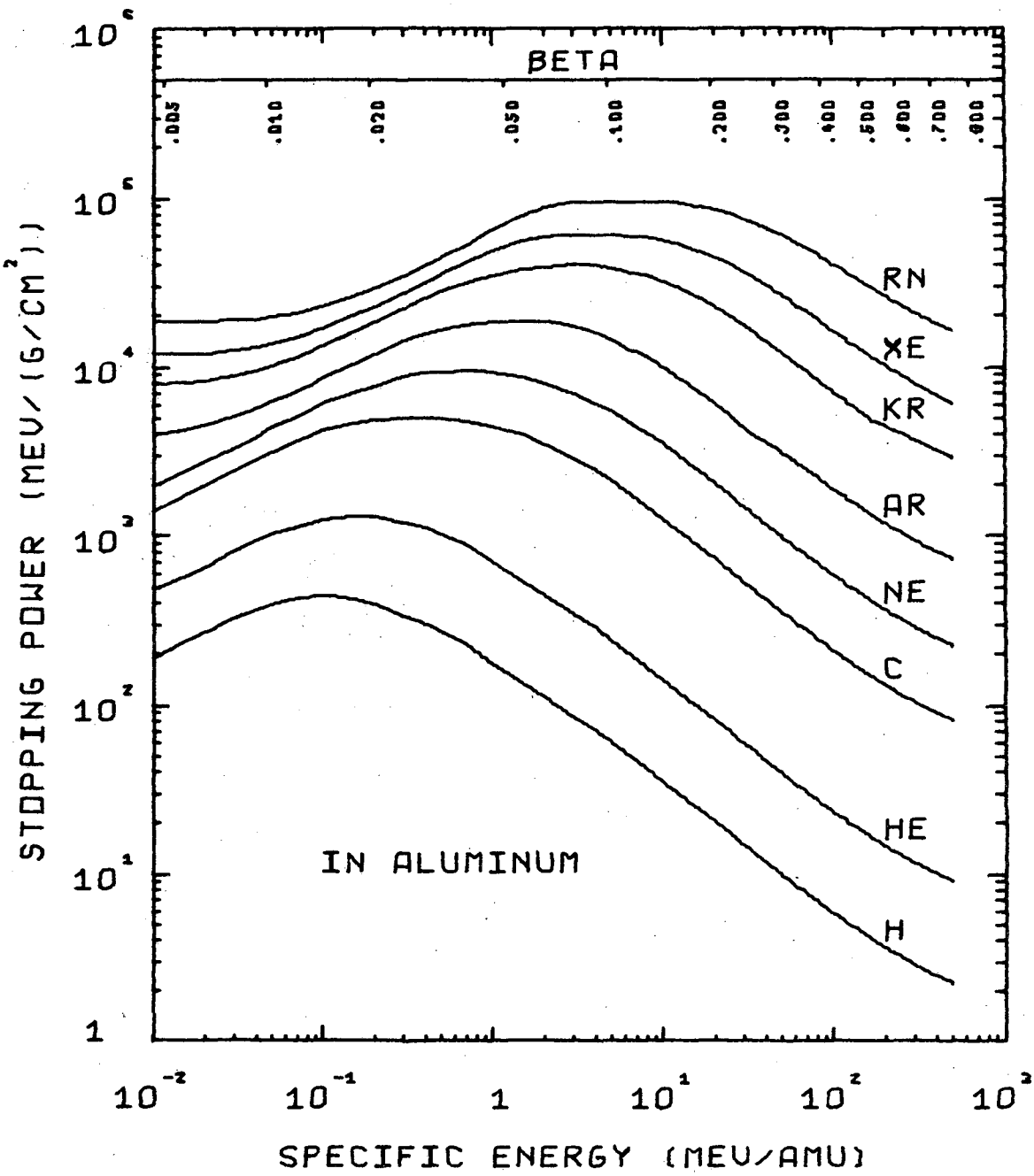

XBL 685-841

Fig. 12. Stopping-power curves as a function of specific energy for various ions in aluminum as calculated by the computer program. At the top of the figure, values of $\beta = V/c$ are displayed.

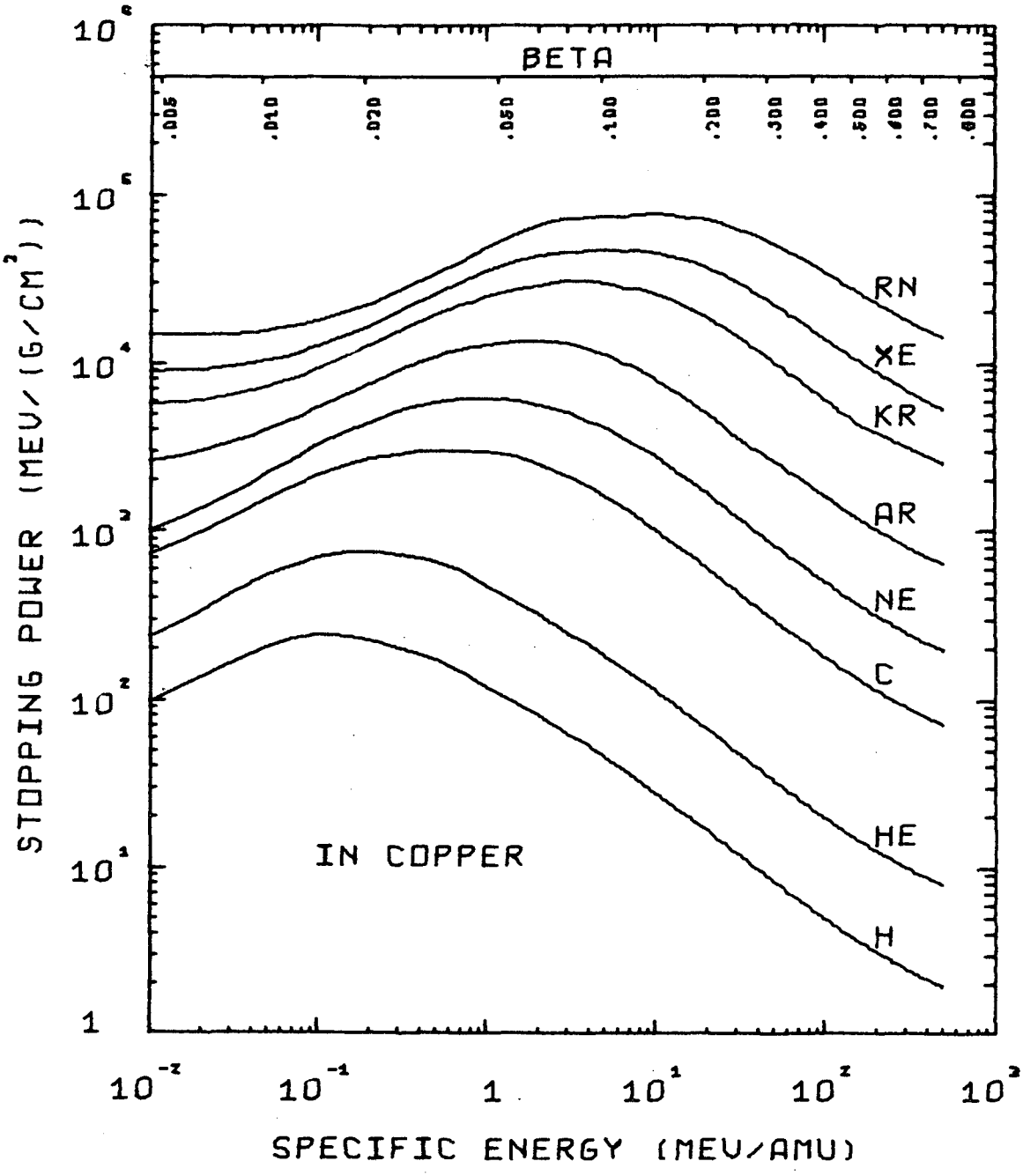

XBL 685-842

Fig. 13. Stopping-power curves as a function of specific energy for various ions in copper as calculated by the computer program. At the top of the figure, values of $\beta = V/c$ are displayed.

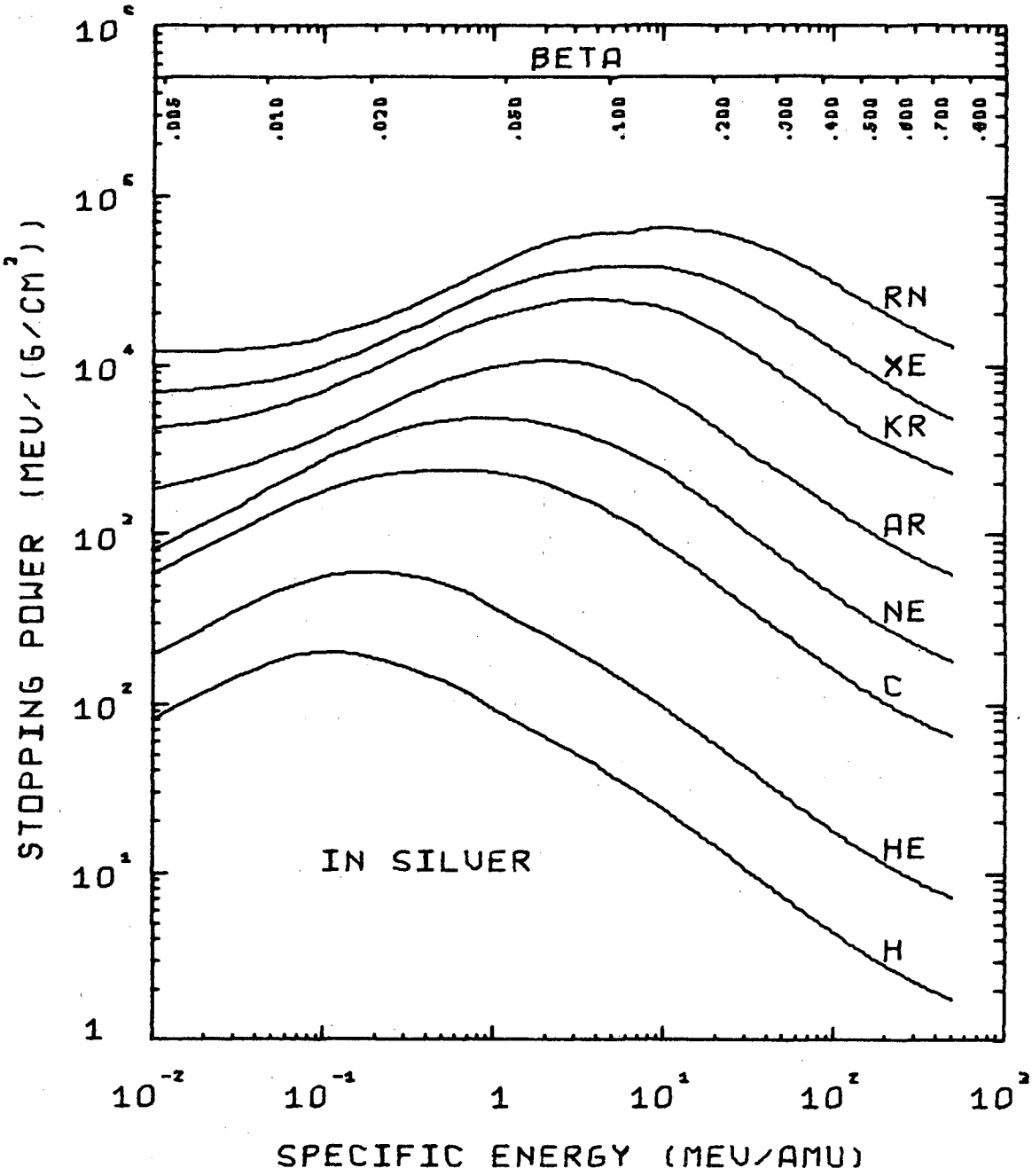

XBL 685-843

Fig. 14. Stopping-power curves as a function of specific energy for various ions in silver as calculated by the computer program. At the top of the figure, values of $\beta = V/c$ are displayed.

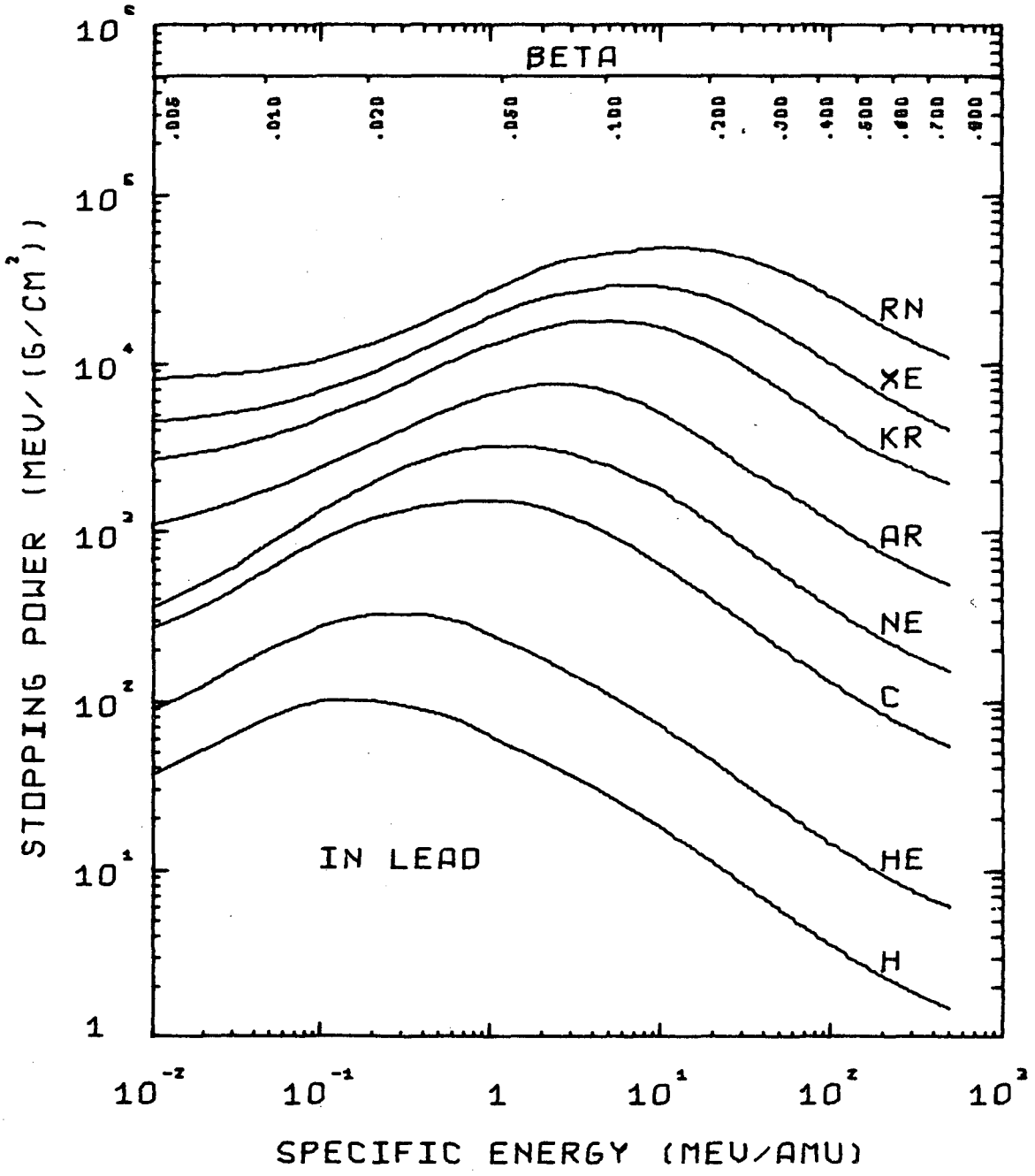

XBL 685-844

Fig. 15. Stopping-power curves as a function of specific energy for various ions in lead as calculated by the computer program. At the top of the figure, values of $\beta = V/c$ are displayed.

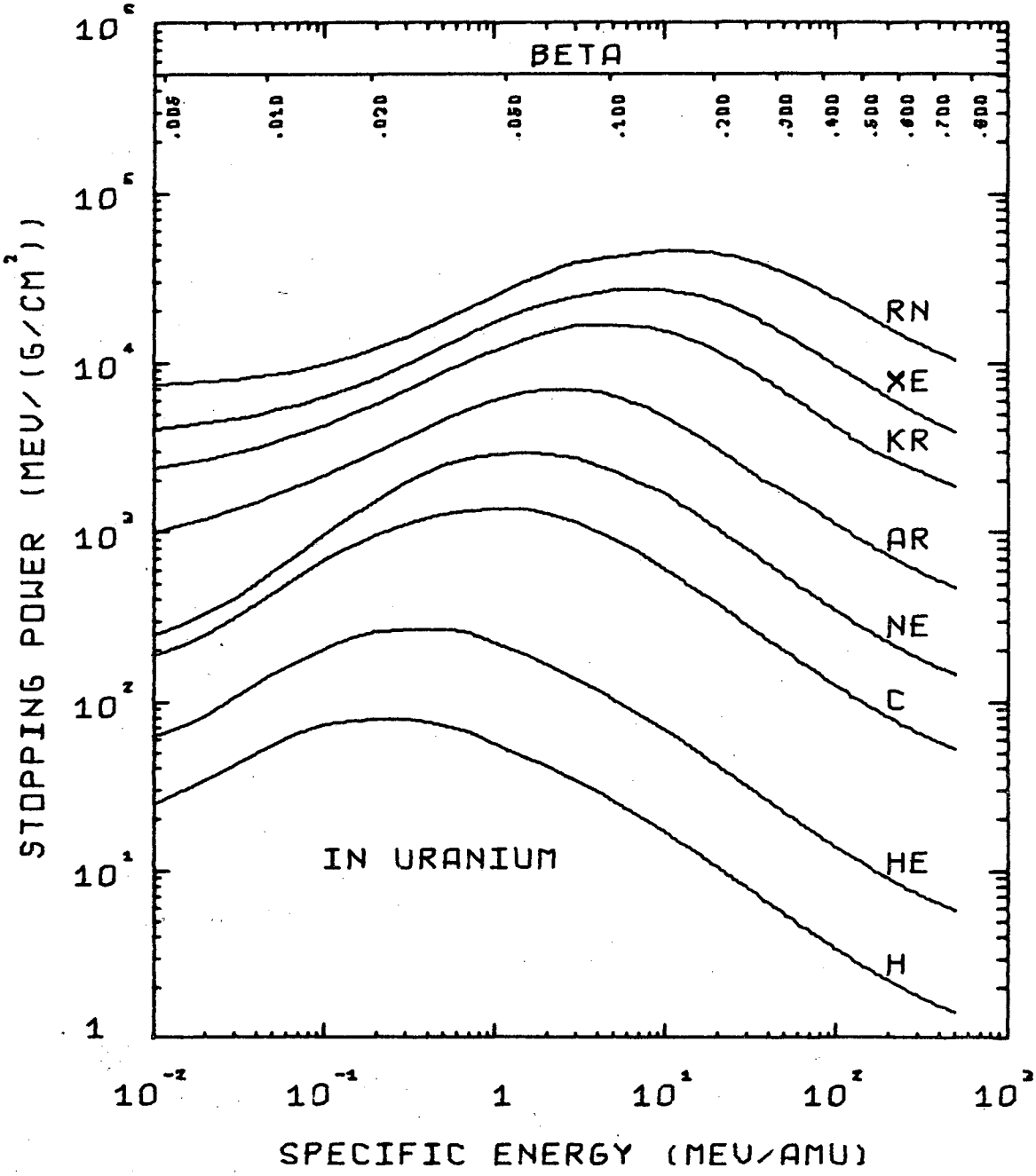

XBL 685-845

Fig. 16. Stopping-power curves as a function of specific energy for various ions in uranium as calculated by the computer program. At the top of the figure, values of $\beta = V/c$ are displayed.

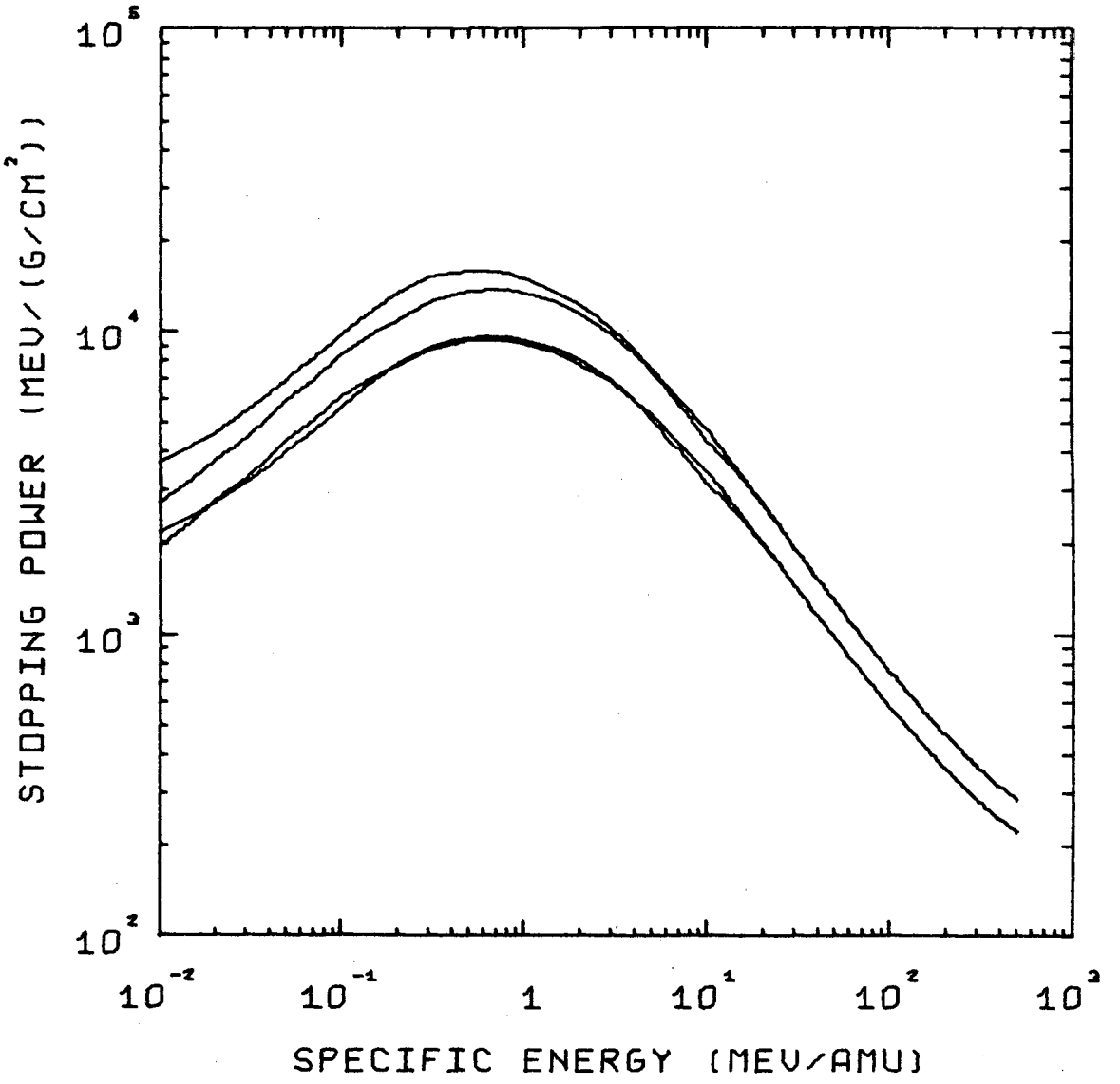

XBL 685-846

Fig. 17. Stopping-power curves as a function of specific energy for a Ne ion in aluminum (lower pair) and in water (upper pair). The member of each pair of curves which shows a decreasing slope for decreasing velocity at very low velocity is calculated by the method normally used only for ions with $Z_1 > 10$. The other member of each pair of curves is calculated by the method used for $Z_1 \leq 10$.

this pair of curves is very good. The percentage difference in magnitude between these two curves is shown by the lower curve in Fig. 18. A negative percentage difference implies that the method for $Z_1 > 10$ gives a stopping power which is less than that for $Z_1 \leq 10$. For specific energies greater than 10 MeV/amu, Fig. 18 gives a magnified view of r^2 of Eq. (43). For Ne ions at 10 MeV/amu r = 0.952 implying that the ion carries an electron nearly half the time. This may be an underestimate of r in this case. The upper pair of curves in Fig. 17 compares the two methods for Ne ions in water. The agreement, which is again displayed in detail in Fig. 18, is not so good in water. There are two main reasons for this, and both have to do with the difficulty of treating hydrogenous stopping media. First and probably most important, the experimental stopping power of hydrogen which is used by the method for $Z_1 \leq 10$ is the stopping power of gaseous hydrogen. The ions at low velocities therefore have a lower charge than they would in condensed hydrogen as discussed in section III A 1. Second, the Thomas-Fermi atomic model, which is used in the low-specific-energy region for $Z_1 > 10$, cannot be applied with rigor to hydrogenous stopping media since the statistical model cannot properly be applied to hydrogen. The method for $Z_1 > 10$ is more properly applied to stopping media heavier than hydrogen.

In Figs. 19 through 24 the stopping power is plotted as a function of ion residual pathlength range. Points of constant specific energy are indicated by symbols at 0.01, 0.1, and 1.0 MeV/amu and by curves at 5, 10, 50, 100, 200, 300, and 500 MeV/amu. From Fig. 19, for instance, we see that a 5 MeV/amu ^{20}Ne in water has a LET of 7500 MeV/(g/cm^2) and a range of 100 microns. The discontinuity in behavior across the $Z_1 = 10$ boundary discussed above is apparent here also.

The H-He, C-Ne, and Xe-Rn crossovers of Fig. 19 are not

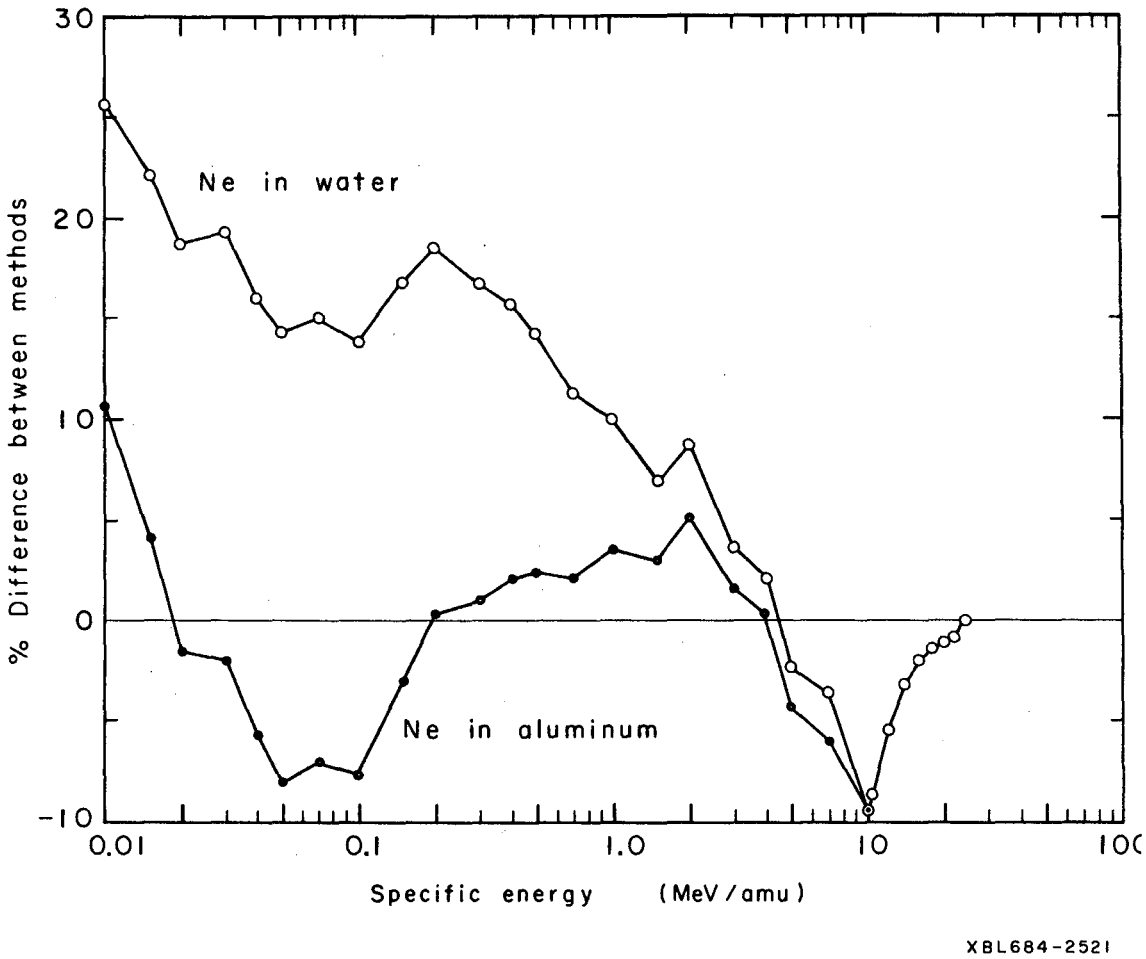

Fig. 18. The percentage difference between the members of each pair of curves in Fig. 17 is plotted as a function of ion specific energy.

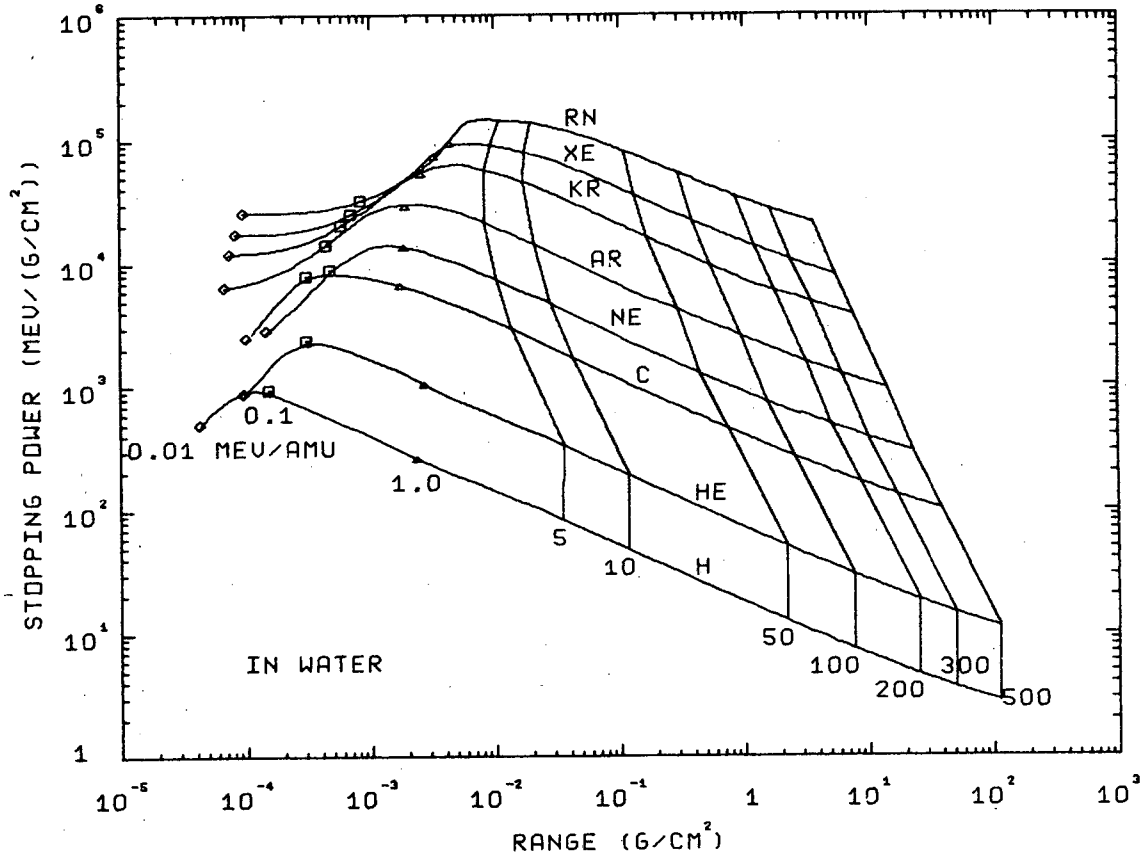

Fig. 19. Stopping-power curves as a function of residual range for various ions in water as calculated by the computer program. Various ion specific energies in units of MeV/amu are designated on each curve by symbols for $\varepsilon \leq 1.0$ and by curves of constant velocity for $\varepsilon \geq 5$. The H-He, C-Ne, and Xe-Rn crossovers are discussed in the text.

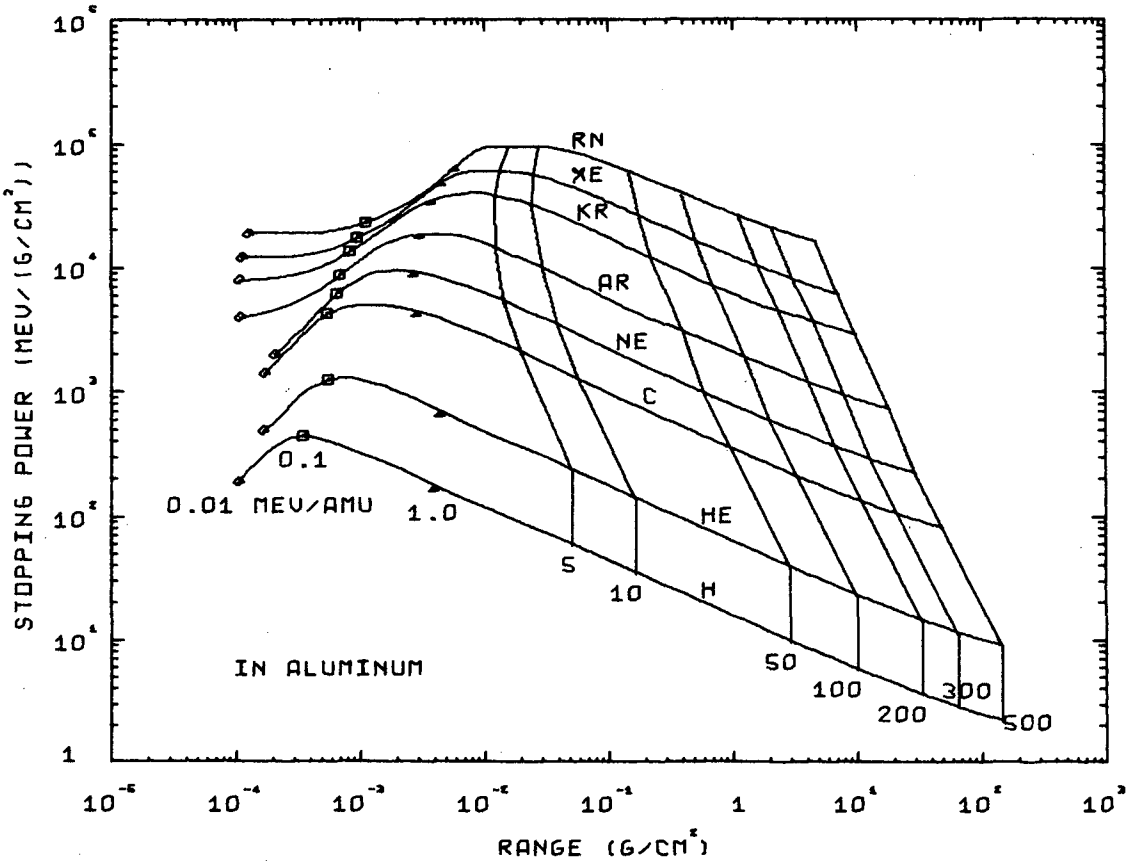

XBL 685-828

Fig. 20. Stopping-power curves as a function of residual range for various ions in aluminum as calculated by the computer program. Various ion specific energies in units of MeV/amu are designated on each curve by symbols for $\varepsilon \leq 1.0$ and by curves of constant velocity for $\varepsilon \geq 5$.

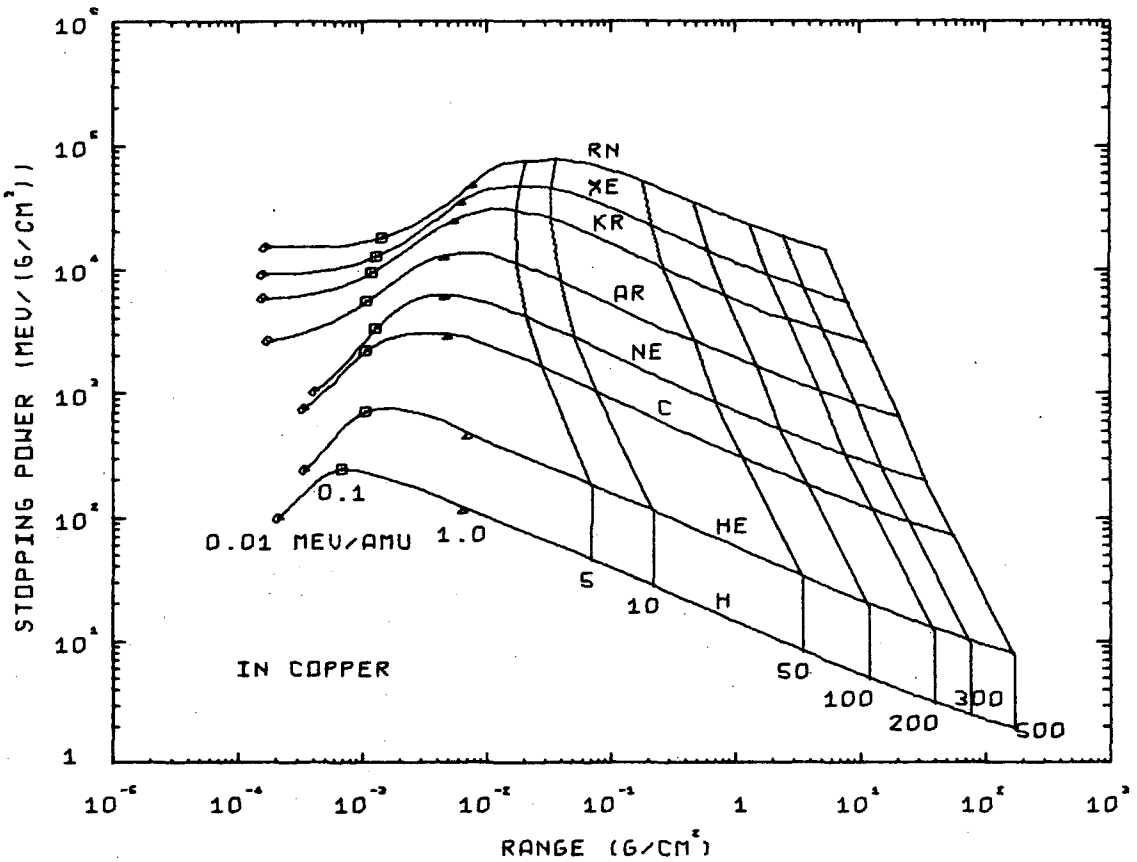

XBL 685-829

Fig. 21. Stopping-power curves as a function of residual range for various ions in copper as calculated by the computer program. Various ion specific energies in units of MeV/amu are designated on each curve by symbols for $\varepsilon \leq 1.0$ and by curves of constant velocity for $\varepsilon \geq 5$.

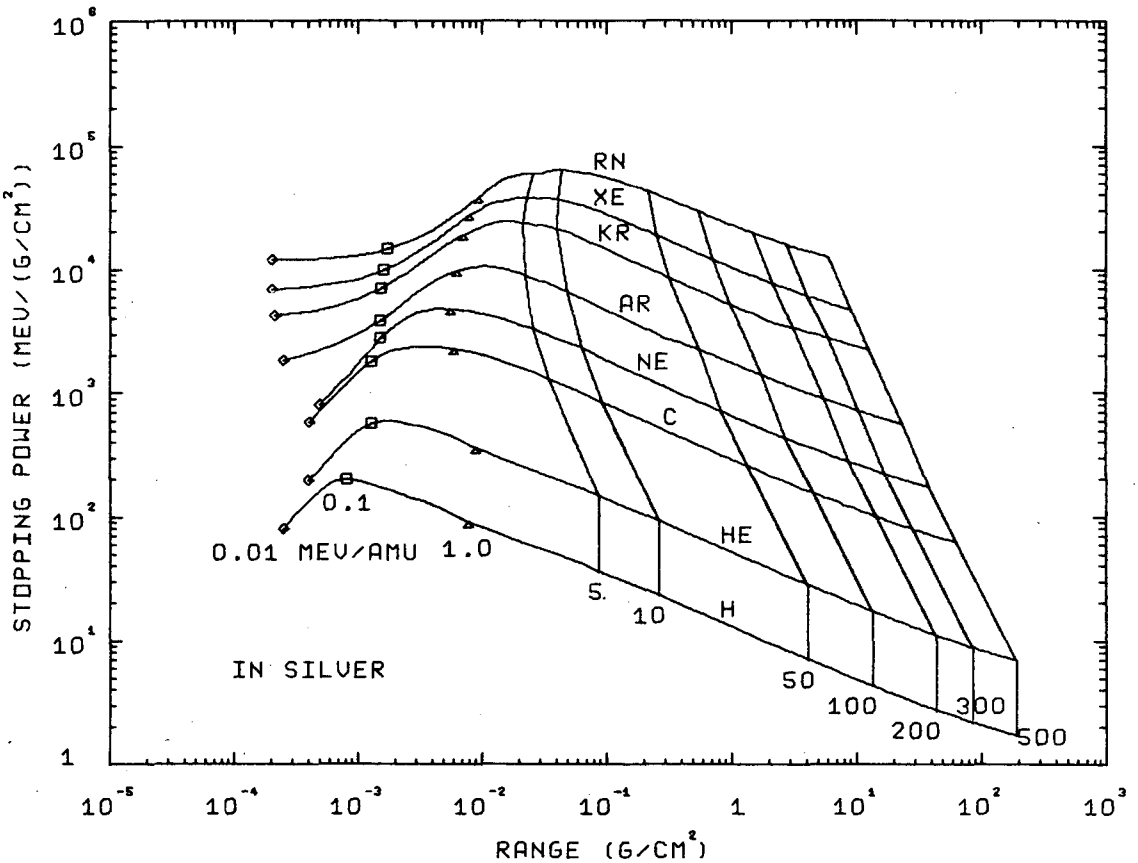

Fig. 22. Stopping-power curves as a function of residual range for various ions in sliver as calculated by the computer program. Various ion specific energies in units of MeV/amu are designated on each curve by symbols for $\varepsilon \leq 1.0$ and by curves of constant velocity for $\varepsilon \geq 5$.

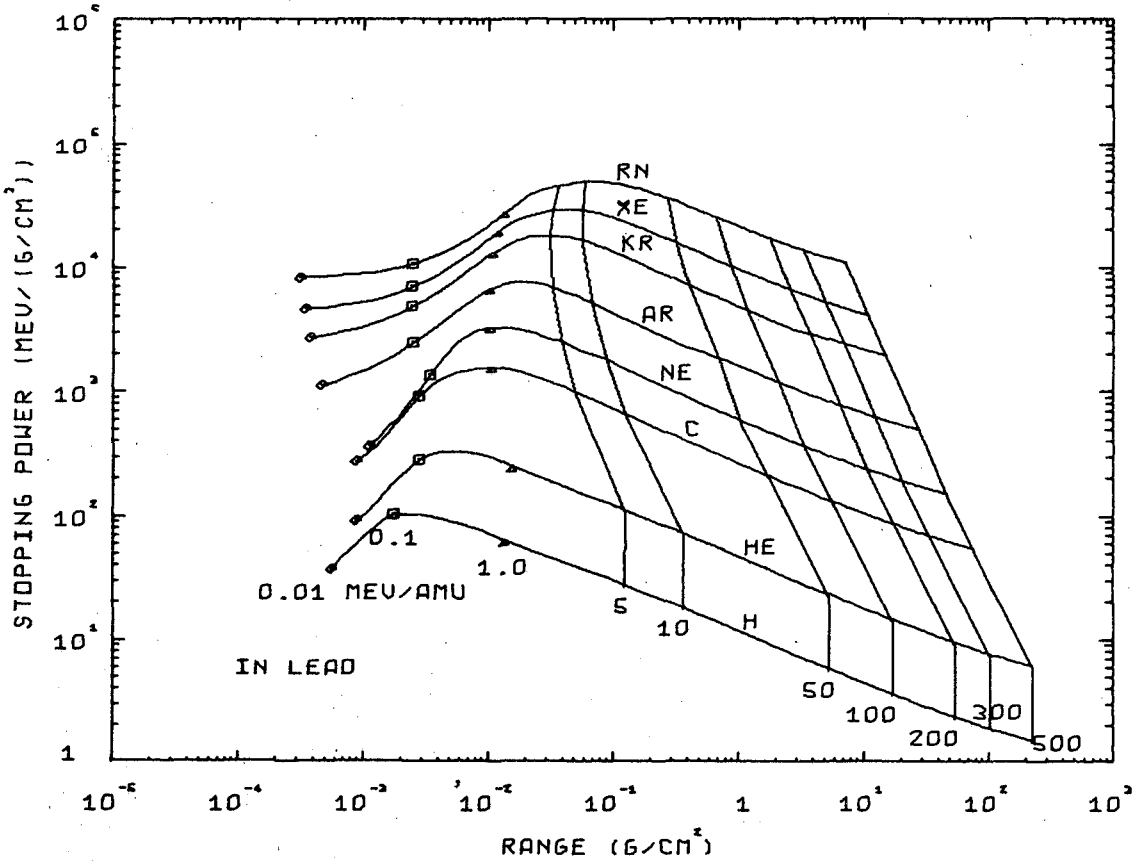

XBL 685-831

Fig. 23. Stopping-power curves as a function of residual range for various ions in lead as calculated by the computer program. Various ion specific energies in units of MeV/amu are designated on each curve by symbols for $\varepsilon \leq 1.0$ and by curves of constant velocity for $\varepsilon \geq 5$.

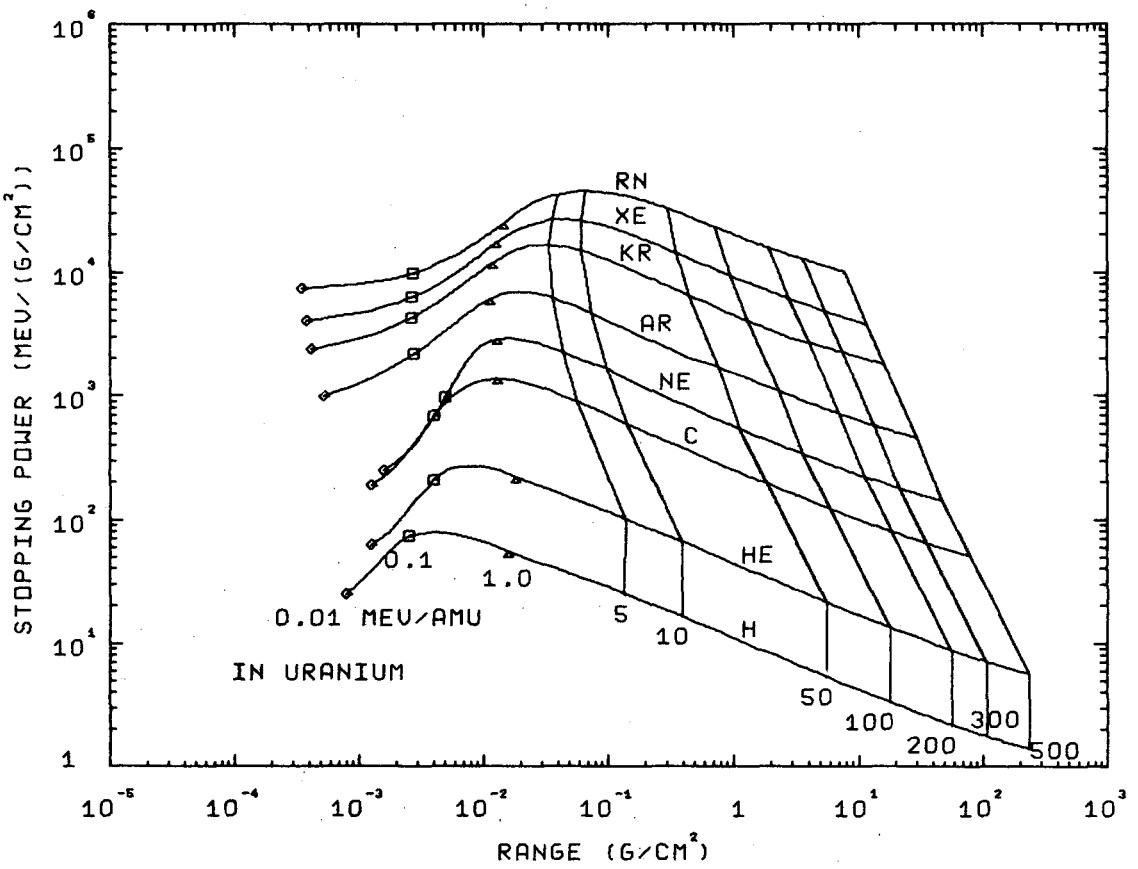

Fig. 24. Stopping-power curves as a function of residual range for various ions in uranium as calculated by the computer program. Various ion specific energies in units of MeV/amu are designated on each curve by symbols for $\varepsilon \leq 1.0$ and by curves of constant velocity for $\varepsilon \geq 5$.

as bizarre as they probably appear, because velocity and not residual range is the natural variable of stopping power. Let us discuss these crossovers one at a time. Since He has 4 times the mass but only twice the charge of H, the two ions have the same range for constant velocity when $r = 1$ because range is proportional to $A_1/(r\ Z_1)^2$. This makes it easier for the He and H curves to cross-over at some low velocity where $r \sim 1$ for H ions but $r < 1$ for He ions.

The error we introduced into Fig. 19 at low velocity for $Z_1 \leq 10$ by using the experimental stopping power in gaseous hydrogen instead of condensed hydrogen has the effect of introducing a value of r which is too small. Since stopping power is proportional to $(r\ Z_1)^2$, the error has the effect of moving a curve plotted on the coordinates of Fig. 19 down and to the right of where it should be. Neon ions would be affected by this error at higher velocities than carbon ions, so the magnitude of the C-Ne crossover may be accentuated by this error.

All three of these crossovers occur in regions where we have relatively low confidence in our method. Thus they may not exist in reality and may be an artifact of the method. This is certainly the case for the Xe-Rn crossovers of Fig. 19. These two curves cross over only slightly in the medium-low-specific-energy region. It is this region that we extend the stopping power from the boundaries into the region by means of a cubic polynomial determined by the slope and magnitude of the stopping power at the boundaries. In Fig. 19, where two curves approach one another near this medium-low-specific energy region, the curvature provided by the cubic can easily be sufficiently erroneous to allow crossovers such as this Xe-Rn crossover.

In Figs. 25 through 30 the velocity is plotted as a function of residual range. The discontinuity in the systematic change of behavior across the $Z_1 = 10$ boundary, as discussed above, is apparent in these curves below 0.1 MeV/amu.

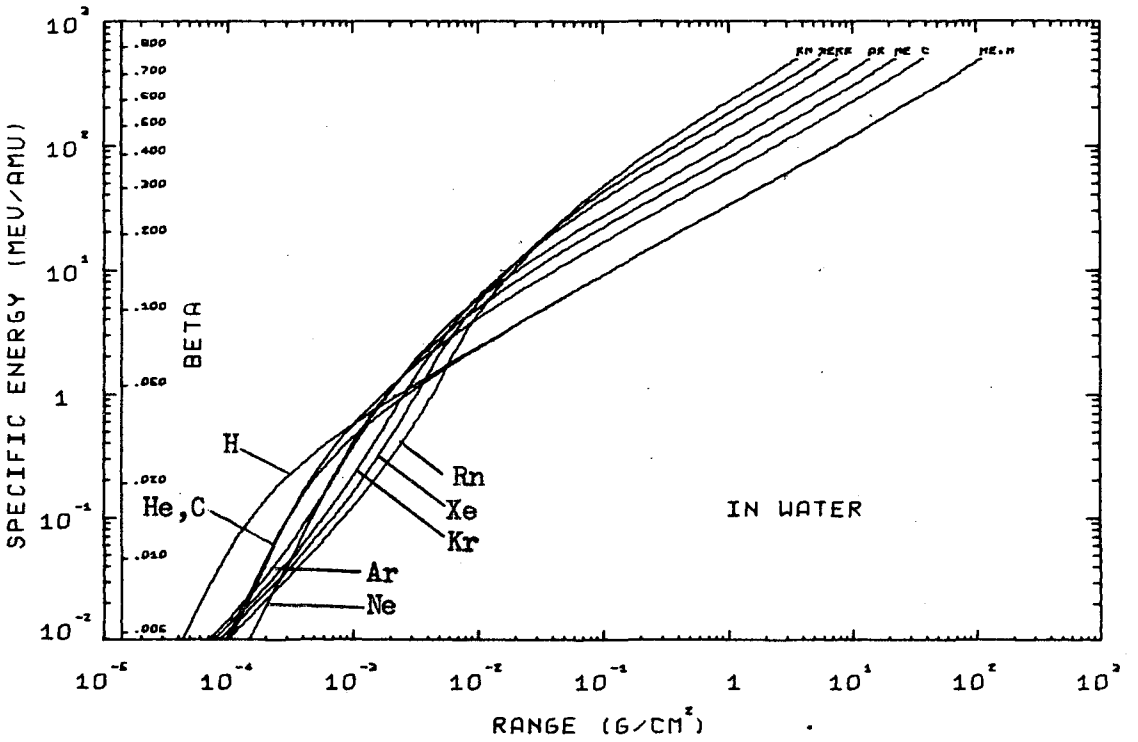

Fig. 25. Energy-range curves for various ions in water as calculated by the computer program. For any specific energy on the ordinate, the residual pathlength range is read from the abscissa. At the left of the figure, values of $\beta = V/c$ are displayed.

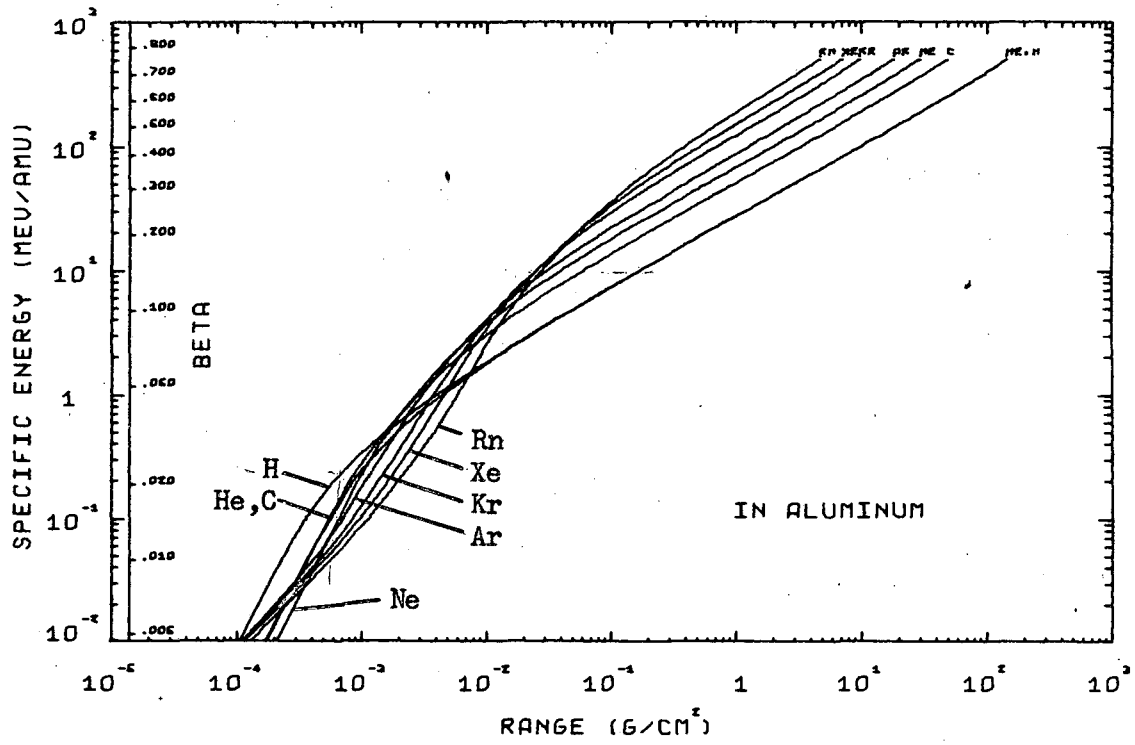

XBL 685-834

Fig. 26. Energy-range curves for various ions in aluminum as calculated by the computer program. For any specific energy on the ordinate, the residual pathlength range is read from the abscissa. At the left of the figure, values of $\beta = V/c$ are displayed.

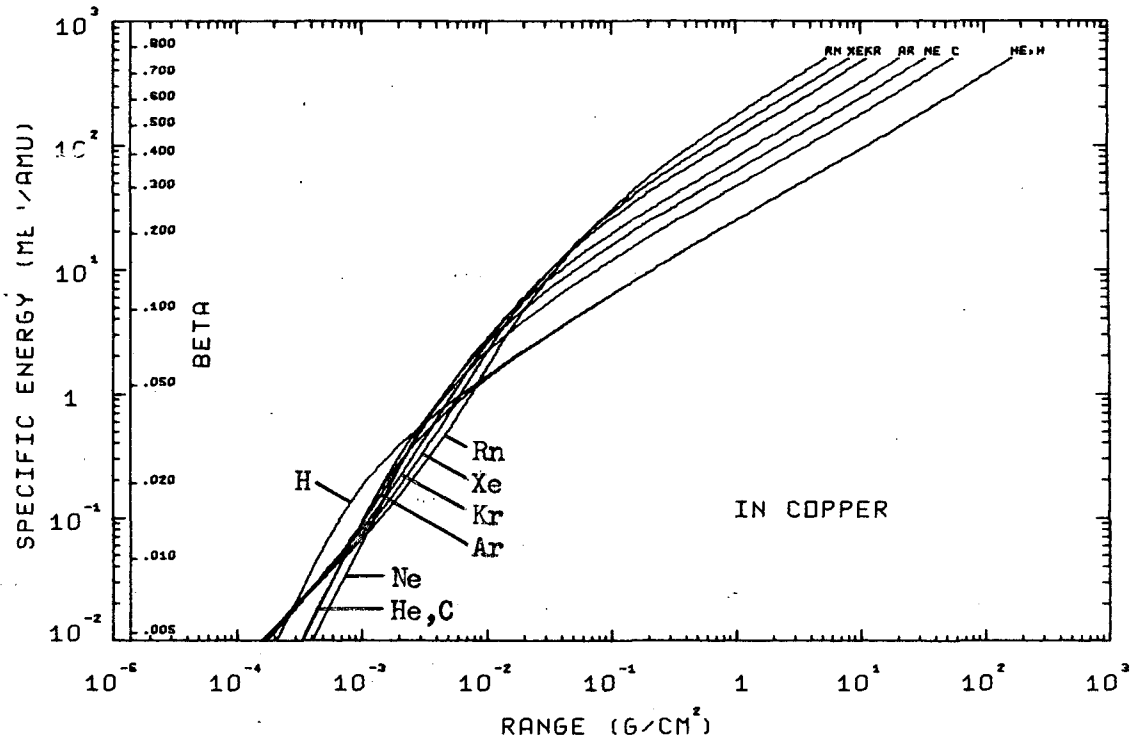

XBL 685-835

Fig. 27. Energy-range curves for various ions in copper as calculated by the computer program. For any specific energy on the ordinate, the residual pathlength range is read from the abscissa. At the left of the figure, values of $\beta = V/c$ are displayed.

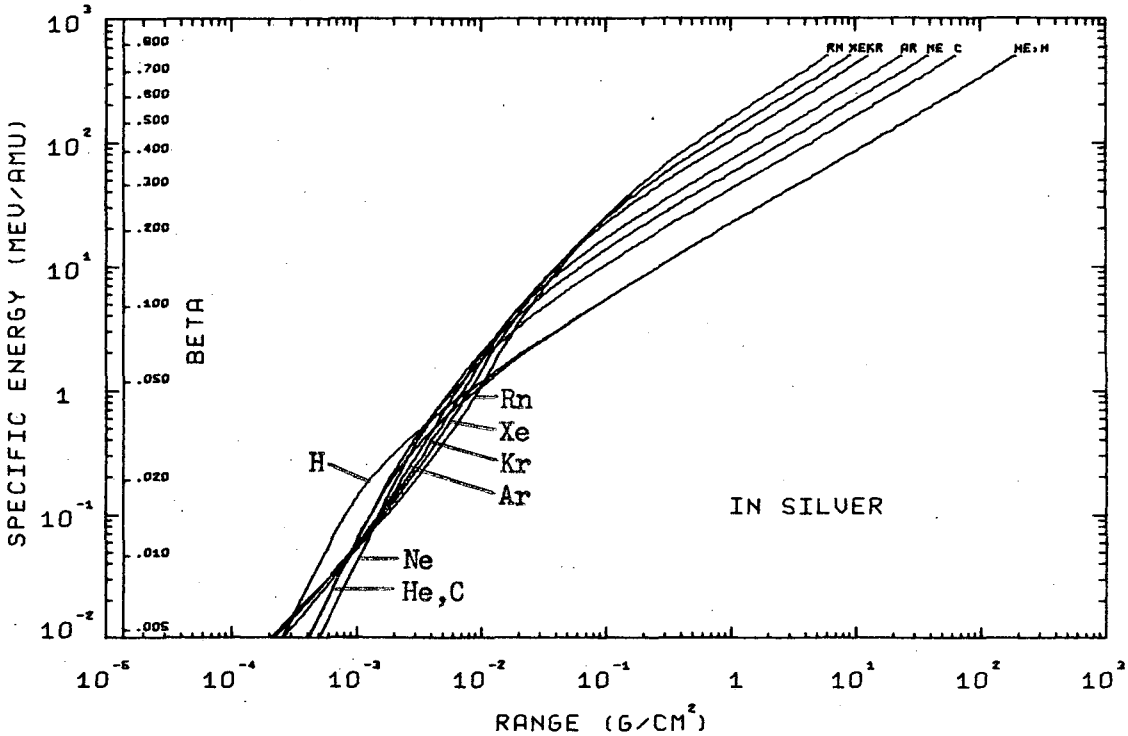

XBL 685-836

Fig. 28. Energy-range curves for various ions in silver as calculated by the computer program. For any specific energy on the ordinate, the residual pathlength range is read from the abscissa. At the left of the figure, values of $\beta = V/c$ are displayed.

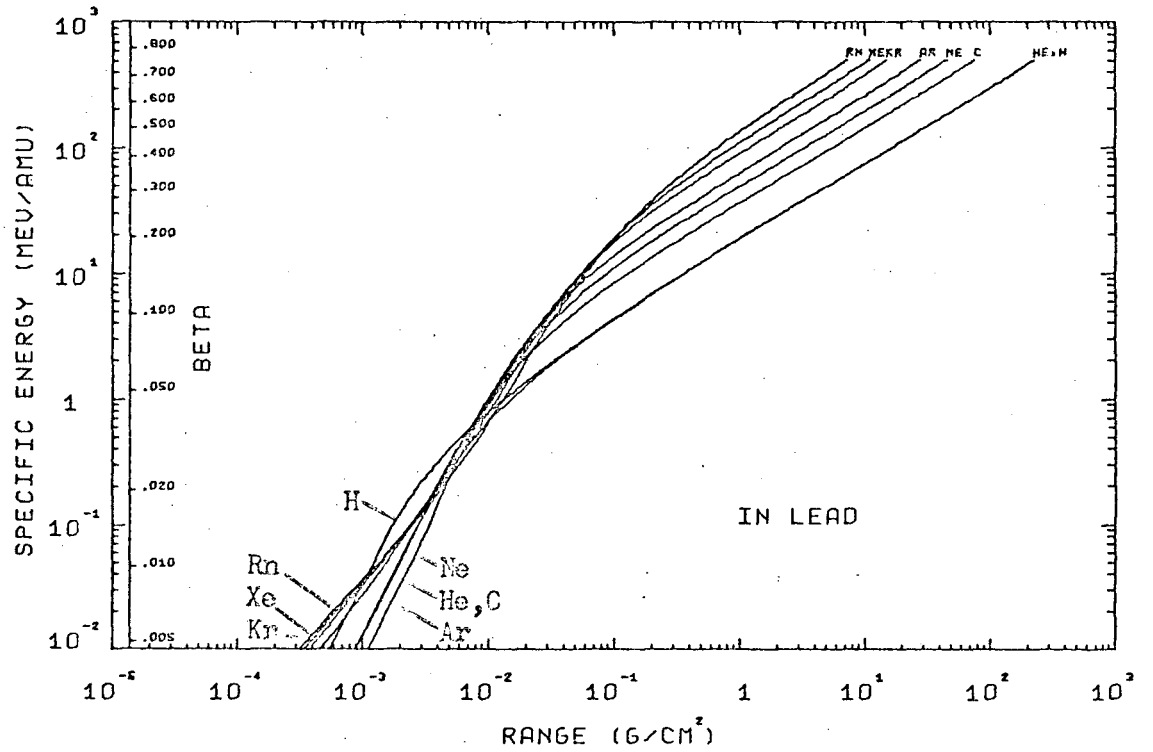

Fig. 29. Energy-range curves for various ions in lead as calculated by the computer program. For any specific energy on the ordinate, the residual pathlength range is read from the abscissa. At the left of the figure, values of $\beta = V/c$ are displayed.

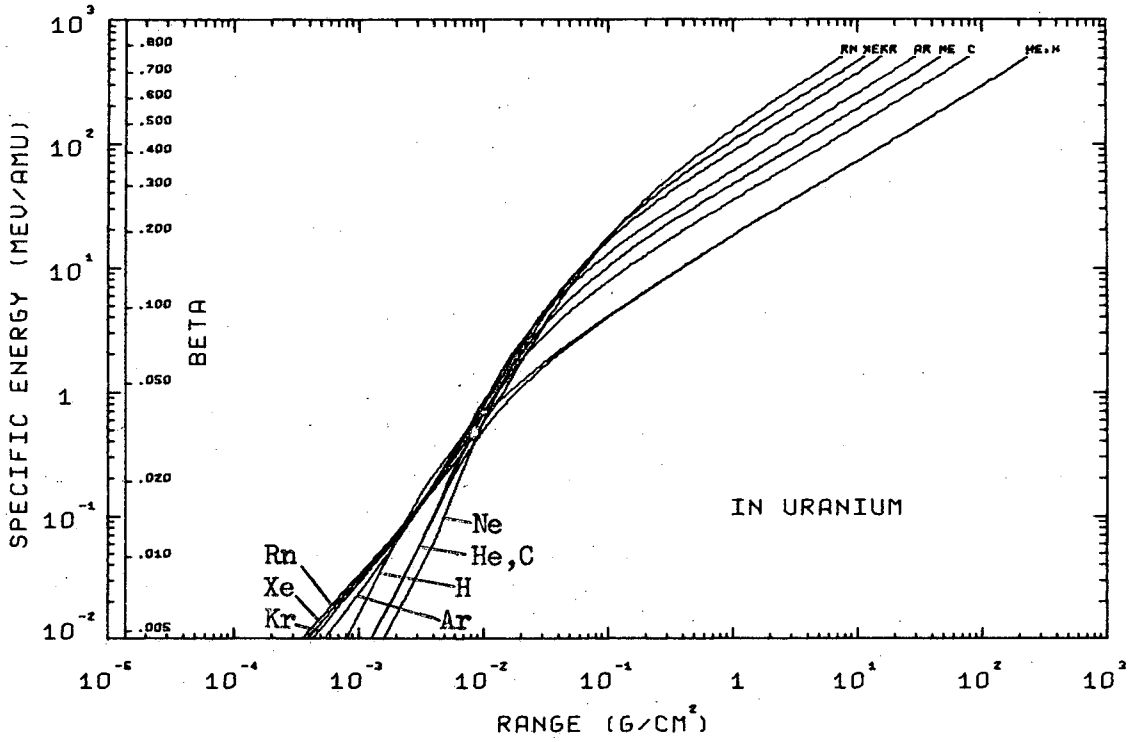

Fig. 30. Energy-range curves for various ions in uranium as calculated by the computer program. For any specific energy on the ordinate, the residual pathlength range is read from the abscissa. At the left of the figure, values of $\beta = V/c$ are displayed.

ACKNOWLEDGMENTS

This research was supported by the Atomic Energy Commission, in part through its Special Fellowship Program in Health Physics, which is administered by the Oak Ridge Associated Universities, and in part through its support of the Biomedical Division of the Lawrence Radiation Laboratory at Berkeley, California.

I wish to express appreciation to the members of my dissertation committee: to Dr. Roger Wallace for his advice and assistance throughout my graduate career; to Dr. Cornelius Tobias for his invaluable support of this project; to Dr. Harvey Amster and Drs. Wallace and Tobias for reviewing the manuscript of this paper.

I am indebted to Mr. Wade Patterson and the entire Health Physics Department of the Lawrence Radiation Laboratory at Berkeley for their cooperation and support throughout my graduate studies. Special recognition go to Mrs. Mary Long and Mrs. Ellen Cimpher who have rendered valuable assistance by typing the various drafts of this paper.

My most tender appreciation goes to my wife, Elsa, whose understanding, patience, and hard work has made this possible.

APPENDICES

A. The Computer Program For Calculating Stopping Power and Mean Pathlength Range.

This computer program utilizes the method described in sections II and III. It is this program which has calculated the results which are presented in section IV. In section A 1 we describe the program, in section A 2 the input to the program is presented, section A 3 is the listing, section A 4 contains four sample problems.

1. Description of the Program.

On page 102 of the listing (section A 3), Tables II, III, IV, and V are stored by DATA statements. Also the forty-eight constants, C_n of Eq. (21), are stored by a DATA statement. The numbers in this statement are in the order given by (((C(I, J, K), I = 1, 2), J = 1, 4), K = 1, 6) where I corresponds to n of Eq. (21), J = 1 to 4 corresponds to Z_1 = 1, 2, 6, and 10 respectively, and K = 1 to 6 corresponds to Z_2 = 1, 6, 13, 28, 47, and 79 respectively.

Pages 103 and 104 of the listing control the input which is presented in section A 2.

Pages 105 through 108 perform the stopping-power and range calculation if $Z_1 \leq 10$. The stopping-power calculation for the velocities indicated in Table V is performed on pages 105, 106, and 107. A variety of calculations are performed on page 108. First several specific energies for which $10 \leq \varepsilon \leq 500$ are chosen. Eqs. (26) and (30) are then solved for these specific energies yielding the range and stopping power. Equation (29) is also solved for the specific energies, for which $\varepsilon < 10$ MeV/amu. Finally, the constant k of Eq. (16) is calculated along with the ranges, velocities, and stopping power for low velocities in the dimensionless units of Lindhard et al. (see Eqs. (12) and (14)).

If $Z_1 > 10$, the range and stopping-power calculation is performed on pages 109 through 112. The specific energies at which the calculation will be made, and the boundaries between the four specific-energy regions are found on pages 109 and 110. For the low specific-energy region, the inelastic (electronic) stopping power, Eq. (31), and the elastic nuclear coulomb stopping power, Eq. (33), and the total stopping power, Eq. (36), are calculated on page 110 of the listing. The range (i. e. the first term of Eq. (46)) is calculated on page 111. The stopping-power calculation for the medium-low-specific-energy region, Eq. (37), and the range calculation (first two terms of Eq. (46)) is begun on page 111 and completed on page 112. The stopping-power and range calculation for the medium-high-specific-energy region (Eq. (44) and the first term of Eq. (46) respectively) is also performed on page 112. Also on page 112 the stopping power and range in the high-specific-energy region (Eqs. (45) and (46)) are calculated. On page 113 the velocity, range, and stopping power are calculated in the dimensionless units of Lindhard et al. for the low-and medium-low-specific-energy regions. The constant k (see Eq. (16) is calculated here too.

In the center of page 113 we calculate the first derivative of the stopping power with respect to energy at each specific energy except at the largest and the smallest. The value of this derivative at ε_1 is assumed to be $1/A_1$ times the slope at ε_i of a parabola which passes through the points $(S_{i-1}, \varepsilon_{i-1})$, (S_i, ε_i), and $(S_{i+1}, \varepsilon_{i+1})$, where S_i is the stopping power at specific energy ε_i. The value of this derivative is useful in certain applications and we include in the program this simple calculation for the few it will benefit.

Finally, at the end of page 113 are the control statements for the plotting subroutines, and the final output statements for the results.

On page 114 of the listing some diagnostic statements, which are normally not executed, appear. Just before terminating the job,

the DATA statements are printed.

The subroutines on pages 115 through 134 are called by the main program described above and by each other. A one or two line description of each subroutine appears as comment statements at the beginning of that subroutine. We now list these subroutines with a few comments about each.

RATIO: This subroutine solves Eq. (43).

BRAKET: This subroutine aids in the interpolation illustrated in Fig. 5.

DEDX: This subroutine solves Eqs. (22 A) and (23 A).

LAMBDA: This subroutine solves Eqs. (22 B) and (23 B).

DEDXL: This subroutine solves Eq. (36).

SPIML: This subroutine solves for the inverse of the stopping power given by Eq. (37).

GLSQ: This subroutine is called by the main program to solve for the coefficients in Eqs. (21) and (37).

XINTG: This subroutine is called by SIMPS (see below) to calculate the value of the integrands appearing in Eq. (46).

YINTERP: This subroutine is called when an ENERGY card appears in the input (see section A 2 below). It linearly interpolates in order to find the stopping powers and ranges at the specific energies read from this card.

STOPL: This subroutine solves Eqs. (31) and (33).

SIMPS: This subroutine solves the integral appearing in Eq. (46) as described in the text following this equation.

CCLOGTC: This subroutine is called by the plotting subroutines in order to construct a logarithmic grid.

GRAPH1: This subroutine plots stopping power as a function of specific energy using the plotting subroutines for the Cal Comp which are available at the Lawrence Radiation Laboratory computing facilities in Berkeley, California.

GRAPH2: This subroutine plots stopping power as a function of range using the system subroutines mentioned under GRAPH1.

GRAPH3: This subroutine plots specific energy as a function of range using the system subroutines mentioned under GRAPH1.

2. Input

There are ten types of input cards. Only the first four types discussed below are normally used. The type of input card is designated by a code word punched in columns 1 through 6. Each type is discussed below under the heading of its code word. The first two types of input cards may be read in any order. The letter b indicates blank columns where no punch appears.

IONbbb: This card is read with A6, 4X, 2E 10.0 format. In columns 11 through 20 the atomic number Z_1, of the ion appears. The atomic weight of the ion, A_1, is punched in columns 21 through 30. If several jobs are to be run, this card needs to be read in only initially or whenever Z_1 and A_1 are changed.

TARGET: This card is read with an A6, 4X, 2E 10.0 format. It also needs to be read only initially or when the stopping medium is changed. Columns 11 through 20 contain the number of elements, NO, in the stopping medium. If these columns are left blank (blanks are read as zero), NO is assumed to be 1.0.

The first NO cards following the TARGET card are read by the format 4E 10.0. Each of these cards contains the necessary information about one element of the stopping medium. Columns 1 through 10 contain the atomic number Z_{2_i}, and columns 11 through 20 contain the atomic weight A_{2_i}. If NO > 1, the relative abundance of this element $RELA_i$, is read from columns 21 through 30. The average adjusted excitation potential for this element, $DIADJ_i$, is read from columns 31 to 40 (see the discussion following Eq. (23) for the meaning of "adjusted").

The average adjusted excitation potential for the stopping medium is determined in one of four ways. For NO $\leq$ 1.0:

1. If a card with the code word IADJ is encountered (see below) the number from this card is taken as IADJ until the next GO card (see below) is encountered.

2. If no IADJ card appears then IADJ is given the value of the number in columns 21 through 30 of the TARGET card if this number is greater than 1.0.

3. If this number is not greater than 1.0 then IADJ is given the value of DIADJ if this number is greater than 1.0.

4. If DIADJ is not greater than 1.0 then IADJ is taken from Table IV or calculated from Eq. (24) depending on whether $Z_2 \leq 10$ or $Z_2 > 10$ respectively.

For NO > 1.0:

1. If a card with the code word IADJ is encountered (see below) the number from this card is taken as IADJ until the next GO card (see below) is encountered. If no IADJ card is encountered then IADJ is found as indicated below.

2. If the number in columns 21 through 30 of the TARGET card is greater than 1.0, then this number is taken as IADJ.

3. If this number is equal to 1.0, then IADJ is calculated from the NO values of $DIADJ_i$ using Eq. (28). When Eq. (28) is used, the value of ρ_i/ρ, $RELDEN_i$, is calculated by

$$RELDEN_i = RELA_i \, A_{2_i} \Big/ \left(\sum_{j=1}^{NO} RELA_j \, A_{2_j} \right);$$

where $RELA_i$ is the relative abundance of the ith element in the stopping medium.

4. If this number is less than 1.0 (or blank), then IADJ is calculated from Table IV and Eqs. (24) and (28).

GObbbb: This card is read with an A6 format, Whenever it is encountered a complete calculation as described above in section A 1 is performed unless a RENORM card has been encountered since the last GO card.

STOPbb: Whenever this card is encountered, the data statements on page 102 of the listing are printed and the problem is terminated.

IADJbb: This card is read with an A6, 4X, E 10.0 format. The number in columns 11 through 20 is taken as IADJ until the next GO card is encountered. This card is intended for use when the stopping medium has not changed since the last GO card, but a different IADJ is desired.

RENORM: This card is read with an A6, 4X, 5 E 10.0 format. When this card is encountered, a calculation as described in section A 1 above is not performed upon encountering the next GO card, but rather a new C_1 and C_2 for Eq. (21) are calculated for the ion ($Z_1 \leq 10$) specified on the last ION card and the stopping medium (single element) specified in the last Target cards.

The numbers in columns 11 to 20, 21 to 30, 31 to 40, 41 to 50, and

51 and 60 are the experimental stopping powers at the specific energies 0.01, 0.04, 0.1, 0.4, and 1.0 MeV/amu respectively, of this stopping medium for the last ion in units of MeV/(g/cm^2). If there is a high confidence in these new experimental stopping power, then the appropriate numbers in the fourth DATA statement on page 102 of the listing may be replaced. (See the discussion on C(I, J, K) in section A 1 above.)

ENERGY: This card is read with an A6, 4X, E 10.0 format. The number in columns 11 through 20 which must be ≤ 50, is the number of specific energies, in units of MeV/amu, to be read in on the next NEN/8 cards (round off the fractions to the next higher integer) read with an 8 E 10.0 format. After the complete calculation is performed, which is triggered by the next GO card, stopping power and range values at each of the NEN specific energies is found by linear interpolation in between the closest members of the table set up by the program. This card essentially allows the user to add energies with data cards to the table calculated by the program.

SEGRAP: This card is read with an A6, 4X, E 10.0 format. Whenever it is encountered, GRAPH1 is called at the end of the calculation triggered by the next GO card. A plot of the stopping power as a function of specific energy is then made. Examples of these plots appear in Fig. 11-16.

A new plotting grid is generated if the number in columns 11-20 is greater than zero or if the last plot was not generated by a SEGRAP card.

This card immediately following the SEGRAP card is read with a A6, 4X, 3A6 format. The symbols in columns 1-6 are used by the plotting subroutine to label the particular curve generated by this SEGRAP card. The symbols in columns 11-29 are used by the plotting

subroutine to label the grid whenever a new plotting grid is generated. Either one or both of these fields may be blank; in this case the labeling controlled by this field is not performed.

SRGRAP: The description of the use of this card is exactly the same as that for SEGRAP with a graph of stopping power as a function of range being plotted by GRAPH2. Examples of these plots appear in Figs. 19-24 and Fig. 31.

REGRAP: The description of the use of this card is exactly the same as that for SEGRAP with a graph of specific energy as a function of residual range being plotted by GRAPH3. Examples of those plots appear in Figs. 25-30.

Note that only one of the above three graph cards can appear in any one problem, i.e. between any two consecutive GO cards.

3. Listing.

This is a listing of the program in FORTRAN IV language.

```
      PROGRAM DEDXR(INPUT ,OUTPUT, TAPE2=INPUT, TAPE3=OUTPUT,TAPE98,
     1TAPE99, PUNCH)
C MAIN PROGRAM
      COMMON EV(200),ZEX(200),R(200),XLOG(200),YLOG(200),DZEX(200)
      COMMON/GEN/IADJ,LI,LAZ,NO,Z,      NN,II,IEV,ANL,JGRAPH,TEST
      COMMON/ABLOK/AMN(3,3),ALPHA(4,4)/BBLOK/CE(10),CN(10),CN1(10),
     1RELDEN(10)/CBLOK/B(5)/GRAF/LTRC,LTRG(3)
      DIMENSION DR(22,5),TABLE(22,10),AT(10),ZT(10),BETA(3),EL(3),
     1D(6,5),IL(5),EQ(22),CIADJ(10),DIADJ(10),ZEE(30),ZEN(30),EPSN(30),
     2ZETA(30),GZEX(30),EN(50),ZEXN(50),RN(50),ALE(6),C(2,4,6),F(4),
     3TEX(17,10),RELA(10),CODE(10),WHAT(7)
      REAL IADJ,LI,LAZ,LE,LL,LAMB2,LAMBDA
C   EXPERIMENTAL STOPPING POWER FOR Z LESS THAN 11 IN ALUMINUM
      DATA EQ/.01,.015,.02,.03,.04,.05,.07,.1,.15,.2,.3,.4,.5,.7,1.0,1.5
     1,2.0,3.,4.,5.,7.,10./,TABLE/183.,230.,265.,320.,360.,390.,430.,440
     2.,410.,380.,330.,290.,265.,220.,172.,131.,109.,83.,69.,58.,45.,34.
     3279,118.,141.,164.,205.,235.,260.,285.,315.,325.,320.,290.,270.,
     4250.,215.,170.,131.,109.,83.,69.,58.,45.,34.279,95.,114.,132.,164.
     5,187.,208.,230.,254.,264.,263.,243.,230.,216.,193.,156.,124.,105.,
     681.6,68.,58.,45.,34.279,71.,86.,99.,122.,140.,155.,175.,193.,203.,
     7206.,196.,189.,181.,166.,142.,117.,101.,80.,67.,57.,45.,34.279,
     848.,58.,66.,80.,93.,103.,120.,132.,142.,149.,150.,149.,147.,140.,
     9129.,111.,98.,79.,67.,57.,45.,34.279,39.,47.,54.,65.,75.,83.,97.,1
     *11.,123.,130.,133.,133.,131.,128.,120.,107.,94.,78.,66.,57.,45.,
     134.279,34.,40.,47.,56.,64.,71.,82.,94.,108.,112.,121.,122.,122.,
     2120.,111.,100.,90.,75.,64.,56.,44.,34.279,28.,33.,38.,47.,54.,60.,
     369.,80.,92.,100.,109.,110.,111.,110.,107.,95.,86.,73.,62.,55.,43.,
     434.279,23.,27.,32.,39.,46.,51.,59.,69.,80.,87.,96.,100.,101.,101.,
     598.,90.,81.,70.,60.,54.,42.,34.279,19.,23.,27.,32.,36.,43.,50.,60.
     6,70.,77.,87.,91.,93.,94.,90.,84.,76.,67.,58.,52.5,42.,34.279/
C   COEFFICIENTS FOR BARKAS POLYNOMIAL FIT TO BETHES THEORY
      DATA AMN/                    -.75265,.73736E-1,.40556E-1,.25398E1,
     6 -.312,.18664E-1,-.24598,.11548,-.99661E-2/,ALPHA/
     7 -.80155E1,.36916,-.14307E-1,.34718E-2,.18371E1,-.1452E-1,
     8 -.30142E-1,.23603E-2,.45233E-1,-.95873E-3,.71303E-2,-.68538E-3,
     9 -.59898E-2,-.52315E-3,-.33802E-3,.39405E-4/,D/30*0./,JGRAPH/0/
C  IONIZATION POTENTIALS FOR ELEMENTS WITH Z LESS THAN 11
      DATA CIADJ/18.7,42.,38.,60.,70.,78.,84.5,88.5,108.,131. /
C  COEFFICIENTS FOR NORMALIZING THE PROGRAM TO EXPERIMENTAL STOPPING POW  ER
C     FOR H, HE, C, AND NE IONS IN H, C, AL, NI, AG, AND AU
      DATA C/                                          8.8811002199177E-02,
     8 1.7138690365610E-02, 4.9497133143262E-02, 1.3540201949725E-02,
     9 5.1855586277785E-02, 1.5541522412133E-02,-7.0320508947949E-02,
     *-1.4255700147520E-02, 3.5990198639876E-03, 1.5967910228485E-03,
     1-5.8195120035795E-04, 8.4052292539332E-04, 9.6868735617298E-03,
     2 4.1480250614850E-03,-7.4582561384904E-03,-1.6385237951375E-03,
     3 5.0138986374204E-04,-2.6552415376993E-04,-1.5773041482136E-03,
     4-6.8461912460993E-04, 8.3666352668449E-03, 2.6876280235695E-03,
     5 1.5035074028774E-03, 1.6737094370482E-04,-1.1241521737316E-02,
     6-4.1837248715580E-03,-7.9827735119005E-03,-2.5753724979494E-03,
     7-1.1763486564892E-02,-4.1226660625563E-03,-1.3449692056030E-02,
     8-4.7899763404858E-03, 1.3976941603226E-02, 9.8137632029485E-04,
     9 9.7438614446294E-03, 5.6591608351300E-05, 1.2115290632189E-02,
     * 7.9626549835530E-04, 1.3788090175256E-02, 1.2567130675785E-03,
     1-1.3176586838630E-02,-5.7053662633375E-03,-1.6323907448869E-02,
     2-6.3370050198126E-03,-1.3188677117176E-02,-5.3555019602713E-03,
     3-1.5092254582325E-02,-5.8882305836342E-03/,TEST/0./
      DATA CODE/
     1 6HION    ,6HTARGET ,6HENERGY ,6HRENORM ,6HIADJ   ,6HSEGRAP ,
```

```
     2 6HSRGRAP ,6HREGRAP ,6HGO     ,6HSTOP   /
  100 CONTINUE
      WRITE (3,370)
  370 FORMAT (20H1DATA CARDS PRINTED./)
      IGRAPH=0
      NEN=0
      NEWB=0
      KA=1
      NN=-1
      NDR=1
      NIADJ=0
C   PROCESS DATA CARDS
  103 READ (2,1) CODEW,(WHAT(I),I=1,7)
    1 FORMAT (A6,4X,7E10.0)
      WRITE (3,371) CODEW,(WHAT(I),I=1,7)
  371 FORMAT (7H ******,A6,7E15.6)
      DO 101 I=1,10
      IF (CODEW.EQ.CODE(I)) GO TO 102
  101 CONTINUE
      WRITE (3,372) CODEW,(WHAT(I),I=1,7)
  372 FORMAT (31H1ILLEGAL DATA CARD, JOB ABORTED ,/1X,A6,7E15.6)
      CALL EXIT
  102 GO TO (1000,1100,1200,1300,1400,1500,1600,1700,1800,1900),I
C   Z IS THE ATOMIC NUMBER OF THE ION
C   A IS THE ATOMIC WEIGHT OF THE ION
 1000 Z=WHAT(1)
      A=WHAT(2)
      GO TO 103
C   NO IS THE NUMBER OF ELEMENTS IN THE STOPPING MEDIUM
 1100 NO=INT(WHAT(1))
      IF (NO.EQ.0) NO=1
 1101 DO 1102 I=1,NO
C   ZT(I) IS THE ATOMIC NUMBER OF THE ITH ELEMENT IN THE STOPPING MEDIUM
C   AT(I) IS THE ATOMIC WEIGHT OF THE ITH ELEMENT IN THE STOPPING MEDIUM
C   RELA(I) IS THE RELATIVE ABUNDANCE OF THE ITH ELEMENT IN THE STOPPING
C    MEDIUM
      READ (2,2) ZT(I),AT(I),RELA(I),DIADJ(I)
    2 FORMAT (4E10.0)
      WRITE (3,373) ZT(I),AT(I),RELA(I),DIADJ(I)
  373 FORMAT (7H ******,8E15.6)
 1102 CONTINUE
      IF (NO.NE.1) GO TO 1103
      RELDEN(1)=1.
      RELA(1)=1.
      IF (NIADJ.EQ.1) GO TO 103
      IADJ=WHAT(2)
      IF (IADJ.GT.1.) GO TO 103
      IADJ=DIADJ(1)
      IF (IADJ.LE.1.) GO TO 20
      GO TO 103
 1103 IF (NIADJ.EQ.1) GO TO 103
      IF (WHAT(2)-1.) 20,45,1104
 1104 IADJ=WHAT(2)
      GO TO 103
 1200 NEN=INT(WHAT(1))
      IF (NEN.LE.50) GO TO 1201
      WRITE (3,358)
  358 FORMAT (////,49H NUMBER OF ENERGIES IS GREATER THAN 50, JOB ABORT)
```

```
      CALL EXIT
 1201 READ (2,3) (EN(I),I=1,NEN)
    3 FORMAT (8E10.0)
      WRITE (3,373) (EN(I),I=1,NEN)
      GO TO 103
 1300 SP1=WHAT(1)
      SP2=WHAT(2)
      SP3=WHAT(3)
      SP4=WHAT(4)
      SP5=WHAT(5)
      NEWB=1
      GO TO 103
 1400 IADJ=WHAT(1)
      NIADJ=1
      GO TO 103
 1500 IGRAPH=1
      TEST=0.
      IF (WHAT(1).NE.0.) TEST=1.
      READ (2,4) LTRC,(LTRG(I),I=1,3)
    4 FORMAT (A6,4X,3A6)
      GO TO 103
 1600 IGRAPH=2
      TEST=0.
      IF (WHAT(1).NE.0.) TEST=1.
      READ (2,4) LTRC,(LTRG(I),I=1,3)
      GO TO 103
 1700 IGRAPH=3
      TEST=0.
      IF (WHAT(1).NE.0.) TEST=1.
      READ (2,4) LTRC,(LTRG(I),I=1,3)
      GO TO 103
 1800 GO TO 50
 1900 GO TO 999
C    CALCULATE IONIZATION POTENTIAL
   20 IF (NO.NE.1) GO TO 41
  422 CONTINUE
      IF (ZT(KA).GT.10.) GO TO 40
      KZ=ZT(KA)+0.1
      IADJ=CIADJ(KZ)
      GO TO 50
   40 IADJ=9.76*ZT(KA)+58.8/ZT(KA)**0.19
      GO TO 50
   41 DO 43 I=1,NO
      IF (ZT(I).GT.10.) GO TO 42
      IND=ZT(I)+0.1
      DIADJ(I)=CIADJ(IND)
      GO TO 43
   42 DIADJ(I)=9.76*ZT(I)+58.8/ZT(I)**0.19
   43 CONTINUE
      GO TO 45
   45 SUM1=0.
      DO 46 I=1,NO
   46 SUM1=SUM1+RELA(I)*ZT(I)*ALOG(DIADJ(I))
      SUM2=0.
      DO 47 I=1,NO
   47 SUM2=SUM2+RELA(I)*ZT(I)
      IADJ=EXP(SUM1/SUM2)
   50 IF (CODEW.EQ.6HTARGET) GO TO 103
```

```
      IF (NN.EQ.0) GO TO 54
      IF(NO.NE.1)GO TO 200
      WRITE(3,300) IADJ,A,Z,AT(1),ZT(1)
  300 FORMAT(////23H TARGET IS PURE ELEMENT//6H IADJ=F10.5/
     1                                       6H A   =F10.5/
     2                                       6H Z   =F10.5/
     3                                       6H AT  =F10.5/
     4                                       6H ZT  =F10.5)
      GO TO 54
  200 WRITE(3,301) IADJ,A,Z,(AT(I),I=1,NO)
  301 FORMAT (////
     *       21H TARGET IS A COMPOUND//6H IADJ=F10.5/6H A   =F10.5/6H Z
     1  =F10.5/5H AT1=F10.5,5H AT2=F10.5,5H AT3=F10.5,5H AT4=F10.5,5H AT
     25= F10.5,5H AT6=F10.5,5H AT7=F10.5,5H AT8=F10.5)
      WRITE(3,302)(ZT(I),I=1,NO)
  302 FORMAT(5H ZT1=F10.5,5H ZT2=F10.5,5H ZT3=F10.5,5H ZT4=F10.5,5H ZT5=
     1F10.5,5H ZT6=F10.5,5H ZT7=F10.5,5H ZT8=F10.5)
      WRITE (3,303) (RELA(I),I=1,NO)
  303 FORMAT                    (5H NT1=F10.5,5H NT2=F10.5,5H NT3=F10.5,5H
     1 NT4=F10.5,5H NT5=F10.5,5H NT6=F10.5,5H NT7=F10.5,5H NT8=F10.5)
      SAT=0.
      DO 51 I=1,NO
   51 SAT=SAT+RELA(I)*AT(I)
      DO 52 I=1,NO
C    RELDEN(I) IS THE RELATIVE DENSITY OF THE ITH ELEMENT IN THE STOPPING
C     MEDIUM
   52 RELDEN(I)=RELA(I)*AT(I)/SAT
      SUM=0.
      DO 53 I=1,NO
   53 SUM=SUM+RELA(I)*ZT(I)
      ZAF=SUM/SAT
      GO TO 55
   54 ZAF=ZT(KA)/AT(KA)
   55 LI=ALOG(IADJ)
      LAZ=ALOG(1./ZAF)
      IF(Z.GT.10.) GO TO 500
C    CALCULATION FOR Z LESS THAN 11
C    LOW ENERGY STOPPING POWER
      NN=0
      ZSQ=Z**2
      JZ=Z+.1
      KZ=ZT(KA)+0.1
      IF (NDR.GT.1) GO TO 429
      OLDZAF=ZAF
      OLDLI=LI
      OLDLAZ=LAZ
      OLDIADJ=IADJ
      DO 420 I=1,21
  420 EV(I)=EQ(I)
  429 CONTINUE
      IF ((ZT(KA).NE.13.).OR.((NO.NE.1).AND.(NDR.EQ.1))) GO TO 416
      DO 415 I=1 ,21
  415 DR(I,NDR)=1.
      GO TO 417
  416 CONTINUE
      R2=DEDX(2.)/112.3138
      R2=0.97*R2
      R10=DEDX(10.)/34.279
```

```
      Q=ALOG(R10/R2)/ALOG(5.)
      P=R2/(2.**Q)
      DO 406 I=1 ,21
  406 DR(I,NDR)=P*EV(I)**Q
  417 CONTINUE
      IF (NEWB.NE.1) GO TO 423
C   CALCULATION OF COEFFICIENTS FOR NORMALIZING THE PROGRAM TO EXPERIMENTAL
C    STOPPING POWER
      AL2=ALOG  (2.)
      ALE(1)=ALOG(.01)
      ALE(2)=ALOG  (0.04)
      ALE(3)=ALOG(.1)
      ALE(4)=ALOG  (0.4)
      ALE(5)=0.
      DO 421 J=1,5
      TEMP=(ALE(J)-AL2)**2
      TEMP2=2*AL2+ALE(J)
      DO 421 I=1,2
  421 D(J,I)=TEMP*TEMP2**(I-1)
      D(1,3)=ALOG(SP1/(DR(1,1)*ZSQ*TABLE(1,JZ)))
      D(2,3)=ALOG(SP2/(DR(5,1)*ZSQ*TABLE(5,JZ)))
      D(3,3)=ALOG(SP3/(DR(8,1)*ZSQ*TABLE(8,JZ)))
      D(4,3)=ALOG(SP4/(DR(12,1)*ZSQ*TABLE(12,JZ)))
      D(5,3)=ALOG(SP5/(DR(15,1)*ZSQ*TABLE(15,JZ)))
      CALL GLSQ (D,B,IL,5,2,SSQ,0.,0.)
      WRITE (3,305) (B(I),I=1,2),SP1,SP2,SP3,SP4,SP5
  305 FORMAT (/////,34H COEF. FOR RELATIVE S. P. ARE. . . ,3HC1=E15.8,
     110X,3HC2=E15.8,                ///,11H EXP. S. P. /5(E20.6/))
      PUNCH 306, (B(I),I=1,2),Z,ZT(1)
  306 FORMAT (2E20.13,2F10.1)
      GO TO 100
  423 CONTINUE
C   INTERPOLATION OF THE RELATIVE STOPPING POWER BETWEEN THE IONS AND
C    STOPPING MEDIA FOR WHICH COEFFICIENTS ARE PROVIDED
      IF (NDR.EQ.5) GO TO 439
      NDR=NDR+1
      IF (NDR.NE.2) GO TO 431
  445 CALL BRAKET (JZ,KZ,JZ1,JZ2,KZ1,KZ2,J1,J2,K1,K2,AT1,AT2)
      ZOLD=Z
      ZTOLD=ZT(KA)
      ATOLD=AT(KA)
  431 IF (NDR-3) 425,426,424
  424 IF (NDR.EQ.5) GO TO 427
      Z=FLOAT (JZ2)
      Z2=Z
      ZT(KA)=FLOAT (KZ1)
      AT(KA)=AT1
      GO TO 428
  425 Z=FLOAT (JZ1)
      Z1=Z
      ZT(KA)=FLOAT (KZ1)
      ZT1=ZT(KA)
      AT(KA)=AT1
      GO TO 428
  426 Z=FLOAT (JZ1)
      ZT(KA)=FLOAT (KZ2)
      ZT2=ZT(KA)
      AT(KA)=AT2
      GO TO 428
```

```
  427 Z=FLOAT (JZ2)
      ZT(KA)=FLOAT (KZ2)
      AT(KA)=AT2
  428 CONTINUE
      IF (NDR.LE.5) GO TO 422
  439 AL2=ALOG(2.)
      DO 419 I=1,17
      ALEV=ALOG  (EV(I))
      DO 432 K=1,4
      NDR=K+1
      IF (K-2) 434,435,433
  433 IF (K.EQ.4) GO TO 436
      M1=J2
      N1=K1
      GO TO 437
  434 M1=J1
      N1=K1
      GO TO 437
  435 M1=J1
      N1=K2
      GO TO 437
  436 M1=J2
      N1=K2
  437 CONTINUE
      ALDR=ALOG(DR(I,NDR))
      TEMP=(ALEV-AL2)**2
      TEMP2=2*AL2+ALEV
      SUM=0.
      DO 418 J=1,2
  418 SUM=SUM+C(J,M1,N1)*TEMP*TEMP2**(J-1)
  432 F(K)=EXP(SUM+ALDR)
      IF ((J1.EQ.J2).AND.(K1.EQ.K2)) GO TO 441
      IF (J1.EQ.J2) GO TO 442
      IF (K1.EQ.K2) GO TO 443
      C2=F(3)-F(1)
      C1=(ZOLD-Z1)/(Z2-Z1)
C   FF IS THE INTERPOLATED RELATIVE STOPPING POWER
      FF=F(1)+C1*C2+(ZTOLD-ZT1)/(ZT2-ZT1)*(F(2)+C1*(F(4)-F(2))-F(1)-C1*C
     12)
      GO TO 430
  441 FF=F(1)
      GO TO 430
  442 FF=F(1)+(ZTOLD-ZT1)*(F(2)-F(1))/(ZT2-ZT1)
      GO TO 430
  443 FF=F(1)+(ZOLD-Z1)*(F(3)-F(1))/(Z2-Z1)
  430 CONTINUE
      JZ=ZOLD+0.1
      ZSQ=ZOLD**2
C   TEX(I,J) IS THE STOPPING POWER FOR THE JTH ELEMENT IN THE STOPPING MEDIUM
C    AT THE ITH ENERGY
      TEX(I,KA)=FF*ZSQ*TABLE(I,JZ)
  419 CONTINUE
      Z=ZOLD
      ZT(KA)=ZTOLD
      AT(KA)=ATOLD
      KA=KA+1
      IF (KA.GT.NO) GO TO 444
      NDR=2
      KZ=ZT(KA)+0.1
```

```
      JZ=Z+0.1
      GO TO 445
  444 CONTINUE
      ZAF=OLDZAF
      LI=OLDLI
      LAZ=OLDLAZ
      IADJ=OLDIADJ
      DO 407 I=17,21
C   ZEX(I) IS THE FINAL STOPPING POWER AT THE ITH ENERGY
  407 ZEX(I)=DR(I,1)*TABLE(I,JZ)*ZSQ
      DO 440 I=1,17
      SUM=0.
      M=I-1
      IF (I.EQ.1) M=17
      DO 438 K=1,NO
  438 SUM=SUM+RELDEN(K)*TEX(M,K)
      IF (I.EQ.1) GO TO 446
      ZEX(M)=CONST*SUM
      GO TO 440
  446 CONST=ZEX(M)/SUM
  440 CONTINUE
      WRITE (3,361) CONST
  361 FORMAT (/ 22H NORMALIZING CONSTANT=  F10.6)
C SET UP TABLE
      EV(22)=10.
      EV(23)=10.38
      I=23
      DO 408 J=12,50,2
      I=I+1
  408 EV(I)=J
      DO 409 J=55,200,5
      I=I+1
  409 EV(I)=J
      DO 410 J=210,500,10
      I=I+1
  410 EV(I)=J
      IEV=I
C   CALCULATION OF THE HIGH ENERGY STOPPING POWER
      DO 411 I=22,IEV
      ZEX(I)=ZSQ*DEDX(EV(I))
  411 CONTINUE
C   CALCULATION OF THE RANGE
      R(1)=2.*EV(1)*A/ZEX(1)
      A2=A/2.
      DO 412 I=2,22
      EOE=EV(I)/EV(I-1)
      EX1=ALOG(EOE*ZEX(I-1)/ZEX(I))/ALOG(EOE)
      R(I)=R(I-1)+A*EV(I-1)/ZEX(I-1)/EX1*(EOE**EX1-1.)
  412 CONTINUE
      ALAMDT=LAMBDA(10.)
      DO 413 I=23,IEV
      R(I)=R(22)+(LAMBDA(EV(I))-ALAMDT)*A/(ZSQ*1.008)
  413 CONTINUE
      IF (NO.GT.1) GO TO 201
C   CALCULATION OF THE STOPPING POWER, RANGE, AND ENERGY IN THE DIMENSIONLESS
C    UNITS OF LINDHARD ET. AL.
      Z23=Z**(2./3.)
      ZS23=Z23+ZT(1)**(2./3.)
      ZS2312=SQRT(ZS23)
```

```
      ATOZT=AT(1)/ZT(1)
      AS=A+AT(1)
      AOAS=A/AS
      FEPSN=3.253E4*AOAS*ATOZT/(Z*ZS2312)
      FZETA=1.6618E8*AOAS/(ZS23*AS)
      FGZEX=1.957E-4*ZS2312*ATOZT/(Z*AOAS)
      XK=0.0793*Z23/(SQRT(ATOZT*(ZS2312*AOAS)**3))
      DO 414 I=1,25
      EPSN(I)=FEPSN*EV(I)
      ZETA(I)=FZETA*R(I)
      GZEX(I)=FGZEX*ZEX(I)
  414 CONTINUE
      WRITE (3,354) XK,(EV(I),EPSN(I),ZEX(I),GZEX(I),R(I),ZETA(I),I=1,
     125)
  354 FORMAT (/// 26H LSS ELECT. S.P. CONSTANT=
     *                  F8.5,/// 8X,1HE,12X, 6HE(LSS),14X, 5HDE/DX, 12X,
     110HDE/DX(LSS), 12X, 1HR,16X, 6HR(LSS),/,1X,9H(MEV/AMU),7X,15H(DIME
     2NSIONLESS),6X, 13H(MEV/GM/SQCM),6X, 15H(DIMENSIONLESS),8X,
     3 9H(GM/SQCM),8X, 15H(DIMENSIONLESS),// 30(1X,F10.3,5E20.6/))
      GO TO 201
C   CALCULATION FOR Z GREATER THAN 10
C DEFINE ENERGY REGION BOUNDARIES AND SET UP TABLE
  500 BETA(1)=(Z**(1./3.)/137.)**2
      BETA(2)=2./465.5
      BETA(3)=(3. *Z/137.)**2
      DO 503 I=1,3
      IF(BETA(I).GT..01) GO TO 501
      EL(I)=465.5*BETA(I)
      GO TO 503
  501 IF(BETA(I).GT..9999) GO TO 502
      GAMMA=1./SQRT(1.-BETA(I))
      EL(I)=931.*(GAMMA-1.)
      GO TO 503
  502 EL(I)=1.E10
  503 CONTINUE
      IF (EL(3).EQ.1.E10) GO TO 541
      WRITE (3,355) (EL(I),I=1,3)
  355 FORMAT (// 47H BOUNDARIES BETWEEN THE FOUR ENERGY REGIONS ARE /10X
     1, 3F20.3)
      GO TO 542
  541 CONTINUE
      WRITE (3,330) (EL(I),I=1,2)
  330 FORMAT (// 47H BOUNDARIES BETWEEN THE FOUR ENERGY REGIONS ARE /
     110X,2F20.3,13X,8HINFINITE)
  542 CONTINUE
      EV(1)=.01
      EV(2)=.015
      DO 519 I=2,9
  519 EV(I+1)=.01*FLOAT(I)
      EV(11)=.1
      EV(12)=.15
      J=12
      DO 524 I=2,9
      J=J+1
  524 EV(J)=0.1*FLOAT(I)
      J=20
      DO 525 I=2,20
      J=J+1
  525 EV(J)=0.5*FLOAT(I)
```

```
      EV(40)=10.38
      I=40
      DO 504 J=12,50,2
      I=I+1
  504 EV(I)=FLOAT(J)
      DO 505 J=55,200,5
      I=I+1
  505 EV(I)=FLOAT(J)
      DO 506 J=210,500,10
      I=I+1
  506 EV(I)=FLOAT(J)
      IEV=I
      DO 507 I=1,IEV
      JK=I
      IF(EV(I).GE.EL(1)) GO TO 509
  507 CONTINUE
  508 GO TO 900
  509 IEL1=JK
      DO 510 I=JK,IEV
      JL=I
      IF(EV(I).GE.EL(2)) GO TO 512
  510 CONTINUE
  511 GO TO 901
  512 IEL2=JL
      IF(EL(3).GE.EV(IEV)) GO TO 516
      DO 513 I=JL,IEV
      JK=I
      IF(EV(I).GE.EL(3)) GO TO 515
  513 CONTINUE
  514 GO TO 902
  515 IEL3=JK-1
      GO TO 517
  516 IEL3=IEV
  517 CONTINUE
C   CALCULATION OF STOPPING POWER AND RANGE IN THE LOW ENERGY REGION
      Z23=Z**(2./3.)
      Z876=7.39E4*Z**1.207
      AOZ=A/Z
      DO 518 I=1,NO
      ZS23=Z23+ZT(I)**(2./3.)
      ZTOAT=ZT(I)/AT(I)
      AS=A+AT(I)
      CE(I)=Z876*ZTOAT/ZS23**1.5
      CN(I)=4.14281E6*(A/AS)**1.5*SQRT(Z*ZTOAT)/ZS23**.75
      CN1(I)=45.1671*(AOZ/(ZTOAT*AS))**.27719/ZS23**.138595
  518 CONTINUE
      UL=EV(1)**.27719
      NN=1
      CALL SIMPS(0.,UL,0.001,10,RI,INDEX)
      IF (INDEX.LE.10) GO TO 327
      WRITE (3,326) NN,INDEX,EV(1),RI
  326 FORMAT (//// 23H SIMPS DID NOT CONVERGE / 4H NN=I2,7H INDEX=I3,
     17H EV(I)=F9.3,4H RI=E15.8)
  327 R(1)=RI*A
      ZEX(1)=DEDXL(EV(1))
      CALL STOPL (EV(1),XZEE,XZEN)
      ZEN(1)=XZEN
      ZEE(1)=XZEE
      DO 520 I=2,IEL1
```

```
      XLL=EV(I-1)**.27719
      UL=EV(I)**.27719
      ZEX(I)=DEDXL(EV(I))
      CALL STOPL (EV(I),XZEE,XZEN)
      ZEN(I)=XZEN
      ZEE(I)=XZEE
      CALL SIMPS(XLL,UL,0.001,10,RI,INDEX)
      IF (INDEX.LE.10) GO TO 328
      WRITE (3,326) NN,INDEX,EV(I),RI
  328 R(I)=R(I-1)+RI*A
  520 CONTINUE
C   CALCULATION IN THE MEDIUM-LOW ENERGY REGION
      SPL=DEDXL(EV(IEL1))
      SQREL=SQRT(EV(IEL1))
      SQRREL=EV(IEL1)**.22281
      CL=ALOG(SPL)
      SUM=0.
      DO 521 I=1,NO
      EXPN=EXP(CN1(I)*EV(IEL1)**.27719)
      SUM=SUM+(.5*(CE(I)+CN(I)/EXPN)/SQREL-.27719*CN(I)*CN1(I)/SQRREL/EX
     1PN)*RELDEN(I)
  521 CONTINUE
      DSPL=SUM
      DCL=DSPL/SPL
      Z2=Z**2
      RAT=RATIO(EV(IEL2))
      RATSQ=RAT**2
      DEX=DEDX(EV(IEL2))
      SPH=Z2*RATSQ*DEX
      CH=ALOG(SPH)
      BEL=SQRT(EV(IEL2)/465.5)
      IF (BEL.LE.Z23/137.) GO TO 522
      DRAT=ANL/EV(IEL2)*(1.-45.7*BEL* ALOG(Z)/(2.*Z-Z23))
      GO TO 523
  522 DRAT=ANL/EV(IEL2)
  523 CONTINUE
      IF(EV(IEL2).LT.7.) GO TO 535
      SUM1=0.
      DO 526 M=1,4
      SUM1=SUM1+ALPHA(M,3)*LI**(M-1)
  526 CONTINUE
      SUM=0.
      DO 527 M=1,4
      SUM=SUM+ALPHA(M,4)*LI**(M-1)
  527 CONTINUE
      DPDE=2./EV(IEL2)*(SUM1+3.*ALOG(EV(IEL2))*SUM)
      GO TO 537
  535 SUM=0.
      DO 536 M=1,3
      SUM=SUM+AMN(M,3)*LI**(M-1)
  536 CONTINUE
      DPDE=2./EV(IEL2)*SUM
  537 CONTINUE
      XLAM=LAMBDA(EV(IEL2))
      DXLAM=DEX*XLAM
      DCH=DRAT /RAT +1./EV(IEL2)-1./DXLAM-DXLAM/EV(IEL2)*DPDE
      DO 540 I=1,6
      DO 540 J=1,5
      D(I,J)=0.
```

```
  540 CONTINUE
      ALE1=ALOG(EV(IEL1))
      IF(ALE1.EQ.0.) ALE1=.001
      DO 528 I=1,4
      D(1,I)=ALE1**(I-1)
  528 CONTINUE
      ALE2=ALOG(EV(IEL2))
      IF(ALE2.EQ.0.) ALE2=.001
      DO 529 I=1,4
      D(2,I)=ALE2**(I-1)
  529 CONTINUE
      DO 530 I=1,4
      D(3,I)=FLOAT(I-1)*ALE1**(I-2)
  530 CONTINUE
      DO 531 I=1,4
      D(4,I)=FLOAT(I-1)*ALE2**(I-2)
  531 CONTINUE
      D(1,5)=CL
      D(2,5)=CH
      D(3,5)=DCL*EV(IEL1)
      D(4,5)=DCH*EV(IEL2)
      CALL GLSQ(D,B,IL,4,4,SSSQ,0.,0.)
      K=IEL1+1
      NN=2
      DO 532 I=K,IEL2
      ZEX(I)=1./SPIML (EV(I))
      ZEE(I)=ZEX(I)
      ZEN(I)=0.
      CALL SIMPS(EV(I-1),EV(I),.0005,10,RI,INDEX)
      IF (INDEX.LE.10) GO TO 329
      WRITE (3,326) NN,INDEX,EV(I),RI
  329 R(I)=R(I-1)+RI*A
  532 CONTINUE
C   CALCULATION IN THE MEDIUM-HIGH ENERGY REGION
      K=IEL2+1
      NN=3
      DO 546 I=K,IEL3
      II=I
      ZEX(I)=Z2*RATIO(EV(I))**2*DEDX(EV(I))
      CALL SIMPS (EV(I-1),EV(I),.0005,10,RI,INDEX)
      IF (INDEX.LE.10) GO TO 545
      WRITE(3,326) NN,INDEX,EV(I),RI
  545 R(I)=R(I-1)+RI*A
  546 CONTINUE
      IF (IEL3.EQ.IEV) GO TO 533
C   CALCULATION IN THE HIGH ENERGY REGION
      K=IEL3+1
      XLAM=LAMBDA(EV(IEL3))
      DO 534 I=K,IEV
      ZEX(I)=Z2  *DEDX(EV(I))
      R(I)=R(IEL3)+A/Z2*(LAMBDA(EV(I))-XLAM)/1.008
  534 CONTINUE
  533 IF (NO.GT.1) GO TO 539
C   CALCULATION OF THE STOPPING POWER, RANGE, AND ENERGY IN THE DIMENSIONLESS
C    UNITS OF LINDHARD ET. AL
      AOAS=A/AS
      FEPSN=3.253E4*AOAS/(ZTOAT*Z*SQRT(ZS23))
      FZETA=1.6618E8*AOAS/(ZS23*AS)
      FGZEX=1.957E-4*SQRT(ZS23)/(Z*ZTOAT*AOAS)
```

```
      XK=0.0793*Z23*SQRT(ZTOAT/AOAS**3)/ZS23**0.75
      DO 538 I=1,IEL2
      EPSN(I)=FEPSN*EV(I)
      ZETA(I)=FZETA*R(I)
      GZEX(I)=FGZEX*ZEX(I)
  538 CONTINUE
      WRITE (3,356) XK,(EV(I),EPSN(I),ZEN(I),ZEE(I),ZEX(I),GZEX(I),R(I),
     1ZETA(I),I=1,IEL2)
  356 FORMAT (///, 26H LSS ELECT. S.P. CONSTANT=
     *                 F8.5,///, 8X, 1HE,10X, 6HE(LSS),9X, 9HNUC. S.P.
     1 8X, 10HELEC. S.P.,10X, 5HDE/DX, 9X, 10HDE/DX(LSS),11X, 1HR,14X,
     2 6HR(LSS), /,1X, 9H(MEV/AMU),4X, 15H(DIMENSIONLESS),3X,
     3 13H(MEV/GM/SQCM),4X, 13H(MEV/GM/SQCM),4X, 13H(MEV/GM/SQCM),3X,
     4 15H(DIMENSIONLESS),5X, 9H(GM/SQCM),5X, 15H(DIMENSIONLESS),//,
     5 30(1X,F10.3,7E17.6/))
      GO TO 201
  539 WRITE (3,357) (EV(I),ZEN(I),ZEE(I),ZEX(I),R(I),I=1,IEL1)
  357 FORMAT (///,8X, 1HE,11X, 9HNUC.S.P.,11X, 10HELEC. S.P.,12X,
     1 5HDE/DX,18X, 1HR,/,1X, 9H(MEV/AMU),8X, 13H(MEV/GM/SQCM),7X,
     2 13H(MEV/GM/SQCM),7X, 13H(MEV/GM/SQCM), 9X, 9H(GM/SQCM),//,
     3 30(1X,F10.3,4E20.6/))
  201 CONTINUE
      IEND=IEV-1
      DZEX(1)=-0.
      DZEX(IEV)=-0.
      DO 204 I=2,IEND
      X1=EV(I)-EV(I+1)
      X2=EV(I+1)-EV(I-1)
      X3=EV(I-1)-EV(I)
      E1SQ=EV(I-1)**2
      E2SQ=EV(I)**2
      E3SQ=EV(I+1)**2
      X1SQ=X1**2
      X3SQ=X3**2
      XNUM=ZEX(I-1)*X1SQ-ZEX(I+1)*X3SQ+ZEX(I)*X2*(X1-X3)
      DNOM=E1SQ*X1+E2SQ*X2+E3SQ*X3
      DZEX(I)=XNUM/(DNOM*A)
  204 CONTINUE
      IF ((IGRAPH.GT.0.).AND.(JGRAPH.NE.IGRAPH)) TEST=1.
      IF ((JGRAPH.NE.2).OR.(TEST.EQ.0.)) GO TO 600
      NN=100
      CALL GRAPH2
  600 IF(IGRAPH.EQ.1) CALL GRAPH1
      NN=1
      IF(IGRAPH.EQ.2) CALL GRAPH2
      IF(IGRAPH.EQ.3) CALL GRAPH3
      IF (IGRAPH.NE.0) JGRAPH=IGRAPH
C OUTPUT AND GO TO THE NEXT PROBLEM
      WRITE(3,350)(EV(I),ZEX(I),R(I),DZEX(I),I=1,IEV)
  350 FORMAT(/// ,8X,1HE,14X,5HDE/DX,15X,4HR(E),11X,14HSLOPE OF DE/DX,/,
     *1X,9H(MEV/AMU),8X,13H(MEV/GM/SQCM),9X,9H(GM/SQCM),11X,9H(SQCM/GM),
     1 // 200(1X,F10.3,3E20.6/))
      IF (NEN.EQ.0) GO TO 203
      DO 202 I=1,NEN
      ZEXN(I)=YINTERP (1,IEV,EV,ZEX,EN(I))
      RN(I)=YINTERP (1,IEV,EV,R,EN(I))
      DZEX(I)=-0.
  202 CONTINUE
      WRITE (3,350) (EN(I),ZEXN(I),RN(I),DZEX(I),I=1,NEN)
```

PUNCH 3578 ~~(ZT(I)~~ Z, A, ZT(1), AT(1), ZT(2)
3578 FORMAT ~~(Z's AND A's ARE --~~ *, ~~8F~~8.0) AT(2)

PUNCH 3579, (EV(I), ZEX(I), I=1,103)
3579 FORMAT (4(F7.3, E13.6))

```
  203 CONTINUE
      CALL SECOND (TIME)
      WRITE (3,374) TIME
  374 FORMAT (///6H TIME=F8.3)
      GO TO 100
C   DIAGNOSTICS--JOB ABORTED.
  900 NSTATE=508
      WRITE (3,351) NSTATE
  351 FORMAT (////,25H PROGRAM ERROR--STATEMENT,I4,30H WAS ENCOUNTERED.
     1JOB ABORTED. )
      CALL EXIT
  901 NSTATE=511
      WRITE (3,351) NSTATE
      CALL EXIT
  902 NSTATE=514
      WRITE (3,351) NSTATE
      CALL EXIT
  999 CONTINUE
C   OUTPUT AT JOB COMPLETION--DATA STATEMENTS PRINTED
      NN=100
      IF (JGRAPH.EQ.2) CALL GRAPH2
      IF (JGRAPH.NE.0) CALL CCEND
      WRITE (3,322)
  322 FORMAT (1H1,50X,23HDATA STATEMENTS PRINTED/////)
      WRITE(3,320) (EQ(I),(TABLE(I,J),J=1,10),I=1,22)
  320 FORMAT(23H DEDX TABLE AS COMPILED   /22(11F10.3/))
      WRITE(3,324)  ((AMN(M,N),N=1,3),M=1,3),((ALPHA(M,N),N=1,4),M=1,4)
  324 FORMAT(/    17H CONSTANTS A(M,N)/3(3E20.8/) 21HOCONSTANTS ALPHA(M,
     1N)/4(4E20.8/))
      WRITE (3,325) (I,I=1,10),(IADJ(I),I=1,10)
  325 FORMAT (/ 4H Z= ,10I10 / 6H IADJ= 10F10.1)
      WRITE (3,321) (((C(I,J,K),K=1,6),I=1,2),J=1,4)
  321 FORMAT (/ 19H CONSTANTS C(I,J,K),/,4(6E22.13/6E22.13//))
      STOP
      END
```

```
      FUNCTION RATIO(E)
C     THIS SUBROUTINE CALCULATES THE RATIO OF THE IONS CHARGE TO ITS NUCLEAR
C      CHARGE
      COMMON/GEN/IADJ,LI,LAZ,NO,Z,      NN,II,IEV,ANL,JGRAPH
      DIMENSION AN(5)
      DATA AN/.413253,1.63475,10.4782,2.21626,.847578/
      Z23=Z**(2./3.)
      XI=E/931.16
      BETA=SQRT(XI*(XI+2.))/(XI+1.)
  201 IF (BETA.LE.Z23/137.) GO TO 202
      IF (BETA.GE.2.*Z/137.) GO TO 204
      G=(137.*BETA+4.*Z-3.*Z23)/(6.*Z-3.*Z23)
      GO TO 203
  202 G=2./3.
      GO TO 203
  204 G=1.
  203 X=137.*BETA/Z**G
      A1=AN(1)*X**(AN(2)**2)
      A2=AN(3)*X**AN(4)
      A3=AN(5)+1.
      RATIO=1.-EXP(-A1)/A3-AN(5)/A3/(A2+1.)
      IF(NN.EQ.1)ANL=A1*AN(2)**2*EXP(-A1)/A3+A2*AN(4)*AN(5)/A3/(A2+1.)**
     12
      IF((E.LT.1.5).OR.(BETA.GT.3.5*Z/137.))GO TO 205
      RETURN
  205 WRITE(3,1) E
    1 FORMAT(37H ENERGY IN RATIC IS OUT OF RANGE   E=E15.8)
      RETURN
      END
```

```
      SUBROUTINE BRAKET (JZ,KZ,JZ1,JZ2,KZ1,KZ2,J1,J2,K1,K2,AT1,AT2)
C     THIS SUBROUTINE RETURNS TO MAIN PROGRAM THE PARAMETERS NEEDED TO
C      INTERPOLATE BETWEEN THE RELATIVE STOPPING POWERS FOR THE CASE Z LESS THAN
C      OR EQUAL TO 10
      IF (JZ.LE.2) GO TO 453
      IF (JZ-6) 455,452,451
  451 IF (JZ.LT.10) GO TO 456
      J1=4
      GO TO 454
  452 J1=3
      GO TO 454
  453 J1=JZ
  454 J2=J1
      JZ1=JZ
      JZ2=JZ
      GO TO 458
  455 J1=2
      J2=3
      JZ1=2
      JZ2=6
      GO TO 458
  456 J1=3
      J2=4
      JZ1=6
      JZ2=10
  458 IF (KZ.EQ.1) GO TO 463
      IF (KZ-6) 471,464,459
  459 IF (KZ-13) 471,465,460
  460 IF (KZ-28) 472,466,461
  461 IF (KZ-47) 473,467,462
  462 IF (KZ-79) 474,468,474
  463 K1=1
      AT1=1.008
      GO TO 469
  464 K1=2
      AT1=12.011
      GO TO 469
  465 K1=3
      AT1=26.98
      GO TO 469
  466 K1=4
      AT1=58.71
      GO TO 469
  467 K1=5
      AT1=107.88
      GO TO 469
  468 K1=6
      AT1=197.
  469 K2=K1
      KZ1=KZ
      KZ2=KZ
      AT2=AT1
      GO TO 476
  471 K1=2
      KZ1=6
      KZ2=13
      AT1=12.011
      AT2=26.98
      GO TO 475
```

```
472 K1=3
    KZ1=13
    KZ2=28
    AT1=26.98
    AT2=58.71
    GO TO 475
473 K1=4
    KZ1=28
    KZ2=47
    AT1=58.71
    AT2=107.88
    GO TO 475
474 K1=5
    KZ1=47
    KZ2=79
    AT1=107.88
    AT2=197.
475 K2=K1+1
476 RETURN
    END
```

```
      FUNCTION DEDX(E)
C     THIS SUBROUTINE CALCULATES THE STOPPING POWER USING BARKAS POLYNOMIAL
C      APPROXIMATION TO BETHES THEORY
      REAL IADJ,LI,LE,LAMBDA
      COMMON/GEN/IADJ,LI,LAZ,NO,Z,      NN,II,IEV,ANL,JGRAPH
      COMMON/ABLOK/AMN(3,3),ALPHA(4,4)
      LE=ALOG(E*1.008)
      IF(LE.EQ.0.) LE=.001
      IF(E.LT.7.) GO TO 221
      IF((E.EQ.7.).AND.(II.EQ.32)) GO TO 221
      SUM=0.
      DO 220 N=2,4
      DO 220 M=1,4
      SUM=SUM+FLOAT(N-1)*ALPHA(M,N)*(LI**(M-1))*(LE**(N-2))
  220 CONTINUE
      DEDX=E*1.008/(SUM*LAMBDA(E))
      RETURN
  221 SUM=0.
      DO 223 N=2,3
      DO 223 M=1,3
      SUM=SUM+FLOAT(N-1)*AMN(M,N)*(LI**(M-1))*(LE**(N-2))
  223 CONTINUE
      DEDX=E*1.008/(SUM*LAMBDA(E))
      IF (E.LT.1.) GO TO 224
      RETURN
  224 WRITE(3,1) E
    1 FORMAT(37H ENERGY IN DEDX IS OUT OF RANGE    E=E15.8)
      RETURN
      END
```

```
      REAL FUNCTION LAMBDA(E)
C     THIS SUBROUTINE CALCULATES THE RANGE USING BARKAS POLYNOMIAL APPROXIMATION
C      TO BETHES THEORY
      REAL IADJ,LAZ,LI,LE,LL
      COMMON/GEN/IADJ,LI,LAZ,NO,Z,      NN,II,IEV,ANL,JGRAPH
      COMMON/ABLOK/AMN(3,3),ALPHA(4,4)
      LE=ALOG(E*1.008)
      IF(LE.EQ.0.) LE=.001
      IF(E.LT.7.) GO TO 221
      IF((E.EQ.7.).AND.(II.EQ.32)) GO TO 221
      SUM=0.
      DO 210 N=1,4
      DO 210 M=1,4
      SUM=SUM+ALPHA(M,N)*(LI**(M-1))*(LE**(N-1))
  210 CONTINUE
      LL=LAZ+SUM
      LAMBDA=EXP(LL)
      RETURN
  221 SUM=0.
      DO 222 N=1,3
      DO 222 M=1,3
      SUM=SUM+AMN(M,N)*LI**(M-1) *(LE**(N-1))
  222 CONTINUE
      LL=LAZ+SUM
      LAMBDA=EXP(LL)*.001
      IF (E.LT.1.)GO TO 211
      RETURN
  211 WRITE(3,1) E
    1 FORMAT(39H ENERGY IN LAMBDA IS OUT OF RANGE    E=E15.8)
      RETURN
      END
```

```
      FUNCTION DEDXL(E)
C     THIS SUBROUTINE CALCULATES THE STOPPING POWER FOR THE CASE OF Z GREATER
C      THAN 10 IN THE LOW ENERGY REGION
      COMMON/GEN/IADJ,LI,LAZ,NO,Z,      NN,II,IEV,ANL,JGRAPH
      COMMON/BBLOK/CE(10),CN(10),CN1(10),RELDEN(10)
      SUM=0.
      SQRE=SQRT(E)
      SQRRE=E**.27719
      DO 230 I=1,NO
      SUM=SUM+(CE(I)+CN(I)/EXP(CN1(I)*SQRRE))*SQRE*RELDEN(I)
  230 CONTINUE
      DEDXL=SUM
      BETA=Z/137.**2
      XI=E/931.16
      BEL=XI*(XI+2.)/(XI+1.)**2
      IF (BEL.GT.BETA) GO TO 232
      RETURN
  232 WRITE(3,1) E
    1 FORMAT(38H ENERGY IN DEDXL IS OUT OF RANGE    E=E15.8)
      RETURN
      END
```

```
      FUNCTION SPIML(E)
C     THIS SUBROUTINE CALCULATES THE INVERSE OF THE STOPPING POWER IN THE
C      MEDIUM-LOW ENERGY REGION FOR THE CASE OF Z GREATER THAN 10
      COMMON/GEN/IADJ,LI,LAZ,NO,Z,      NN,II,IEV,ANL,JGRAPH
      COMMON/CBLOK/B(5)
      BETA1=Z**(1./3.)/137.**2
      BETA2=2.5/465.5
      IF (E.EQ.1.) GO TO 251
      XLE=ALOG(E)
      SUM=0.
      DO 250 I=1,4
      SUM=SUM+B(I)*XLE**(I-1)
  250 CONTINUE
      SPIML=1./EXP(SUM)
      XI=E/931.16
      BEL=XI*(XI+2.)/(XI+1.)**2
      IF ((BEL.GT.BETA2).OR.(BEL.LT.BETA1)) GO TO 252
      RETURN
  251 SPIML=1./EXP(B(1))
      IF ((.002148.GT.BETA2).OR.(.002148.LT.BETA1)) GO TO 252
      RETURN
  252 WRITE(3,1) E
    1 FORMAT(37H ENERGY IN SPIML IS OUT OF RANGE   E=E15.8)
      RETURN
      END
```

```
      SUBROUTINE GLSQ(A,X,IL,N,M,ALPHA,E1,E2)
C     THIS SUBROUTINE CALCULATES THE LEAST SQUARE COEFFICIENTS FOR EACH OF M
C      FUNCTIONS WHICH ALLOW THEIR SUM TO APPROXIMATE THE N DATA POINTS
      DIMENSION A(6,5), X(5), IL(5)
      MM=M+1
      LL=1
      DO 60J=1,MM
 60   IL(J)=0
      I=1
      DO 3K=1,MM
      II=I+1
      DO 4J=II,N
      IF(ABS(A(J,K))-E1) 4,4,6
 6    T1=SQRT ((A(J,K))**2+(A(I,K))**2)
      S=A(J,K)/T1
      C=A(I,K)/T1
      DO 5L=K,MM
      T2=C*A(I,L)+S*A(J,L)
      A(J,L)=-S*A(I,L)+C*A(J,L)
 5    A(I,L)=T2
      LL=LL+1
 4    CONTINUE
      IF (ABS (A(I,K))-E2)3,3,8
 8    IL(K)=I
      I=I+1
 3    CONTINUE
      X(MM)=-1.0
      II=M
      DO 35I=1,M
 35   X(I)=0.
      DO 30J=1,M
      IF (IL(II))30,30,31
 31   S=0.
      LL=II+1
      I=IL(II)
      DO 32K=LL,MM
 32   S=S+A(I,K)*X(K)
      X(II)=-S/A(I,II)
 30   II=II-1
      IF (IL(MM))50,51,50
 51   ALPHA=0.
      GO TO 52
 50   I=IL(MM)
      ALPHA=A(I,MM)
 52   RETURN
      END
```

```
      FUNCTION XINTG(X)
C     THIS SUBROUTINE CALCULATES THE INTEGRAND FOR SIMPS
      COMMON/GEN/IADJ,LI,LAZ,NO,Z,      NN,II,IEV,ANL,JGRAPH
      COMMON/BBLOK/CE(10),CN(10),CN1(10),RELDEN(10)
      GO TO (1,2,3  ),NN
    1 SUM=0.
      DO 260 I=1,NO
      SUM=SUM+RELDEN(I)*(CE(I)+CN(I)/EXP(CN1(I)*X))
  260 CONTINUE
      XINTG=3.6076*      X**.80399/SUM
      RETURN
    2 XINTG=SPIML(X)
      RETURN
    3 XINTG=1./((Z*RATIO(X))**2*DEDX(X))
      RETURN
      END
```

```
      FUNCTION YINTERP(IMIN,IMAX,XTABLE,YTABLE,X)
C     THIS SUBROUTINE LINEARLY INTERPOLATES BETWEEN VALUES OF THE ARRAY YTABLE
      DIMENSION XTABLE(1),YTABLE(1)
      N=IMIN
      M=IMAX
      L1=N
      L2=M
      K=N
      IF(X-XTABLE(N))1,15,3
    3 K=M
      IF(XTABLE(M)-X)1,15,9
    9 K=M/2
      IF(X-XTABLE(K))20,15,29
   20 L2=K
      GO TO 23
   29 L1=K
   23 IF(L2-L1-1)1,14,25
   25 M=L1+L2
      GO TO 9
   14 YINTERP=YTABLE(L1)+(X-XTABLE(L1))*(YTABLE(L2)-YTABLE(L1))/
     1(XTABLE(L2)-XTABLE(L1))
      RETURN
   15 YINTERP=YTABLE(K)
      RETURN
    1 YINTERP=0.0
      WRITE(3,300)L1,L2,K,M,IMAX,IMIN,X
  300 FORMAT(41H  ERROR IN FUNCTION YINTERP...JOB ABORTED/1X,6I8,E20.8)
      CALL EXIT
      END
```

```
      SUBROUTINE STOPL (E,XELEC,XNUC)
C     IN THE CASE FOR Z GREATER THAN 10 THIS SUBROUTINE CALCULATES THE ELECTRONI
C      AND NUCLEAR STOPPING POWER IN THE LOW ENERGY REGION
      COMMON/BBLOK/CE(10),CN(10),CN1(10),RELDEN(10)
      COMMON/GEN/IADJ,LI,LAZ,NO,Z,      NN,II,IEV,ANL,JGRAPH
      SQRE=SQRT(E)
      SUM=0.
      DO 230 I=1,NO
      SUM=SUM+CE(I)*RELDEN(I)
  230 CONTINUE
      XELEC=SUM*SQRE
      SQRRE=E**0.27719
      SUM=0.
      DO 231 I=1,NO
      SUM=SUM+CN(I)/EXP(CN1(I)*SQRRE)*RELDEN(I)
  231 CONTINUE
      XNUC=SUM*SQRE
      BETA=Z/137.**2
      XI=E/931.16
      BEL=XI*(XI+2.)/(XI+1.)**2
      IF (BEL.GT.BETA) GO TO 233
      RETURN
  233 WRITE (3,1) E
    1 FORMAT (38H ENERGY IN STOPL IS OUT OF RANGE    E=E15.8)
      RETURN
      END
```

```
      SUBROUTINE SIMPS (A,B,E,MAXI,XIP,INDEX)
C     THIS SUBROUTINE NUMERICALLY INTEGRATES USING SIMPSONS RULE
      FAFB=XINTG(A)+XINTG(B)
      XH=B-A
      XIR=XH*.5
      XJ=XIR*FAFB
      XNEW=A+XIR
      XHA=XIR/3.
      INDEX=0
 1006 FNEWX=XINTG(XNEW)
 1001 IF (INDEX .GT. 0) GO TO 1003
 1002 INDEX=1
      XI=XHA*(FAFB+FNEWX*4.)
 1004 XJ=(XJ+XI*3.)*.25
      INDEX=INDEX+1
      IF (INDEX .GT. MAXI) GO TO 1009
 1010 XH=XH*.5
      XNEW=A+XH*.5
      S=0.
 1005 IF (XNEW .LT. B) GO TO 1006
 1007 XIP=(XJ+XH*2.*S)/3.
      IF (ABS (XIP-XI) .LE. ABS (E*XIP)) GO TO 1009
 1008 XI=XIP
      GO TO 1004
 1003 S=S+FNEWX
      XNEW=XNEW+XH
      GO TO 1005
 1009 RETURN
      END
```

```
      SUBROUTINE CCLOGTC(KAXIS,NC,TICLL,TICLL1)
C     THIS SUBROUTINE PLOTS LOG SPACED TIC MARKS USING THE CAL COMP ROUTINES
C     KAXIS OF 1=LOWER AXIS, 2=RIGHT HAND AXIS, 3=UPPER AXIS, 4=LEFT HAND AXIS
C     NC=NUMBER OF CYCLES
C     TICLL=LENGTH OF SECONDARY TIC MARKS IN INCHES
C     TICLL1=LENGTH OF PRIMARY TIC MARKS IN INCHES
      COMMON/CCPOOL/XMIN,XMAX,YMIN,YMAX,CCXMIN,CCXMAX,CCYMIN,CCYMAX
      COMMON/CCFACT/FACTOR
      DIMENSION XTIC(30),YTIC(30)
      X1SAVE=XMIN $ X2SAVE=XMAX $ Y1SAVE=YMIN $ Y2SAVE=YMAX
      GO TO (100,110,120,130),KAXIS
  100 XMIN=0. $ XMAX=FLOAT(NC) $ YMIN=0. $ YMAX=1.
      B=100./(FACTOR*(CCYMAX-CCYMIN))
      GO TO 200
  110 XMIN=1. $ XMAX=0. $ YMIN=0. $ YMAX=FLOAT(NC)
      B=100./(FACTOR*(CCXMAX-CCXMIN))
      GO TO 200
  120 XMIN=0. $ XMAX=FLOAT(NC) $ YMIN=1. $ YMAX=0.
      B=100./(FACTOR*(CCYMAX-CCYMIN))
      GO TO 200
  130 XMIN=0. $ XMAX=1. $ YMIN=0. $ YMAX=FLOAT(NC)
      B=100./(FACTOR*(CCXMAX-CCXMIN))
  200 TICL=TICLL*B
      TICL1=TICLL1*B
      DO 205 K=1,NC
      L=1
      DO 204 J=1,9
      AJ=J
      XTICC=ALOG10(AJ)+K-1.
      DO 203 I=1,3
      XTIC(L)=XTICC
      GO TO (201,202,201),I
  201 YTIC(L)=0.
      GO TO 203
  202 YTIC(L)=TICL
      IF ((J.EQ.1).AND.(K.NE.1)) YTIC(L)=TICL1
  203 L=L+1
  204 CONTINUE
      XTIC(L)=K
      YTIC(L)=0.
      GO TO (206,207,206,207),KAXIS
  206 CALL CCPLOT(XTIC,YTIC,L,4HJOIN)
      GO TO 205
  207 CALL CCPLOT (YTIC,XTIC,L,4HJOIN)
  205 CONTINUE
      XMIN=X1SAVE $ XMAX=X2SAVE $ YMIN=Y1SAVE $ YMAX=Y2SAVE
      RETURN
      END
```

```
      SUBROUTINE GRAPH1
C     THIS SUBROUTINE PLOTS STOPPING POWER VS ENERGY
      REAL IADJ
      COMMON EV(200),ZEX(200),R(200),XLOG(200),YLOG(200)
      COMMON/GEN/IADJ,LI,LAZ,NO,Z,     NN,II,IEV,ANL,JGRAPH,TEST
      COMMON/GRAF/LTRC,LTRG(3)
      COMMON/CCPOOL/XMIN,XMAX,YMIN,YMAX,CCXMIN,CCXMAX,CCYMIN,CCYMAX
      DIMENSION XTC(47),YTC(47),BETA(15)
      DATA BETA/0.005,0.01,0.02,0.05,0.1,0.2,0.3,0.4,0.5,0.6,0.7,0.8/
      XMIN=0.
      XMAX=5.
      YMIN=0.
      YMAX=6.
      CCXMIN= 80.
      CCXMAX=580.
      CCYMIN=280.
      CCYMAX=880.
      DO 290 I=1,IEV
      XLOG(I)=ALOG10(EV(I)*1.E2)
      YLOG(I)=ALOG10(ZEX(I))
  290 CONTINUE
      IF (TEST.EQ.0.) GO TO 311
      CALL CCNEXT
      WRITE(98,1) IADJ
    1 FORMAT(5HIADJ=F5.1)
      CALL CCLOGTC(1,5,.05,.1)
      CALL CCLOGTC(2,6,.05,.1)
      CALL CCLOGTC(4,6,.05,.1)
      CALL CCLOGTC(3,5,.05,.1)
      CALL CCLTR (35.,870.,0,2,2H10)
      CALL CCLTR (63.,885.,0,1,1H6)
      CALL CCLTR (35.,770.,0,2,2H10)
      CALL CCLTR (63.,785.,0,1,1H5)
      CALL CCLTR (35.,670.,0,2,2H10)
      CALL CCLTR (63.,685.,0,1,1H4)
      CALL CCLTR (35.,570.,0,2,2H10)
      CALL CCLTR (63.,585.,0,1,1H3)
      CALL CCLTR (35.,470.,0,2,2H10)
      CALL CCLTR (63.,485.,0,1,1H2)
      CALL CCLTR (35.,370.,0,2,2H10)
      CALL CCLTR (63.,385.,0,1,1H1)
      CALL CCLTR (42.,280.,0,2,1H1)
      CALL CCLTR (15.,388.,1,2,25HSTOPPING POWER (MEV/(G/CM )
      CALL CCLTR (-1.,738.,1,1,1H2)
      CALL CCLTR (15.,745.,1,2,2H)))
      CALL CCLTR ( 59.,240.,0,2,2H10)
      CALL CCLTR ( 87.,255.,0,1,2H-2)
      CALL CCLTR (159.,240.,0,2,2H10)
      CALL CCLTR (187.,255.,0,1,2H-1)
      CALL CCLTR (280.,240.,0,2,1H1)
      CALL CCLTR (362.,240.,0,2,2H10)
      CALL CCLTR (390.,255.,0,1,1H1)
      CALL CCLTR (462.,240.,0,2,2H10)
      CALL CCLTR (490.,255.,0,1,1H2)
      CALL CCLTR (562.,240.,0,2,2H10)
      CALL CCLTR (590.,255.,0,1,1H3)
```

```
      CALL CCLTR (155.,205.,0,2,25HSPECIFIC ENERGY (MEV/AMU))
      CALL CCLTR (900.,300.,1,2)
      Y1=ALOG10(5.)+5.
      Y2=Y1-0.05
      YTC(1)=Y1
      XTC(1)=XMIN
      L=2
      CALL CCLTR (302.,285.+100.*Y1,0,2,4HBETA)
      DO 100 I=1,12
      FACT1=1./SQRT(1.-BETA(I)**2)-1.
      FACT2=ALOG10(931.16*FACT1)+2.
      DO 101 J=1,3
      XTC(L)=FACT2
      GO TO (102,103,102),J
  102 YTC(L)=Y1
      GO TO 101
  103 YTC(L)=Y2
  101 L=L+1
      WRITE (98,4) BETA(I)
    4 FORMAT (F4.3)
      CALL CCLTR (88.+100.*FACT2,242.+100.*Y1,1,1)
  100 CONTINUE
      XTC(L)=XMAX
      YTC(L)=Y1
      CALL CCPLOT (XTC,YTC,L,4HJOIN)
      IF (LTRG(1).EQ.6H       ) GO TO 311
    2 FORMAT (3A6)
      WRITE (98,2) (LTRG(I),I=1,3)
      CALL CCLTR (180.,380.,0,2)
  311 CONTINUE
      CALL CCPLOT(XLOG,YLOG,IEV,4HJOIN)
      IF (LTRC.EQ.6H       ) RETURN
    3 FORMAT (A6)
      WRITE (98,3) LTRC
      I=73
      IF (Z.GT.10.) I=90
      CALL CCLTR (80.+100.*XLOG(I),285.+100.*YLOG(I),0,2)
      RETURN
      END
```

```
      SUBROUTINE GRAPH2
C     THIS SUBROUTINE PLOTS STOPPING POWER VS RANGE
      REAL IADJ
      COMMON EV(200),ZEX(200),R(200),XLOG(200),YLOG(200)
      COMMON/GEN/IADJ,LI,LAZ,NO,Z,      NN,II,IEV,ANL,JGRAPH,TEST
      COMMON/GRAF/LTRC,LTRG(3)
      COMMON/CCPOOL/XMIN,XMAX,YMIN,YMAX,CCXMIN,CCXMAX,CCYMIN,CCYMAX
      DIMENSION XE1(20),XE2(20),XE3(20),XE4(20),XE5(20),XE6(20),XE7(20),
     2XE8(20),XE9(20),XE10(20),YE1(20),YE2(20),YE3(20),YE4(20),YE5(20),
     3YE6(20),YE7(20),YE8(20),YE9(20),YE10(20)
      IF(NN.EQ.100) GO TO 327
      XMIN=0.
      XMAX=8.
      YMIN=0.
      YMAX=6.
      CCXMIN=80.
      CCXMAX=880.
      CCYMIN=280.
      CCYMAX=880.
      DO 290 I=1,IEV
      XLOG(I)=ALOG10(R(I)*1.E5)
      YLOG(I)=ALOG10(ZEX(I))
  290 CONTINUE
      IF (TEST.EQ.0.) GO TO 311
      CALL CCNEXT
      WRITE(98,1) IADJ
    1 FORMAT(5HIADJ=F5.1)
      NS=1
      CALL CCLOGTC(1,8,.05,0.1)
      CALL CCLOGTC(2,6,.05,0.1)
      CALL CCLOGTC(4,6,.05,0.1)
      CALL CCLOGTC(3,8,.05,0.1)
      CALL CCLTR (35.,870.,0,2,2H10)
      CALL CCLTR (63.,885.,0,1,1H6)
      CALL CCLTR (35.,770.,0,2,2H10)
      CALL CCLTR (63.,785.,0,1,1H5)
      CALL CCLTR (35.,670.,0,2,2H10)
      CALL CCLTR (63.,685.,0,1,1H4)
      CALL CCLTR (35.,570.,0,2,2H10)
      CALL CCLTR (63.,585.,0,1,1H3)
      CALL CCLTR (35.,470.,0,2,2H10)
      CALL CCLTR (63.,485.,0,1,1H2)
      CALL CCLTR (35.,370.,0,2,2H10)
      CALL CCLTR (63.,385.,0,1,1H1)
      CALL CCLTR (42.,280.,0,2,1H1)
      CALL CCLTR (15.,388.,1,2,25HSTOPPING POWER (MEV/(G/CM )
      CALL CCLTR ( 0.,738.,1,1,1H2)
      CALL CCLTR (15.,745.,1,2,2H)))
      CALL CCLTR ( 59.,240.,0,2,2H10)
      CALL CCLTR ( 87.,255.,0,1,2H-5)
      CALL CCLTR (159.,240.,0,2,2H10)
      CALL CCLTR (187.,255.,0,1,2H-4)
      CALL CCLTR (259.,240.,0,2,2H10)
      CALL CCLTR (287.,255.,0,1,2H-3)
      CALL CCLTR (359.,240.,0,2,2H10)
      CALL CCLTR (387.,255.,0,1,2H-2)
```

```
      CALL CCLTR (459.,240.,0,2,2H10)
      CALL CCLTR (487.,255.,0,1,2H-1)
      CALL CCLTR (580.,240.,0,2,1H1)
      CALL CCLTR (662.,240.,0,2,2H10)
      CALL CCLTR (690.,255.,0,1,1H1)
      CALL CCLTR (762.,240.,0,2,2H10)
      CALL CCLTR (790.,255.,0,1,1H2)
      CALL CCLTR (862.,240.,0,2,2H10)
      CALL CCLTR (890.,255.,0,1,1H3)
      CALL CCLTR (393.,205.,0,2,11HRANGE (G/CM )
      CALL CCLTR (546.,220.,0,1,1H2)
      CALL CCLTR (553.,205.,0,2,1H))
      CALL CCLTR(1100.,300.,1,2)
      IF (LTRG(1).EQ.6H      ) GO TO 311
    3 FORMAT (3A6)
      WRITE (98,3) (LTRG(I),I=1,3)
      CALL CCLTR (180.,350.,0,2)
  311 CONTINUE
      SEND=.01
      K=1
      DO 324 J=1,10
      DO 312 I=K,IEV
      L=I
      IF(EV(I).EQ.SEND)GOTO(313,314,315,316,317,318,319,320,321,322),J
  312 CONTINUE
  323 WRITE(3,2)
    2 FORMAT(52H STATEMENT 323 OF SUBROUTINE GRAPH2 WAS ENCOUNTERED.)
      GO TO 325
  313 XE1(NS)=XLOG(L)
      YE1(NS)=YLOG(L)
      K=L
      SEND=.1
      GO TO 324
  314 XE2(NS)=XLOG(L)
      YE2(NS)=YLOG(L)
      K=L
      SEND=1.
      GO TO 324
  315 XE3(NS)=XLOG(L)
      YE3(NS)=YLOG(L)
      K=L
      SEND=5.
      GO TO 324
  316 XE4(NS)=XLOG(L)
      YE4(NS)=YLOG(L)
      K=L
      SEND=10.
      GO TO 324
  317 XE5(NS)=XLOG(L)
      YE5(NS)=YLOG(L)
      K=L
      SEND=50.
      GO TO 324
  318 XE6(NS)=XLOG(L)
      YE6(NS)=YLOG(L)
      K=L
```

```
      SEND=100.
      GO TO 324
  319 XE7(NS)=XLOG(L)
      YE7(NS)=YLOG(L)
      K=L
      SEND=200.
      GO TO 324
  320 XE8(NS)=XLOG(L)
      YE8(NS)=YLOG(L)
      K=L
      SEND=300.
      GO TO 324
  321 XE9(NS)=XLOG(L)
      YE9(NS)=YLOG(L)
      K=L
      SEND=500.
      GO TO 324
  322 XE10(NS)=XLOG(L)
      YE10(NS)=YLOG(L)
      GO TO 325
  324 CONTINUE
  325 NS=NS+1
      CALL CCPLOT(XLOG,YLOG,IEV,4HJOIN)
      IF (LTRC.EQ.6H      ) RETURN
    4 FORMAT (A6)
      WRITE (98,4) LTRC
      I=28
      IF (Z.GT.10.) I=45
      CALL CCLTR (81.+100.*XLOG(I),285.+100.*YLOG(I),0,2)
      RETURN
  327 N=NS-1
      CALL CCLTR (24.+100.*XE1(1),255.+100.*YE1(1),0,2,12H0.01 MEV/AMU)
      CALL CCPLOT(XE1,YE1,N,6HNOJOIN,6,1)
      CALL CCLTR (62.+100.*XE2(1),255.+100.*YE2(1),0,2,3H0.1)
      CALL CCPLOT(XE2,YE2,N,6HNOJOIN,7,1)
      CALL CCLTR (61.+100.*XE3(1),253.+100.*YE3(1),0,2,3HL.0)
      CALL CCPLOT(XE3,YE3,N,6HNOJOIN,8,1)
      CALL CCLTR (73.+100.*XE4(1),258.+100.*YE4(1),0,2,1H5)
      CALL CCPLOT(XE4,YE4,N,4HJOIN)
      CALL CCLTR (61.+100.*XE5(1),258.+100.*YE5(1),0,2,2H10)
      CALL CCPLOT(XE5,YE5,N,4HJOIN)
      CALL CCLTR (61.+100.*XE6(1),258.+100.*YE6(1),0,2,2H50)
      CALL CCPLOT(XE6,YE6,N,4HJOIN)
      CALL CCLTR (45.+100.*XE7(1),258.+100.*YE7(1),0,2,3H100)
      CALL CCPLOT(XE7,YE7,N,4HJOIN)
      CALL CCLTR (45.+100.*XE8(1),258.+100.*YE8(1),0,2,3H200)
      CALL CCPLOT(XE8,YE8,N,4HJOIN)
      CALL CCLTR (68.+100.*XE9(1),288.+100.*YE9(1),0,2,3H300)
      CALL CCPLOT(XE9,YE9,N,4HJOIN)
      CALL CCLTR (82.+100.*XE10(1),273.+100.*YE10(1),0,2,3H500)
      CALL CCPLOT(XE10,YE10,N,4HJOIN)
      RETURN
      END
```

```
      SUBROUTINE GRAPH3
C     THIS SUBROUTINE PLOTS ENERGY VS RANGE
      REAL IADJ
      COMMON EV(200),ZEX(200),R(200),XLOG(200),YLOG(200)
      COMMON/GEN/IADJ,LI,LAZ,NO,Z,      NN,II,IEV,ANL,JGRAPH,TEST
      COMMON/GRAF/LTRC,LTRG(3)
      COMMON/CCPOOL/XMIN,XMAX,YMIN,YMAX,CCXMIN,CCXMAX,CCYMIN,CCYMAX
      DIMENSION XTC(47),YTC(47),BETA(15)
      DATA BETA/0.005,0.01,0.02,0.05,0.1,0.2,0.3,0.4,0.5,0.6,0.7,0.8/
      XMIN=0.
      XMAX=8.
      YMIN=0.
      YMAX=5.
      CCXMIN=80.
      CCXMAX=880.
      CCYMIN=280.
      CCYMAX=780.
      DO 290 I=1,IEV
      XLOG(I)=ALOG10(R(I))+5.
      YLOG(I)=ALOG10(EV(I))+2.
  290 CONTINUE
      IF (TEST.EQ.0.) GO TO 311
      CALL CCNEXT
      WRITE(98,1) IADJ
    1 FORMAT(5HIADJ=F5.1)
      CALL CCLOGTC(1,8,.05,0.1)
      CALL CCLOGTC(2,5,.05,0.1)
      CALL CCLOGTC(4,5,.05,0.1)
      CALL CCLOGTC(3,8,.05,0.1)
      CALL CCLTR (35.,770.,0,2,2H10)
      CALL CCLTR (63.,785.,0,1,1H3)
      CALL CCLTR (35.,670.,0,2,2H10)
      CALL CCLTR (63.,685.,0,1,1H2)
      CALL CCLTR (35.,570.,0,2,2H10)
      CALL CCLTR (63.,585.,0,1,1H1)
      CALL CCLTR (42.,470.,0,2,1H1)
      CALL CCLTR (30.,370.,0,2,2H10)
      CALL CCLTR (58.,385.,0,1,2H-1)
      CALL CCLTR (30.,280.,0,2,2H10)
      CALL CCLTR (58.,295.,0,1,2H-2)
      CALL CCLTR (15.,355.,1,2,25HSPECIFIC ENERGY (MEV/AMU))
      CALL CCLTR ( 59.,240.,0,2,2H10)
      CALL CCLTR ( 87.,255.,0,1,2H-5)
      CALL CCLTR (159.,240.,0,2,2H10)
      CALL CCLTR (187.,255.,0,1,2H-4)
      CALL CCLTR (259.,240.,0,2,2H10)
      CALL CCLTR (287.,255.,0,1,2H-3)
      CALL CCLTR (359.,240.,0,2,2H10)
      CALL CCLTR (387.,255.,0,1,2H-2)
      CALL CCLTR (459.,240.,0,2,2H10)
      CALL CCLTR (487.,255.,0,1,2H-1)
      CALL CCLTR (580.,240.,0,2,1H1)
      CALL CCLTR (662.,240.,0,2,2H10)
      CALL CCLTR (690.,255.,0,1,1H1)
      CALL CCLTR (762.,240.,0,2,2H10)
      CALL CCLTR (790.,255.,0,1,1H2)
```

```
      CALL CCLTR (862.,240.,0,2,2H10)
      CALL CCLTR (890.,255.,0,1,1H3)
      CALL CCLTR (393.,205.,0,2,11HRANGE (G/CM )
      CALL CCLTR (546.,220.,0,1,1H2)
      CALL CCLTR (553.,205.,0,2,1H))
      CALL CCLTR(1100.,300.,1,2)
      X1=ALOG10(1.4)
      X2=X1+0.05
      XTC(1)=X1
      YTC(1)=YMIN
      CALL CCLTR (100.*X1+143.,502.,1,2,4HBETA)
      L=2
      DO 100 I=1,12
      FACT1=1./SQRT(1.-BETA(I)**2)-1.
      FACT2=ALOG10(931.16*FACT1)+2.
      DO 101 J=1,3
      YTC(L)=FACT2
      GO TO (102,103,102),J
  102 XTC(L)=X1
      GO TO 101
  103 XTC(L)=X2
  101 L=L+1
      WRITE (98,5) BETA(I)
    5 FORMAT (F4.3)
      CALL CCLTR (90.+100.*X1,280.+100.*FACT2,0,1)
  100 CONTINUE
      XTC(L)=X1
      YTC(L)=YMAX
      CALL CCPLOT (XTC,YTC,L,4HJOIN)
      IF (LTRG(1).EQ.6H      ) GO TO 311
    2 FORMAT (3A6)
      WRITE (98,2) (LTRG(I),I=1,3)
      CALL CCLTR (580.,380.,0,2)
  311 CONTINUE
      CALL CCPLOT(XLOG,YLOG,IEV,4HJOIN)
      IF (LTRC.EQ.6H      ) RETURN
    3 FORMAT (A6)
      WRITE (98,3) LTRC
      CALL CCLTR (80.+100.*XLOG(IEV),283.+100.*YLOG(IEV),0,1)
      RETURN
      END
```

4. Sample Problems

The 20 data cards which appear on the following page instructs the program which is listed on the previous pages to perform stopping power and range calculations for the following combinations of ions and stopping media:

1. Carbon ions in water.
2. Argon ions in water.
3. Neon ions in aluminum.
4. Uranium ions in uranium.

The output for these 4 problems are respectively representative of the output for 4 types of problems defined by:

1. $Z_1 \leq 10$ and the stopping medium is a compound or a mixture.
2. $Z_1 > 10$ and the stopping medium is a compound or a mixture.
3. $Z_1 \leq 10$ and the stopping medium is a pure element.
4. $Z_1 > 10$ and the stopping medium is a pure element.

The first 2 problems each contain a SRGRAP card (the final H is not read since it is outside the field defined by the A6 format) which is the instruction that causes the graph to be plotted which appears as Fig. 31. The output for the 4 problems appears on pages 138 through 150. Note that for the second and fourth types of problems, the nuclear coulomb stopping power (elastic) and the electronic stopping power (inelastic) are listed separately in the low-specific-energy region. For the third and fourth types, the output at low specific energies is also given in the dimensionless units of Lindhard et al. (LSS). The electronic stopping power constant k (see Eq. (16)) is also given for the last two types of problems.

```
ION          6.          12.
TARGET       2.
1.           1.          2.
8.           16.         1.
SRGRAPH
C            IN WATER
GO
SRGRAPH
AR
ION          18.         40.
GO
TARGET
13.          26.9815
ION          10.         20.
GO
ION          92.         238.
TARGET
92.          238.
GO
STOP
```

XBL 686-910

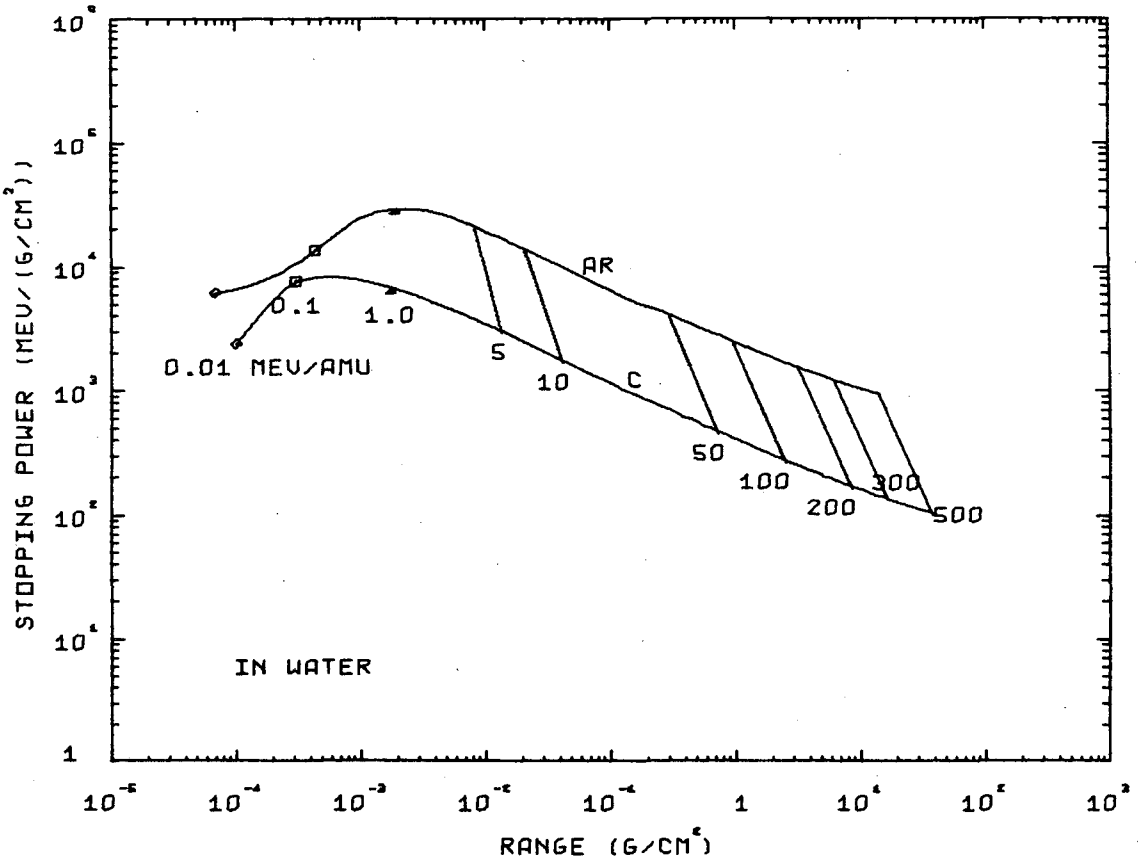

Fig. 31. This figure is a part of the sample problems. It was generated in response to the SRGRAP cards which appear in the first two problems (see page 101).

DATA CARDS PRINTED.

```
******ION      6.000000E+00   1.200000E+01  -0.          -0.          -0.          -0.          -0.
******TARGET   2.000000E+00  -0.            -0.          -0.          -0.          -0.          -0.
******   1.000000E+00   1.000000E+00   2.000000E+00  -0.
******   8.000000E+00   1.600000E+01   1.000000E+00  -0.
******SRGRAP  -0.           -0.           -0.          -0.          -0.          -0.          -0.
******GO      -0.           -0.           -0.          -0.          -0.          -0.          -0.
```

TARGET IS A COMPOUND

```
IADJ=  64.85193
A    =  12.00000
Z    =   6.00000
AT1=   1.00000 AT2=  16.00000 AT3=
ZT1=   1.00000 ZT2=   8.00000 ZT3=
NT1=   2.00000 NT2=   1.00000 NT3=
```

NORMALIZING CONSTANT= 1.032052

E (MEV/AMU)	DE/DX (MEV/GM/SQCM)	R(E) (GM/SQCM)	SLOPE OF DE/DX (SQCM/GM)
.010	2.368944E+03	1.013110E-04	-0.
.015	3.050073E+03	1.235016E-04	1.042160E+04
.020	3.619536E+03	1.415077E-04	8.701976E+03
.030	4.474398E+03	1.711692E-04	6.576427E+03
.040	5.197878E+03	1.959861E-04	5.304613E+03
.050	5.747505E+03	2.179091E-04	4.307580E+03
.070	6.650455E+03	2.566042E-04	3.157053E+03
.100	7.460166E+03	3.075679E-04	1.750475E+03
.150	8.011728E+03	3.850072E-04	6.585454E+02
.200	8.250420E+03	4.587569E-04	2.275391E+02
.300	8.114792E+03	6.054981E-04	-1.511697E+02
.400	7.887613E+03	7.555977E-04	-2.130211E+02
.500	7.603541E+03	9.106652E-04	-2.130658E+02
.700	7.205754E+03	1.235430E-03	-1.705613E+02
1.000	6.565723E+03	1.760449E-03	-1.647515E+02
1.500	5.707563E+03	2.746015E-03	-1.343989E+02
2.000	4.952936E+03	3.879278E-03	-1.090751E+02
3.000	4.044742E+03	6.583256E-03	-6.537663E+01
4.000	3.383897E+03	9.845034E-03	-4.782788E+01
5.000	2.896873E+03	1.369270E-02	-3.594563E+01
7.000	2.256883E+03	2.316911E-02	-2.224066E+01
10.000	1.695200E+03	4.179387E-02	-1.170942E+01
10.380	1.644054E+03	4.452569E-02	-1.089579E+01
12.000	1.458803E+03	5.710344E-02	-8.524393E+00
14.000	1.283994E+03	7.467944E-02	-6.449044E+00
16.000	1.149249E+03	9.447070E-02	-5.039963E+00
18.000	1.042076E+03	1.164313E-01	-4.052856E+00
20.000	9.547123E+02	1.405192E-01	-3.333388E+00
22.000	8.820735E+02	1.666957E-01	-2.792192E+00
24.000	8.206870E+02	1.949248E-01	-2.374492E+00
26.000	7.680979E+02	2.251723E-01	-2.045135E+00
28.000	7.225205E+02	2.574064E-01	-1.780699E+00
30.000	6.826244E+02	2.915966E-01	-1.565069E+00
32.000	6.473972E+02	3.277138E-01	-1.386859E+00

XBL 686-897

34.000	6.160551E+02	3.657306E-01	-1.237833E+00
36.000	5.879813E+02	4.056203E-01	-1.111909E+00
38.000	5.626835E+02	4.473575E-01	-1.004520E+00
40.000	5.397643E+02	4.909178E-01	-9.121762E-01
42.000	5.188990E+02	5.362775E-01	-8.321754E-01
44.000	4.998199E+02	5.834139E-01	-7.623986E-01
46.000	4.823039E+02	6.323049E-01	-7.011644E-01
48.000	4.661640E+02	6.829292E-01	-6.471243E-01
50.000	4.512419E+02	7.352662E-01	-6.003684E-01
55.000	4.184274E+02	8.734712E-01	-5.037364E-01
60.000	3.907935E+02	1.021958E+00	-4.269895E-01
65.000	3.671887E+02	1.180449E+00	-3.667744E-01
70.000	3.467806E+02	1.348681E+00	-3.186318E-01
75.000	3.289529E+02	1.526409E+00	-2.795163E-01
80.000	3.132387E+02	1.713400E+00	-2.472893E-01
85.000	2.992781E+02	1.909432E+00	-2.204125E-01
90.000	2.867892E+02	2.114296E+00	-1.977557E-01
95.000	2.755474E+02	2.327793E+00	-1.784733E-01
100.000	2.653724E+02	2.549731E+00	-1.619223E-01
105.000	2.561168E+02	2.779928E+00	-1.476063E-01
110.000	2.476596E+02	3.018210E+00	-1.351373E-01
115.000	2.399003E+02	3.264409E+00	-1.242083E-01
120.000	2.327546E+02	3.518365E+00	-1.145739E-01
125.000	2.261514E+02	3.779923E+00	-1.060356E-01
130.000	2.200303E+02	4.048935E+00	-9.843210E-02
135.000	2.143396E+02	4.325256E+00	-9.163053E-02
140.000	2.090347E+02	4.608749E+00	-8.552105E-02
145.000	2.040771E+02	4.899280E+00	-8.001206E-02
150.000	1.994332E+02	5.196720E+00	-7.502670E-02
155.000	1.950739E+02	5.500944E+00	-7.050007E-02
160.000	1.909732E+02	5.811832E+00	-6.637708E-02
165.000	1.871086E+02	6.129266E+00	-6.261069E-02
170.000	1.834599E+02	6.453133E+00	-5.916056E-02
175.000	1.800093E+02	6.783323E+00	-5.599192E-02
180.000	1.767409E+02	7.119730E+00	-5.307469E-02
185.000	1.736404E+02	7.462249E+00	-5.038269E-02
190.000	1.706950E+02	7.810781E+00	-4.789311E-02
195.000	1.678932E+02	8.165226E+00	-4.558596E-02
200.000	1.652247E+02	8.525489E+00	-4.346734E-02
210.000	1.602506E+02	9.263104E+00	-3.965516E-02
220.000	1.557074E+02	1.002291E+01	-3.628999E-02
230.000	1.515410E+02	1.080424E+01	-3.333994E-02
240.000	1.477058E+02	1.160643E+01	-3.073876E-02
250.000	1.441637E+02	1.242889E+01	-2.843301E-02
260.000	1.408819E+02	1.327102E+01	-2.637912E-02
270.000	1.378327E+02	1.413226E+01	-2.454132E-02
280.000	1.349920E+02	1.501208E+01	-2.289002E-02
290.000	1.323391E+02	1.590998E+01	-2.140055E-02
300.000	1.298559E+02	1.682545E+01	-2.005219E-02
310.000	1.275266E+02	1.775803E+01	-1.882748E-02
320.000	1.253373E+02	1.870726E+01	-1.771159E-02
330.000	1.232758E+02	1.967272E+01	-1.669183E-02
340.000	1.213312E+02	2.065398E+01	-1.575737E-02
350.000	1.194940E+02	2.165064E+01	-1.489883E-02
360.000	1.177555E+02	2.266232E+01	-1.410811E-02
370.000	1.161081E+02	2.368864E+01	-1.337817E-02
380.000	1.145447E+02	2.472924E+01	-1.270286E-02
390.000	1.130594E+02	2.578378E+01	-1.207680E-02
400.000	1.116463E+02	2.685191E+01	-1.149525E-02
410.000	1.103005E+02	2.793332E+01	-1.095404E-02
420.000	1.090173E+02	2.902768E+01	-1.044948E-02
430.000	1.077926E+02	3.013470E+01	-9.978291E-03

XBL 686-898

440.000	1.066226E+02	3.125408E+01	-9.537557E-03
450.000	1.055036E+02	3.238554E+01	-9.124675E-03
460.000	1.044326E+02	3.352880E+01	-8.737318E-03
470.000	1.034067E+02	3.468358E+01	-8.373396E-03
480.000	1.024230E+02	3.584964E+01	-8.031032E-03
490.000	1.014792E+02	3.702672E+01	-7.708534E-03
500.000	1.005730E+02	3.821458E+01	-0.

TIME= 1.123

XBL 686-899

DATA CARDS PRINTED.

```
******SRGRAP  -0.            -0.            -0.          -0.          -0.          -0.          -0.
******ION      1.800000E+01   4.000000E+01  -0.          -0.          -0.          -0.          -0.
******GO      -0.            -0.            -0.          -0.          -0.          -0.          -0.
```

TARGET IS A COMPOUND

```
IADJ=  64.85193
A    =  40.00000
Z    =  18.00000
AT1=    1.00000 AT2=   16.00000 AT3=
ZT1=    1.00000 ZT2=    8.00000 ZT3=
NT1=    2.00000 NT2=    1.00000 NT3=
```

BOUNDARIES BETWEEN THE FOUR ENERGY REGIONS ARE
.170 2.000 82.012

E (MEV/AMU)	NUC.S.P., (MEV/GM/SQCM)	ELEC. S.P. (MEV/GM/SQCM)	DE/DX (MEV/GM/SQCM)	R (GM/SQCM)
.010	1.844193E+03	4.219608E+03	6.063801E+03	6.852845E-05
.015	1.338278E+03	5.167943E+03	6.506221E+03	1.003913E-04
.020	1.027047E+03	5.967426E+03	6.994474E+03	1.300332E-04
.030	6.674182E+02	7.308575E+03	7.975993E+03	1.835205E-04
.040	4.699450E+02	8.439215E+03	8.909160E+03	2.309122E-04
.050	3.481253E+02	9.435329E+03	9.783455E+03	2.737123E-04
.060	2.672254E+02	1.033589E+04	1.060311E+04	3.129527E-04
.070	2.106568E+02	1.116403E+04	1.137469E+04	3.493505E-04
.080	1.695529E+02	1.193485E+04	1.210441E+04	3.834204E-04
.090	1.387798E+02	1.265882E+04	1.279760E+04	4.155431E-04
.100	1.151812E+02	1.334357E+04	1.345875E+04	4.460089E-04
.150	5.255081E+01	1.634247E+04	1.639502E+04	5.800083E-04
.200	2.808268E+01	1.887066E+04	1.889874E+04	6.933386E-04

E (MEV/AMU)	DE/DX (MEV/GM/SQCM)	R(E) (GM/SQCM)	SLOPE OF DE/DX (SQCM/GM)
.010	6.063801E+03	6.852845E-05	-0.
.015	6.506221E+03	1.003913E-04	2.326682E+03
.020	6.994474E+03	1.300332E-04	2.445441E+03
.030	7.975993E+03	1.835205E-04	2.393358E+03
.040	8.909160E+03	2.309122E-04	2.259327E+03
.050	9.783455E+03	2.737123E-04	2.117438E+03
.060	1.060311E+04	3.129527E-04	1.989043E+03
.070	1.137469E+04	3.493505E-04	1.876618E+03
.080	1.210441E+04	3.834204E-04	1.778642E+03
.090	1.279760E+04	4.155431E-04	1.692933E+03
.100	1.345875E+04	4.460089E-04	1.622084E+03
.150	1.639502E+04	5.800083E-04	1.359997E+03
.200	1.889874E+04	6.933386E-04	1.137148E+03
.300	2.252964E+04	8.854855E-04	7.330933E+02
.400	2.476349E+04	1.054166E-03	4.592215E+02

.500	2.620341E+04	1.210859E-03	2.983058E+02
.600	2.714993E+04	1.360635E-03	1.959437E+02
.700	2.777096E+04	1.506188E-03	1.272525E+02
.800	2.816795E+04	1.649124E-03	7.936043E+01
.900	2.840584E+04	1.790477E-03	4.501047E+01
1.000	2.852804E+04	1.930950E-03	2.275915E+01
1.500	2.820430E+04	2.633735E-03	-3.189856E+01
2.000	2.725210E+04	3.354473E-03	-5.421587E+01
2.500	2.603566E+04	4.105019E-03	-6.214956E+01
3.000	2.476611E+04	4.892517E-03	-6.323734E+01
3.500	2.350617E+04	5.721428E-03	-6.187112E+01
4.000	2.229127E+04	6.595224E-03	-5.915870E+01
4.500	2.113982E+04	7.516683E-03	-5.578565E+01
5.000	2.005984E+04	8.488076E-03	-5.216539E+01
5.500	1.905320E+04	9.511296E-03	-4.853974E+01
6.000	1.811825E+04	1.058796E-02	-4.504423E+01
6.500	1.725143E+04	1.171945E-02	-3.662759E+01
7.000	1.665315E+04	1.290667E-02	-3.176494E+01
7.500	1.598084E+04	1.413287E-02	-3.243373E+01
8.000	1.535580E+04	1.540981E-02	-3.016530E+01
8.500	1.477423E+04	1.673786E-02	-2.808308E+01
9.000	1.423248E+04	1.811731E-02	-2.617668E+01
9.500	1.372716E+04	1.954840E-02	-2.443350E+01
10.000	1.325514E+04	2.103130E-02	-2.283482E+01
10.380	1.291690E+04	2.219303E-02	-2.174924E+01
12.000	1.164657E+04	2.748317E-02	-1.789167E+01
14.000	1.038434E+04	3.476966E-02	-1.422349E+01
16.000	9.370812E+03	4.289040E-02	-1.152545E+01
18.000	8.540267E+03	5.184295E-02	-9.520360E+00
20.000	7.847554E+03	6.162405E-02	-7.995949E+00
22.000	7.260915E+03	7.223038E-02	-6.812964E+00
24.000	6.757480E+03	8.365891E-02	-5.878067E+00
26.000	6.320424E+03	9.590712E-02	-5.127241E+00
28.000	5.937121E+03	1.089732E-01	-4.515589E+00
30.000	5.597930E+03	1.228560E-01	-4.010961E+00
32.000	5.295368E+03	1.375552E-01	-3.562642E+00
34.000	5.027907E+03	1.530702E-01	-2.632880E+00
36.000	4.874107E+03	1.692310E-01	-1.893821E+00
38.000	4.724896E+03	1.859022E-01	-1.832005E+00
40.000	4.580986E+03	2.030987E-01	-1.762876E+00
42.000	4.442836E+03	2.208328E-01	-1.689297E+00
44.000	4.310699E+03	2.391147E-01	-1.613530E+00
46.000	4.184671E+03	2.579521E-01	-1.537319E+00
48.000	4.064728E+03	2.773512E-01	-1.461978E+00
50.000	3.950754E+03	2.973164E-01	-1.389172E+00
55.000	3.690666E+03	3.497222E-01	-1.219469E+00
60.000	3.462967E+03	4.056963E-01	-1.068042E+00
65.000	3.263449E+03	4.652193E-01	-9.372833E-01
70.000	3.088053E+03	5.282492E-01	-8.257408E-01
75.000	2.933153E+03	5.947304E-01	-7.310534E-01
80.000	2.795632E+03	6.645992E-01	-5.991238E-01
85.000	2.693503E+03	7.372037E-01	-5.363241E-01
90.000	2.581102E+03	8.130794E-01	-5.339404E-01
95.000	2.479927E+03	8.921522E-01	-4.818780E-01
100.000	2.388351E+03	9.743515E-01	-4.371902E-01
105.000	2.305051E+03	1.059610E+00	-3.985370E-01
110.000	2.228936E+03	1.147862E+00	-3.648707E-01
115.000	2.159103E+03	1.239047E+00	-3.353625E-01
120.000	2.094791E+03	1.333105E+00	-3.093494E-01
125.000	2.035363E+03	1.429978E+00	-2.862962E-01
130.000	1.980273E+03	1.529612E+00	-2.657667E-01
135.000	1.929056E+03	1.631953E+00	-2.474024E-01

XBL 686-901

140.000	1.881312E+03	1.736951E+00	-2.309068E-01
145.000	1.836693E+03	1.844555E+00	-2.160326E-01
150.000	1.794899E+03	1.954718E+00	-2.025721E-01
155.000	1.755665E+03	2.067393E+00	-1.903502E-01
160.000	1.718759E+03	2.182537E+00	-1.792181E-01
165.000	1.683977E+03	2.300105E+00	-1.690489E-01
170.000	1.651139E+03	2.420056E+00	-1.597335E-01
175.000	1.620084E+03	2.542349E+00	-1.511782E-01
180.000	1.590668E+03	2.666944E+00	-1.433017E-01
185.000	1.562763E+03	2.793803E+00	-1.360333E-01
190.000	1.536255E+03	2.922888E+00	-1.293114E-01
195.000	1.511039E+03	3.054164E+00	-1.230821E-01
200.000	1.487022E+03	3.187595E+00	-1.173618E-01
210.000	1.442255E+03	3.460786E+00	-1.070689E-01
220.000	1.401367E+03	3.742197E+00	-9.798297E-02
230.000	1.363869E+03	4.031576E+00	-9.001783E-02
240.000	1.329353E+03	4.328686E+00	-8.299466E-02
250.000	1.297473E+03	4.633299E+00	-7.676912E-02
260.000	1.267937E+03	4.945198E+00	-7.122361E-02
270.000	1.240494E+03	5.264177E+00	-6.626157E-02
280.000	1.214928E+03	5.590038E+00	-6.180307E-02
290.000	1.191052E+03	5.922591E+00	-5.778148E-02
300.000	1.168703E+03	6.261654E+00	-5.414092E-02
310.000	1.147739E+03	6.607053E+00	-5.083421E-02
320.000	1.128035E+03	6.958622E+00	-4.782128E-02
330.000	1.109482E+03	7.316199E+00	-4.506795E-02
340.000	1.091981E+03	7.679629E+00	-4.254490E-02
350.000	1.075446E+03	8.048763E+00	-4.022684E-02
360.000	1.059800E+03	8.423459E+00	-3.809190E-02
370.000	1.044973E+03	8.803578E+00	-3.612106E-02
380.000	1.030903E+03	9.188986E+00	-3.429772E-02
390.000	1.017534E+03	9.579554E+00	-3.260735E-02
400.000	1.004817E+03	9.975159E+00	-3.103717E-02
410.000	9.927046E+02	1.037568E+01	-2.957591E-02
420.000	9.811561E+02	1.078100E+01	-2.821360E-02
430.000	9.701337E+02	1.119101E+01	-2.694139E-02
440.000	9.596030E+02	1.160559E+01	-2.575140E-02
450.000	9.495326E+02	1.202465E+01	-2.463662E-02
460.000	9.398937E+02	1.244808E+01	-2.359076E-02
470.000	9.306600E+02	1.287578E+01	-2.260817E-02
480.000	9.218072E+02	1.330765E+01	-2.168379E-02
490.000	9.133130E+02	1.374361E+01	-2.081304E-02
500.000	9.051567E+02	1.418356E+01	-0.

TIME= 2.071

XBL 686-902

DATA CARDS PRINTED.

```
******TARGET  -0.          -0.          -0.          -0.          -0.          -0.          -0.
******   1.300000E+01  2.698150E+01  -0.          -0.
******ION      1.000000E+01  2.000000E+01  -0.          -0.          -0.          -0.          -0.
******GO     -0.          -0.          -0.          -0.          -0.          -0.          -0.
```

TARGET IS PURE ELEMENT

IADJ= 162.99837
A = 20.00000
Z = 10.00000
AT = 26.98150
ZT = 13.00000

NORMALIZING CONSTANT= 1.000000

LSS ELECT. S.P. CONSTANT= .16152

E (MEV/AMU)	E(LSS) (DIMENSIONLESS)	DE/DX (MEV/GM/SQCM)	DE/DX(LSS) (DIMENSIONLESS)	R (GM/SQCM)	R(LSS) (DIMENSIONLESS)
.010	9.012425E+00	1.952161E+03	5.940107E-01	2.049012E-04	3.033632E+01
.015	1.351864E+01	2.357567E+03	7.173692E-01	2.512874E-04	3.720397E+01
.020	1.802485E+01	2.762600E+03	8.406142E-01	2.903638E-04	4.298936E+01
.030	2.703728E+01	3.265490E+03	9.936355E-01	3.566544E-04	5.280392E+01
.040	3.604970E+01	3.870240E+03	1.177651E+00	4.127516E-04	6.110930E+01
.050	4.506213E+01	4.372824E+03	1.330579E+00	4.612877E-04	6.829523E+01
.070	6.308698E+01	5.073043E+03	1.543644E+00	5.459396E-04	8.082824E+01
.100	9.012425E+01	6.073143E+03	1.847958E+00	6.536049E-04	9.676846E+01
.150	1.351864E+02	7.066917E+03	2.150348E+00	8.056154E-04	1.192741E+02
.200	1.802485E+02	7.760089E+03	2.361268E+00	9.403989E-04	1.392293E+02
.300	2.703728E+02	8.748166E+03	2.661924E+00	1.182303E-03	1.750440E+02
.400	3.604970E+02	9.137371E+03	2.780353E+00	1.405784E-03	2.081312E+02
.500	4.506213E+02	9.328991E+03	2.838660E+00	1.622327E-03	2.401910E+02
.700	6.308698E+02	9.417378E+03	2.865555E+00	2.048970E-03	3.033570E+02
1.000	9.012425E+02	9.007508E+03	2.740838E+00	2.701338E-03	3.999423E+02
1.500	1.351864E+03	8.401254E+03	2.556365E+00	3.853815E-03	5.705706E+02
2.000	1.802485E+03	7.600000E+03	2.312556E+00	5.108816E-03	7.563778E+02
3.000	2.703728E+03	6.700000E+03	2.038701E+00	7.925350E-03	1.173375E+03
4.000	3.604970E+03	5.800000E+03	1.764845E+00	1.114755E-02	1.650433E+03
5.000	4.506213E+03	5.250000E+03	1.597489E+00	1.478017E-02	2.188254E+03
7.000	6.308698E+03	4.200000E+03	1.277992E+00	2.336953E-02	3.459940E+03
10.000	9.012425E+03	3.409098E+03	1.037333E+00	3.935314E-02	5.826369E+03
10.380	9.354897E+03	3.311431E+03	1.007614E+00	4.161538E-02	6.161300E+03
12.000	1.081491E+04	2.955592E+03	8.993385E-01	5.199088E-02	7.697429E+03
14.000	1.261740E+04	2.616660E+03	7.962069E-01	6.640472E-02	9.831448E+03

E (MEV/AMU)	DE/DX (MEV/GM/SQCM)	R(E) (GM/SQCM)	SLOPE OF DE/DX (SQCM/GM)
.010	1.952161E+03	2.049012E-04	-0.
.015	2.357567E+03	2.512874E-04	4.052198E+03

XBL 686-903

.020	2.762600E+03	2.903638E-04	3.538372E+03
.030	3.265490E+03	3.566544E-04	2.769100E+03
.040	3.870240E+03	4.127516E-04	2.768333E+03
.050	4.372824E+03	4.612877E-04	2.258794E+03
.070	5.073043E+03	5.459396E-04	1.717062E+03
.100	6.073143E+03	6.536049E-04	1.414436E+03
.150	7.066917E+03	8.056154E-04	8.434729E+02
.200	7.760089E+03	9.403989E-04	6.267942E+02
.300	8.748166E+03	1.182303E-03	3.443206E+02
.400	9.137371E+03	1.405784E-03	1.452061E+02
.500	9.328991E+03	1.622327E-03	7.123880E+01
.700	9.417378E+03	2.048970E-03	-1.406659E+01
1.000	9.007508E+03	2.701338E-03	-6.542931E+01
1.500	8.401254E+03	3.853815E-03	-7.037539E+01
2.000	7.600000E+03	5.108816E-03	-6.841692E+01
3.000	6.700000E+03	7.925350E-03	-4.500000E+01
4.000	5.800000E+03	1.114755E-02	-3.625000E+01
5.000	5.250000E+03	1.478017E-02	-2.708333E+01
7.000	4.200000E+03	2.336953E-02	-2.102268E+01
10.000	3.409098E+03	3.935314E-02	-1.288809E+01
10.380	3.311431E+03	4.161538E-02	-1.249593E+01
12.000	2.955592E+03	5.199088E-02	-9.859698E+00
14.000	2.616660E+03	6.640472E-02	-7.530028E+00
16.000	2.353190E+03	8.255041E-02	-5.931087E+00
18.000	2.142173E+03	1.003888E-01	-4.800440E+00
20.000	1.969155E+03	1.198844E-01	-3.969906E+00
22.000	1.824580E+03	1.410050E-01	-3.341016E+00
24.000	1.701873E+03	1.637205E-01	-2.852851E+00
26.000	1.596352E+03	1.880030E-01	-2.466003E+00
28.000	1.504593E+03	2.138262E-01	-2.154030E+00
30.000	1.424030E+03	2.411655E-01	-1.898630E+00
32.000	1.352703E+03	2.699972E-01	-1.686799E+00
34.000	1.289086E+03	3.002991E-01	-1.509086E+00
36.000	1.231976E+03	3.320497E-01	-1.358482E+00
38.000	1.180408E+03	3.652287E-01	-1.229698E+00
40.000	1.133600E+03	3.998165E-01	-1.118681E+00
42.000	1.090913E+03	4.357942E-01	-1.022283E+00
44.000	1.051817E+03	4.731436E-01	-9.380263E-01
46.000	1.015871E+03	5.118473E-01	-8.639379E-01
48.000	9.827023E+02	5.518882E-01	-7.984329E-01
50.000	9.519963E+02	5.932501E-01	-7.416419E-01
55.000	8.843340E+02	7.023306E-01	-6.239664E-01
60.000	8.272031E+02	8.193333E-01	-5.302220E-01
65.000	7.782896E+02	9.440385E-01	-4.564398E-01
70.000	7.359151E+02	1.076241E+00	-3.972870E-01
75.000	6.988321E+02	1.215746E+00	-3.491081E-01
80.000	6.660935E+02	1.362373E+00	-3.093266E-01
85.000	6.369668E+02	1.515949E+00	-2.760837E-01
90.000	6.108767E+02	1.676308E+00	-2.480101E-01
95.000	5.873648E+02	1.843296E+00	-2.240786E-01
100.000	5.660610E+02	2.016764E+00	-2.035061E-01
105.000	5.466636E+02	2.196569E+00	-1.856872E-01
110.000	5.289236E+02	2.382575E+00	-1.701474E-01
115.000	5.126341E+02	2.574652E+00	-1.565107E-01
120.000	4.976214E+02	2.772676E+00	-1.444761E-01
125.000	4.837389E+02	2.976525E+00	-1.337999E-01
130.000	4.708615E+02	3.186084E+00	-1.242833E-01
135.000	4.588822E+02	3.401242E+00	-1.157627E-01
140.000	4.477089E+02	3.621891E+00	-1.081027E-01
145.000	4.372617E+02	3.847927E+00	-1.011901E-01
150.000	4.274709E+02	4.079250E+00	-9.492988E-02
155.000	4.182757E+02	4.315763E+00	-8.924162E-02

XBL 686-904

160.000	4.096226E+02	4.557373E+00	-8.405708E-02
165.000	4.014643E+02	4.803988E+00	-7.931795E-02
170.000	3.937590E+02	5.055520E+00	-7.497413E-02
175.000	3.864694E+02	5.311885E+00	-7.098243E-02
180.000	3.795625E+02	5.572998E+00	-6.730540E-02
185.000	3.730084E+02	5.838781E+00	-6.391051E-02
190.000	3.667804E+02	6.109154E+00	-6.076931E-02
195.000	3.608545E+02	6.384041E+00	-5.785690E-02
200.000	3.552090E+02	6.663369E+00	-5.518109E-02
210.000	3.446823E+02	7.235062E+00	-5.036330E-02
220.000	3.350637E+02	7.823679E+00	-4.610735E-02
230.000	3.262394E+02	8.428694E+00	-4.237361E-02
240.000	3.181142E+02	9.049610E+00	-3.907915E-02
250.000	3.106077E+02	9.685949E+00	-3.615695E-02
260.000	3.036515E+02	1.033726E+01	-3.355240E-02
270.000	2.971868E+02	1.100311E+01	-3.122057E-02
280.000	2.911632E+02	1.168308E+01	-2.912427E-02
290.000	2.855371E+02	1.237678E+01	-2.723247E-02
300.000	2.802702E+02	1.308382E+01	-2.551911E-02
310.000	2.753294E+02	1.380385E+01	-2.396219E-02
320.000	2.706854E+02	1.453652E+01	-2.254302E-02
330.000	2.663122E+02	1.528147E+01	-2.124561E-02
340.000	2.621871E+02	1.603841E+01	-2.005628E-02
350.000	2.582897E+02	1.680700E+01	-1.896319E-02
360.000	2.546018E+02	1.758696E+01	-1.795612E-02
370.000	2.511073E+02	1.837799E+01	-1.702616E-02
380.000	2.477914E+02	1.917981E+01	-1.616555E-02
390.000	2.446410E+02	1.999216E+01	-1.536746E-02
400.000	2.416444E+02	2.081477E+01	-1.462592E-02
410.000	2.387907E+02	2.164740E+01	-1.393563E-02
420.000	2.360701E+02	2.248980E+01	-1.329192E-02
430.000	2.334739E+02	2.334174E+01	-1.269064E-02
440.000	2.309939E+02	2.420298E+01	-1.212810E-02
450.000	2.286227E+02	2.507331E+01	-1.160098E-02
460.000	2.263535E+02	2.595252E+01	-1.110635E-02
470.000	2.241801E+02	2.684039E+01	-1.064154E-02
480.000	2.220969E+02	2.773673E+01	-1.020418E-02
490.000	2.200985E+02	2.864134E+01	-9.792124E-03
500.000	2.181800E+02	2.955404E+01	-0.

TIME= 2.487

XBL 686-905

DATA CARDS PRINTED.

```
******ION      9.200000E+01   2.380000E+02  -0.          -0.          -0.          -0.          -0.
******TARGET  -0.            -0.           -0.          -0.          -0.          -0.          -0.
******   9.200000E+01   2.380000E+02  -0.          -0.
******GO      -0.            -0.           -0.          -0.          -0.          -0.          -0.
```

TARGET IS PURE ELEMENT

IADJ= 922.82334
A = 238.00000
Z = 92.00000
AT = 238.00000
ZT = 92.00000

BOUNDARIES BETWEEN THE FOUR ENERGY REGIONS ARE
.505 2.000 INFINITE

LSS ELECT. S.P. CONSTANT= .17618

E (MEV/AMU)	E(LSS) (DIMENSIONLESS)	NUC. S.P. (MEV/GM/SQCM)	ELEC. S.P. (MEV/GM/SQCM)	DE/DX (MEV/GM/SQCM)	DE/DX(LSS) (DIMENSIONLESS)	R (GM/SQCM)	R(LSS) (DIMENSIONLESS)
.010	7.163816E-01	5.366298E+03	2.575220E+03	7.941519E+03	5.580031E-01	3.473605E-04	1.487648E+00
.015	1.074572E+00	4.992354E+03	3.153988E+03	8.146342E+03	5.723949E-01	4.951227E-04	2.120473E+00
.020	1.432763E+00	4.650822E+03	3.641912E+03	8.292733E+03	5.826809E-01	6.398297E-04	2.740213E+00
.030	2.149145E+00	4.081919E+03	4.460412E+03	8.542331E+03	6.002186E-01	9.224732E-04	3.950697E+00
.040	2.865526E+00	3.633593E+03	5.150441E+03	8.784034E+03	6.172016E-01	1.197175E-03	5.127169E+00
.050	3.581908E+00	3.271323E+03	5.758368E+03	9.029691E+03	6.344625E-01	1.464372E-03	6.271498E+00
.060	4.298290E+00	2.971779E+03	6.307976E+03	9.279755E+03	6.520330E-01	1.724333E-03	7.384841E+00
.070	5.014671E+00	2.719410E+03	6.813393E+03	9.532803E+03	6.698131E-01	1.977340E-03	8.468400E+00
.080	5.731053E+00	2.503525E+03	7.283823E+03	9.787348E+03	6.876985E-01	2.223698E-03	9.523483E+00
.090	6.447435E+00	2.316525E+03	7.725661E+03	1.004219E+04	7.056045E-01	2.463727E-03	1.055146E+01
.100	7.163816E+00	2.152844E+03	8.143562E+03	1.029641E+04	7.234669E-01	2.697746E-03	1.155370E+01
.150	1.074572E+01	1.566697E+03	9.973786E+03	1.154048E+04	8.108808E-01	3.788252E-03	1.622403E+01
.200	1.432763E+01	1.204829E+03	1.151674E+04	1.272156E+04	8.938684E-01	4.769438E-03	2.042618E+01
.300	2.149145E+01	7.852506E+02	1.410506E+04	1.489031E+04	1.046253E+00	6.494214E-03	2.781292E+01
.400	2.865526E+01	5.540566E+02	1.628712E+04	1.684118E+04	1.183329E+00	7.994585E-03	3.423859E+01
.500	3.581908E+01	4.110763E+02	1.820956E+04	1.862063E+04	1.308361E+00	9.336978E-03	3.998769E+01
.600	4.298290E+01	3.159388E+02	1.994757E+04	2.026351E+04	1.423796E+00	1.056117E-02	4.523055E+01
.700	5.014671E+01	0.	2.177510E+04	2.177510E+04	1.530006E+00	1.169333E-02	5.007928E+01
.800	5.731053E+01	0.	2.316491E+04	2.316491E+04	1.627660E+00	1.275243E-02	5.461514E+01
.900	6.447435E+01	0.	2.445837E+04	2.445837E+04	1.718544E+00	1.375189E-02	5.889553E+01
1.000	7.163816E+01	0.	2.567351E+04	2.567351E+04	1.803924E+00	1.470135E-02	6.296179E+01
1.500	1.074572E+02	0.	3.094420E+04	3.094420E+04	2.174264E+00	1.890330E-02	8.095760E+01
2.000	1.432763E+02	0.	3.538222E+04	3.538222E+04	2.486097E+00	2.249146E-02	9.632468E+01

E (MEV/AMU)	DE/DX (MEV/GM/SQCM)	R(E) (GM/SQCM)	SLOPE OF DE/DX (SQCM/GM)
.010	7.941519E+03	3.473605E-04	-0.
.015	8.146342E+03	4.951227E-04	1.475692E+02

XBL 686-906

.020	8.292733E+03	6.398297E-04	1.169693E+02
.030	8.542331E+03	9.224732E-04	1.032144E+02
.040	8.784034E+03	1.197175E-03	1.023865E+02
.050	9.029691E+03	1.464372E-03	1.041431E+02
.060	9.279755E+03	1.724333E-03	1.056958E+02
.070	9.532803E+03	1.977340E-03	1.066373E+02
.080	9.787348E+03	2.223698E-03	1.070133E+02
.090	1.004219E+04	2.463727E-03	1.069448E+02
.100	1.029641E+04	2.697746E-03	1.064364E+02
.150	1.154048E+04	3.788252E-03	1.018974E+02
.200	1.272156E+04	4.769438E-03	9.654169E+01
.300	1.489031E+04	6.494214E-03	8.654655E+01
.400	1.684118E+04	7.994585E-03	7.836808E+01
.500	1.862063E+04	9.336978E-03	7.189768E+01
.600	2.026351E+04	1.056117E-02	6.627024E+01
.700	2.177510E+04	1.169333E-02	6.095371E+01
.800	2.316491E+04	1.275243E-02	5.637133E+01
.900	2.445837E+04	1.375189E-02	5.270171E+01
1.000	2.567351E+04	1.470135E-02	4.992868E+01
1.500	3.094420E+04	1.890330E-02	4.079290E+01
2.000	3.538222E+04	2.249146E-02	3.240456E+01
2.500	3.865648E+04	2.569792E-02	2.282019E+01
3.000	4.081342E+04	2.868808E-02	1.521600E+01
3.500	4.227789E+04	3.154958E-02	1.046277E+01
4.000	4.330356E+04	3.432880E-02	7.424147E+00
4.500	4.404484E+04	3.705240E-02	5.437743E+00
5.000	4.459775E+04	3.973660E-02	4.110879E+00
5.500	4.502323E+04	4.239174E-02	3.205372E+00
6.000	4.536062E+04	4.502461E-02	2.573386E+00
6.500	4.563569E+04	4.763985E-02	4.573833E+00
7.000	4.644920E+04	5.024006E-02	4.889606E+00
7.500	4.679942E+04	5.279226E-02	2.842683E+00
8.000	4.712575E+04	5.532611E-02	2.662522E+00
8.500	4.743310E+04	5.784299E-02	2.516344E+00
9.000	4.772464E+04	6.034405E-02	2.392140E+00
9.500	4.800243E+04	6.283023E-02	2.281777E+00
10.000	4.826771E+04	6.530240E-02	2.179599E+00
10.380	4.846142E+04	6.717234E-02	1.609356E+00
12.000	4.820662E+04	7.514399E-02	-8.095354E-01
14.000	4.773391E+04	8.506557E-02	-1.064673E+00
16.000	4.719305E+04	9.509337E-02	-1.193378E+00
18.000	4.659781E+04	1.052429E-01	-1.295102E+00
20.000	4.596011E+04	1.155278E-01	-1.373153E+00
22.000	4.529057E+04	1.259603E-01	-1.430192E+00
24.000	4.459857E+04	1.365510E-01	-1.468894E+00
26.000	4.389219E+04	1.473092E-01	-1.491922E+00
28.000	4.317826E+04	1.582430E-01	-1.501809E+00
30.000	4.246246E+04	1.693595E-01	-1.500863E+00
32.000	4.174944E+04	1.806647E-01	-1.491127E+00
34.000	4.104291E+04	1.921638E-01	-1.474369E+00
36.000	4.034584E+04	2.038613E-01	-1.452095E+00
38.000	3.966052E+04	2.157609E-01	-1.425570E+00
40.000	3.898869E+04	2.278660E-01	-1.395847E+00
42.000	3.833167E+04	2.401791E-01	-1.363795E+00
44.000	3.769036E+04	2.527025E-01	-1.330127E+00
46.000	3.706539E+04	2.654381E-01	-1.295422E+00
48.000	3.645712E+04	2.783873E-01	-1.260148E+00
50.000	3.586573E+04	2.915513E-01	-1.224747E+00
55.000	3.446086E+04	3.254063E-01	-1.137497E+00
60.000	3.315849E+04	3.606164E-01	-1.053652E+00
65.000	3.195317E+04	3.971819E-01	-9.749119E-01
70.000	3.083819E+04	4.350979E-01	-9.019910E-01

XBL 686-907

75.000	2.980643E+04	4.743553E-01	-8.350378E-01
80.000	2.885080E+04	5.149420E-01	-7.738829E-01
85.000	2.796459E+04	5.568436E-01	-7.181889E-01
90.000	2.714152E+04	6.000441E-01	-6.675414E-01
95.000	2.637584E+04	6.445263E-01	-6.215013E-01
100.000	2.566234E+04	6.902721E-01	-5.796360E-01
105.000	2.499631E+04	7.372629E-01	-5.415353E-01
110.000	2.437349E+04	7.854798E-01	-5.068200E-01
115.000	2.379007E+04	8.349036E-01	-4.751445E-01
120.000	2.324264E+04	8.855151E-01	-4.461969E-01
125.000	2.272813E+04	9.372952E-01	-4.196981E-01
130.000	2.224376E+04	9.902248E-01	-3.953985E-01
135.000	2.178708E+04	1.044285E+00	-3.730762E-01
140.000	2.135584E+04	1.099458E+00	-3.525339E-01
145.000	2.094805E+04	1.155724E+00	-3.335962E-01
150.000	2.056188E+04	1.213066E+00	-3.161074E-01
155.000	2.019571E+04	1.271466E+00	-2.999287E-01
160.000	1.984805E+04	1.330907E+00	-2.849369E-01
165.000	1.951756E+04	1.391372E+00	-2.710222E-01
170.000	1.920302E+04	1.452843E+00	-2.580865E-01
175.000	1.890332E+04	1.515305E+00	-2.460423E-01
180.000	1.861744E+04	1.578742E+00	-2.348112E-01
185.000	1.834447E+04	1.643137E+00	-2.243231E-01
190.000	1.808355E+04	1.708476E+00	-2.145149E-01
195.000	1.783392E+04	1.774744E+00	-2.053300E-01
200.000	1.759486E+04	1.841925E+00	-1.968014E-01
210.000	1.714592E+04	1.978972E+00	-1.812527E-01
220.000	1.673210E+04	2.119506E+00	-1.673236E-01
230.000	1.634946E+04	2.263420E+00	-1.549307E-01
240.000	1.599463E+04	2.410613E+00	-1.438569E-01
250.000	1.566470E+04	2.560988E+00	-1.339220E-01
260.000	1.535716E+04	2.714451E+00	-1.249751E-01
270.000	1.506982E+04	2.870912E+00	-1.168893E-01
280.000	1.480077E+04	3.030286E+00	-1.095573E-01
290.000	1.454833E+04	3.192490E+00	-1.028880E-01
300.000	1.431102E+04	3.357445E+00	-9.680357E-02
310.000	1.408754E+04	3.525076E+00	-9.123717E-02
320.000	1.387673E+04	3.695309E+00	-8.613132E-02
330.000	1.367756E+04	3.868073E+00	-8.143623E-02
340.000	1.348910E+04	4.043302E+00	-7.710868E-02
350.000	1.331052E+04	4.220929E+00	-7.311098E-02
360.000	1.314109E+04	4.400893E+00	-6.941016E-02
370.000	1.298013E+04	4.583132E+00	-6.597725E-02
380.000	1.282704E+04	4.767588E+00	-6.278677E-02
390.000	1.268126E+04	4.954205E+00	-5.981618E-02
400.000	1.254231E+04	5.142927E+00	-5.704552E-02
410.000	1.240973E+04	5.333703E+00	-5.445704E-02
420.000	1.228310E+04	5.526481E+00	-5.203493E-02
430.000	1.216204E+04	5.721211E+00	-4.976506E-02
440.000	1.204621E+04	5.917847E+00	-4.763479E-02
450.000	1.193530E+04	6.116341E+00	-4.563275E-02
460.000	1.182900E+04	6.316649E+00	-4.374872E-02
470.000	1.172706E+04	6.518727E+00	-4.197348E-02
480.000	1.162921E+04	6.722534E+00	-4.029870E-02
490.000	1.153523E+04	6.928028E+00	-3.871684E-02
500.000	1.144492E+04	7.135170E+00	-0.

TIME= 3.857

XBL 686-908

DATA STATEMENTS PRINTED

DEDX TABLE AS COMPILED

.010	183.000	118.000	95.000	71.000	48.000	39.000	34.000	28.000	23.000	19.000
.015	230.000	141.000	114.000	86.000	58.000	47.000	40.000	33.000	27.000	23.000
.020	265.000	164.000	132.000	99.000	66.000	54.000	47.000	38.000	32.000	27.000
.030	320.000	205.000	164.000	122.000	80.000	65.000	56.000	47.000	39.000	32.000
.040	360.000	235.000	187.000	140.000	93.000	75.000	64.000	54.000	46.000	38.000
.050	390.000	260.000	208.000	155.000	103.000	83.000	71.000	60.000	51.000	43.000
.070	430.000	285.000	230.000	175.000	120.000	97.000	82.000	69.000	59.000	50.000
.100	440.000	315.000	254.000	193.000	132.000	111.000	94.000	80.000	69.000	60.000
.150	410.000	325.000	264.000	203.000	142.000	123.000	108.000	92.000	80.000	70.000
.200	380.000	320.000	263.000	206.000	149.000	130.000	112.000	100.000	87.000	77.000
.300	330.000	290.000	243.000	196.000	150.000	133.000	121.000	109.000	96.000	87.000
.400	290.000	270.000	230.000	189.000	149.000	133.000	122.000	110.000	100.000	91.000
.500	265.000	250.000	216.000	181.000	147.000	131.000	122.000	111.000	101.000	93.000
.700	220.000	215.000	193.000	166.000	140.000	128.000	120.000	110.000	101.000	94.000
1.000	172.000	170.000	156.000	142.000	129.000	120.000	111.000	107.000	98.000	90.000
1.500	131.000	131.000	124.000	117.000	111.000	107.000	100.000	95.000	90.000	84.000
2.000	109.000	109.000	105.000	101.000	98.000	94.000	90.000	86.000	81.000	76.000
3.000	83.000	83.000	81.600	80.000	79.000	78.000	75.000	73.000	70.000	67.000
4.000	69.000	69.000	68.000	67.000	67.000	66.000	64.000	62.000	60.000	58.000
5.000	58.000	58.000	58.000	57.000	57.000	57.000	56.000	55.000	54.000	52.500
7.000	45.000	45.000	45.000	45.000	45.000	45.000	44.000	43.000	42.000	42.000
10.000	34.279	34.279	34.279	34.279	34.279	34.279	34.279	34.279	34.279	34.279

CONSTANTS A(M,N)

-7.52650000E-01	2.53980000E+00	-2.45980000E-01
7.37360000E-02	-3.12000000E-01	1.15480000E-01
4.05560000E-02	1.86640000E-02	-9.96610000E-03

CONSTANTS ALPHA(M,N)

-8.01550000E+00	1.83710000E+00	4.52330000E-02	-5.98980000E-03
3.69160000E-01	-1.45200000E-02	-9.58730000E-04	-5.23150000E-04
-1.43070000E-02	-3.01420000E-02	7.13030000E-03	-3.38020000E-04
3.47180000E-03	2.36030000E-03	-6.85380000E-04	3.94050000E-05

Z=	1	2	3	4	5	6	7	8	9	10
IADJ=	18.7	42.0	38.0	60.0	70.0	78.0	84.5	88.5	108.0	131.0

CONSTANTS C(I,J,K)

8.88110021991 77E-02	3.5990198639876E-03	5.0138986374204E-04	-1.1241521737316E-02	1.3976941603226E-02	-1.3176586838630E-02
1.7138690365610E-02	1.5967910228485E-03	-2.6562415376993E-04	-4.1837248715580E-03	9.8137632029485E-04	-5.7053662633375E-03
4.9497133143262E-02	-5.8195120035795E-04	-1.5773041482136E-03	-7.9827735119005E-03	9.7438614446294E-03	-1.6323907448869E-02
1.3540201949725E-02	8.4062292539332E-04	-6.8461912460993E-04	-2.5753724979494E-03	5.6591608351300E-05	-6.3370050198126E-03
5.1855586277785E-02	9.6868735617298E-03	8.3666352668449E-03	-1.1763486564892E-02	1.2115290632189E-02	-1.3188677117176E-02
1.5541522412133E-02	4.1480250614850E-03	2.6876280235695E-03	-4.1226660625563E-03	7.9626549835530E-04	-5.3555019602713E-03
-7.0320508947949E-02	-7.4582561384904E-03	1.5035074028774E-03	-1.3449692056030E-02	1.3788090175256E-02	-1.5092254582325E-02
-1.4255700147520E-02	-1.6385237951375E-03	1.6737094370482E-04	-4.7899763404858E-03	1.2567130675785E-03	-5.8882305836342E-03

XBL 686-909

B. Method For Calculating The Mean Projected Range

Many experimental ranges are reported as the mean distance which the ion travels in the initial direction of flight. For heavy stopping media and low ion velocity, the percentage deviation of this range from the pathlength range may be significant. For example, this deviation is 9% for a 1.12 MeV/amu Sr^{89} fission product in U, and 11% for a 0.437 MeV/amu Ce^{144} fission product in U. We therefore prepared a method for calculating this projected range and the deviation of this projected range from the pathlength range so that we could make more meaningful comparisons between the theory and experiments.

We have adopted a method proposed by Lindhard et al.[18, 63] and used by Schiott.[64] In order to avoid a complex and time consuming numerical solution to an integro-differential equation, Lindhard et al. were forced to assume that either $A_2 \ll A_1$ or that the average projected range $\bar{R}_p$ (g/cm^2) is proportional to the ion energy E. We chose to develop this method in a more general manner and solve the integro-differential equation directly by taking advantage of the excellent computing facilities available to us.

Let $P(E, R_p)dR_p$ be the probability that the projected range of an ion of kinetic energy E will be within dR_p of R_p. (The simpler terminology (R_p, dR_p) will hereafter be equivalent to "within dR_p of R_p".) We normalize this probability function such that $\int_0^\infty P(E, R_p)dR_p = 1.0$. We now have $\bar{R}_p(E) = \int_0^\infty R_p P(E, R_p)dR_p$ and define $P(E, R_p)$ such that $R_p P(E, R_p) = 0$ at $R_p = 0$ and at $R_p = \infty$.

We assume that elastic coulomb collisions with nuclei and inelastic electronic collisions can be considered in this development to be uncorrelated. Then the probability that the ion will have a coulomb nuclear collision in δR and a range (R_p, dR_p) projected onto

the direction of flight before the collision is

$$N\delta R_p dR_p \int_0^{T_{nmax}} \cos\phi_n(E, T)\, \sigma_n(E, T)\, P(R_p - \delta R_p, E-T)dT\,, \qquad \text{(B 1)}$$

where N is the number of nuclei per gram of the stopping medium, $\cos\phi_e(E, T)$ is the cosine of the scattering angle in the laboratory system of the ion with a kinetic energy T lost to the recoiling nucleus, $\sigma_n(E, T)$ is the cross section for an ion collision with energy transfer T, and $T_{n\,max}$ is the maximum energy transferred to a nucleus determined by the condition that the nuclear potentials of the ion and nucleus must not overlap. Note that we may use δR_p instead of δR in expression (B 1) because the probability of the collision is proportional to the distance traveled before the collision. Thus δR and δR_p are equivalent in this case. The expression for electronic collisions which corresponds to expression (B 1) is

$$N\delta R_p dR_p \int_0^{T_{emax}} \cos\phi_e(E, T)\, \sigma_e(E, T)\, P(R_p - \delta R_p, E-T)dT\,. \qquad \text{(B 2)}$$

The probability that an ion which has a projected range (R_p, dR_p) will not suffer a collision in δR is

$$\left\{1-N\delta R_p\left[\int_0^{T_{emax}}\sigma_e(E,T)dT+\int_0^{T_{nmax}}\sigma_n(E,T)dT\right]\right\}P(R_p-\delta R_p,E)dR_p\ . \qquad (B\ 3)$$

Equating the sum of expressions (B 1), (B 2), and (B 3) to $P(E, R_p)dR_p$ and dividing by dR_p we have

$$P(R_p,E)-P(R_p-\delta R_p,E)=N\delta R_p\left\{\int_0^{T_{nmax}}\sigma_n(E,T)\right.$$

$$\times\left[\cos\phi_n(E,T)\,P(R_p-\delta R_p,E-T)-P(R_p-\delta R_p,E)\right]dT$$

$$\left.+\int_0^{T_{emax}}\sigma_e(E,T)\left[\cos\phi_e(E,T)\,P(R_p-\delta R_p,E-T)-P(R_p-\delta R_p,E)\right]dT\right\}\ .$$

Dividing by δR_p and taking the limit as δR_p approaches zero we have

$$\frac{\partial P}{\partial R_p}=N\int_0^{T_{nmax}}\sigma_n(E,T)\left[\cos\phi_n(E,T)\,P(R_p,E-T)-P(R_p,E)\right]dT$$

$$+N\int_0^{T_{emax}}\sigma_e(E,T)\left[\cos\phi_e(E,T)\,P(R_p,E-T)-P(R_p,E)\right]dT\ .$$

Multiplying both sides of this equation by $R_p dR_p$ and integrating over R_p from 0 to ∞ we get

$$-1.0=N\int_0^{T_{nmax}}\sigma_n(E,T)[\bar{R}_p(E-T)\cos\phi_n(E,T)-\bar{R}_p(E)]\,dT$$

$$+N\int_0^{T_{emax}}\sigma_e(E,T)[\bar{R}_p(E-T)\cos\phi_e(E,T)-\bar{R}_p(E)]\,dT\,, \qquad \text{(B 4)}$$

where the left hand side has been integrated by parts and we have assumed the integrands of the T integrals on the right hand side to be sufficiently well behaved to allow the R_p integrations to be performed first. We shall hereafter replace $\bar{R}_p$ by R_p and deal only with average ranges. Since the mass of the ion is much greater than the mass of the electron, $T_{e\,max} \ll E$. We may then expand $R_p(E, T)$ from the second term on the right in a power series about T = 0. Truncating this series after two terms, this second term of Eq. (B 4) becomes

$$N\int_0^{T_{emax}}\sigma_e(E,T)\left\{R_p(E)[\cos\phi_e(E,T)-1]\right\}\,dT$$

$$-N\frac{dR_p}{dE}\int_0^{T_{emax}}T\sigma_e(E,T)\cos\phi_e(E,T)dT\,.$$

Again, since the mass of the ion is so much greater than that of an electron, $\cos\phi_e(E, T) \sim 1.0$. Also,

$$N\int_0^{T_{emax}}T\sigma_e(E,T)dT$$

is the electronic stopping power. Making use of these facts and substituting into Eq. (B 4) we have

$$S_e(E)\frac{dR_p}{dE}=1+N\int_0^{T_{nmax}}\sigma_n(E, T)[R_p(E-T)\cos\phi_n(E, T)-R_p(E)]\,dT$$

$$-NR_p(E)\int_0^{T_{emax}}\sigma_e(E, T)[1-\cos\phi_e(E, T)]\,dT\,, \qquad \text{(B 5)}$$

where $S_e(E)$ is the electronic stopping power of the ion with kinetic energy E. We estimated $[1-\cos\phi_e(E, T)]$ by temporarily assuming the collisions with electrons to be elastic. Since $\cos\phi_e(E, T)$ is very nearly 1.0, we can make a two term expansion which yields

$$[1-\cos\phi_e(E, T)]\sim\left(\frac{0.51}{931A_1}\right)^2\frac{1}{0.51(\gamma^2-1)}\left[T-\frac{T^2}{1.02(\gamma^2-1)}\right]$$

where $\gamma = E/(931\,A_1) + 1$, E and T are in units of MeV. This equation can be found from Eqs. (B 9), (B 10), and (B 11) below by assuming $A_1 >> A_2$. Substituting this into the third term of Eq. (B 5) and performing the integration gives one term involving the electronic stopping power and another term involving the variance in energy transfer per unit pathlength (i.e. energy straggling). The energy straggling is estimated from an expression given by Evans.[65] We have estimated the right hand side of Eq. (B 5) for a wide variety of ions, stopping media, and energies. As one would expect the third term is always several orders of magnitude less than the sum of the first two. Therefore we neglect the third term. We now change variables making the substitutions $E = A_1\,\varepsilon$, $T = A_2\,\tau$, $\sigma_n(E, T)\,dT =$

$\sigma_n(\varepsilon,\tau)d\tau$, and $N = 6.023\times10^{23}/A_2$. Equation (B 5) then becomes

$$\frac{dR_p}{d\varepsilon}=\frac{A_1}{S_e(\varepsilon)}\left\{1-\frac{6.023\times10^{23}}{A_2}\right.$$

$$\left.\times\int_0^{\tau_{max}(\varepsilon)}\sigma_n(\varepsilon,\tau)[R_p(\varepsilon)-R_p(\varepsilon-\frac{A_2}{A_1}\tau)\cos\phi_n(\varepsilon,\tau)]\,d\tau\right\}. \qquad \text{(B 6)}$$

The corresponding equation for the pathlength range would be

$$\frac{dR}{d\varepsilon}=\frac{A_1}{S_e(\varepsilon)}\left\{1-\frac{6.023\times10^{23}}{A_2}\int_0^{\tau_{max}(\varepsilon)}\sigma_n(\varepsilon,\tau)[R(\varepsilon)-R(\varepsilon-\frac{A_2}{A_1}\tau)]\,d\tau\right\}. \qquad \text{(B 7)}$$

If we define the difference between the pathlength and projecter ranges as $D = R-R_p$, from Eqs. (B 6) and (B 7) we have

$$\frac{dD}{d\varepsilon}=\frac{6.023\times10^{23}}{S_e(\varepsilon)}\frac{A_1}{A_2}\int_0^{\tau_{max}(\varepsilon)}\sigma_n(\varepsilon,\tau)$$

$$\times\left\{R(\varepsilon-\frac{A_2}{A_1}\tau)[1-\cos\phi_n(\varepsilon,\tau)]+D(\varepsilon-\frac{A_2}{A_1}\tau)\cos\phi_n(\varepsilon,\tau)-D(\varepsilon)\right\}d\tau\,. \qquad \text{(B 8)}$$

Equations (B 6), (B 7), and (B 8) are ready for numerical solution as soon as expressions for $\cos\phi(\varepsilon,\tau)$, $\sigma_n(\varepsilon,\tau)d\tau$, and $\tau_{max}(\varepsilon)$ are given. The cosine of the scattering angle for the ion in the

laboratory system, assuming an elastic collision, can be found using expressions presented in Ref. (66). The result is

$$\cos\phi(\varepsilon,\tau)=\left\{1+\frac{\dfrac{\tau}{931\gamma_{2c}^2(\gamma_{2c}^2-1)}\left[2+\dfrac{\tau}{931(\gamma_{2c}^2+1)}\right]}{\left[1-\dfrac{\tau}{931(\gamma_{2c}^2+1)}+\dfrac{A_1}{A_2}\dfrac{\gamma_{1c}}{\gamma_{2c}}\right]^2}\right\}^{-1/2} \tag{B 9}$$

where

$$\gamma_{1c}=\frac{\gamma+\dfrac{A_1}{A_2}}{\left[1+2\dfrac{A_1}{A_2}\gamma+\left(\dfrac{A_1}{A_2}\right)^2\right]^{1/2}}, \tag{B 10}$$

$$\gamma_{2c}=\frac{\gamma+\dfrac{A_2}{A_1}}{\left[1+2\dfrac{A_2}{A_1}\gamma+\left(\dfrac{A_2}{A_1}\right)^2\right]^{1/2}}, \text{ and} \tag{B 11}$$

$$\gamma=\frac{\varepsilon}{931}+1 \ . \tag{B 12}$$

The elastic differential scattering cross section $\sigma_n(\varepsilon, \tau)d\tau$ is derived from the Thomas-Fermi potential. This cross section takes into consideration the fact that for soft collisions the electron clouds of the ion and the atom of the stopping medium do not penetrate each other sufficiently for the two nuclei to experience a 1/r coulomb potential. For hard collisions, this cross section smoothly joins the Rutherford cross section when the two nuclei become sufficiently close.

Lindhard et al.[18] give the cross section in the form

$$d\sigma = \pi a^2 \frac{dt}{2t^{3/2}} f(t^{1/2}) \qquad \text{(B 13)}$$

where a is given in Eq. (13), $t^{1/2} = \epsilon \sin\frac{\theta}{2}$, ϵ is found in Eq. (14), θ is the scattering angle in the center-of-mass system, and $f(t^{1/2})$ is graphically presented in Fig. 1 of Ref. (18) and tabulated in Table IX below. From Eq. (14) and Ref. (66) we find

$$t^{1/2} = \frac{3.253\times10^4}{Z_1 Z_2 (Z_1^{2/3}+Z_2^{2/3})^{1/2}} \frac{A_1 A_2}{A_1+A_2} \left[\frac{\tau}{2\times 931(\gamma_{2c}^2-1)}\right]^{1/2} \varepsilon, \qquad \text{(B 14)}$$

where γ_{2c} is given by Eq. (B 11). Eq. (B 13) becomes

$$\sigma_n(\varepsilon, \tau)d\tau = 4.573\times10^{-20} \frac{Z_1 Z_2}{(Z_1^{2/3}+Z_2^{2/3})^{1/2}} \frac{A_1+A_2}{A_1 A_2} \frac{(\gamma_{2c}^2-1)^{1/2}}{\varepsilon} f(t^{1/2}) \frac{d\tau}{\tau^{3/2}}, \qquad \text{(B 15)}$$

where we obtain values for $f(t^{1/2})$ by interpolating between the entries in Table IX. Whenever $t^{1/2} > 10$ we use the Rutherford cross section in the form

$$\sigma_n(\varepsilon, \tau)d\tau = \frac{2.119\times10^{-21}}{A_2\varepsilon^{1/2}} \frac{Z_1Z_2}{(Z_1^{2/3}+Z_2^{2/3})^{1/2}} \frac{0.5}{t^{1/2}} \frac{d\tau}{\tau^{3/2}}, \qquad \text{(B 16)}$$

In order to find $\tau_{max}(\varepsilon)$, we assume a $1/r$ potential and require that the nuclear potentials of the ion and nucleus of the scattering center do not overlap. We find

$$\tau_{max}(\varepsilon) = \frac{2.0736\times10^{-26}}{\varepsilon}\left(\frac{Z_1Z_2}{A_2}\right)^2 \qquad \text{(B 17)}$$

$$\times\left[b_{min}^2 + 5.184\times10^{-25}\left(\frac{A_1+A_2}{A_1A_2}\frac{Z_1Z_2}{\varepsilon}\right)^2\right]^{-1}$$

where the square of the minimum impact parameter b_{min}^2 is given by

$$b_{min}^2 = (R+r)^2\left[1-\frac{1.44\times10^{-13}Z_1Z_2}{931A_1(\gamma_{1c}-1)(R+r)}\right]. \qquad \text{(B 18)}$$

Table IX. The function $f(t^{1/2})$ used with Eq. (B 13) to give the elastic nuclear coulomb differential scattering cross section based upon a Thomas-Fermi potential.

$t^{1/2}$	$f(t^{1/2})$
0.002	0.161
0.005	0.225
0.01	0.282
0.02	0.333
0.05	0.396
0.1	0.431
0.13	0.435
0.2	0.427
0.3	0.404
0.5	0.361
1.	0.277
2.	0.184
3.	0.137
5.	0.0914
10.	0.05001

Here R and r are the radii of the nuclear potentials of the nucleus of the stopping medium and that of the ion respectively. The former is given by

$$R = 1.2 \times 10^{-13} A_2^{1/3}$$

and the latter by

$$r = 1.2 \times 10^{-13} A_1^{1/3} + \frac{1.973 \times 10^{-11}}{931 A_1 (\gamma^2 - 1)^{1/2}}$$

where the second term is the de Broglie wavelength of the ion. When the factor in the brackets of Eq. (B 18) is negative, then the ion is not energetic enough for the nuclear fields to overlap even for a head-on collision. In this case $\tau_{max}(\varepsilon)$ is determined by conservation of momentum and energy and is given by

$$\tau_{max}(\varepsilon) = 2 \times 931 \, (\gamma_{2c}^2 - 1) \qquad \text{(B 19)}$$

We are now ready to solve Eqs. (B 6), (B 7), and (B 8). We use the computer subroutine ZAM, which is in the computer library at the Lawrence Radiation Laboratory in Berkeley. It solves simultaneous, first order, differential equations using the fourth-order Adams Moulton predictor-corrector method with a starting procedure based on Zonneveld's formulas, see Refs. (67) and (68). Here, of course, we have only single differential equations with rather complex derivatives. The method requires an initial value; it then in effect integrates the derivative in such small increments of the independent variable ε that the value of the derivative changes very little between increments. The solution, $R_p(\varepsilon)$ in the case of Eq. (B6), is thus found for increasing values of ε.

Fortunately, since the solution is found for increasing values of ε, the integrations indicated in Eqs. (B 6), (B 7), and (B 8) are over those values of the solution which have already been found. For purposes of these integrations, the solution is extrapolated linearly to zero from the initial value, assumed linear between the incremental values of the solution found by ZAM, and linearly extrapolated from the last two values found to higher values when necessary.

Equation (B 6) and (B 7) each have the property that, if the initial value is in error, the solution very quickly converges upon the true solution as ε increases. That is to say, the value of R_p or R which we obtain for $\varepsilon = 0.01$ MeV/amu is quite insensitive to the initial value we choose for $\varepsilon = 0.0001$. The solution $D(\varepsilon)$ of Eq. (B 8) also converges for increasing ε, but we find it advantageous to take as the initial value of D the difference between the solutions of Eqs. (B 6) and (B 7) at a fairly large velocity, say $\varepsilon = 0.03$.

The electronic stopping power required in order to calculate the derivatives in Eqs. (B 6), (B 7), and (B 8) is found from Eq. (31) whenever the ions have $Z_1 \geq 10$ and are in the low-specific-energy region. Otherwise it is assumed to be the total stopping power calculated by the methods of section II.

The range values required in the integrand of Eq. (B 8) are also calculated by the methods of section II.

The computer programs described here were designated to find the effect of multiple scattering on the ion range only for specific energies up to about 2 to 4 MeV/amu. For velocities greater than this, computer time becomes prohibitive (greater than 5 to 10 minutes on the CDC 6600), and other methods of solving the problems are probably more appropriate.

C. Stopping Power From Bloch's Theory Using The Computer

As discussed in section III B 3, we calculated stopping power using Bloch's theory in the medium-high-specific-energy region whenever $Z_1 > Z_2$ in order to test the use of the Born approximation by Bethe's theory where it is not rigorously valid. We discontinued the use of Bloch's theory when it became apparent that the major uncertainty lay in the choice of the function r(X) and not in the use of the Born approximation. In this appendix we describe the approximations made in this use of Bloch's theory.

The stopping power from Bloch's theory is calculated by evaluating Eqs. (8) and (11). The term $\psi[1]$ of Eq. (11) is the logarithmic derivative of the gamma function evaluated at 1.0. Its value is 0.4228. The term $\mathrm{Re}\,\psi[1 + i(rZ_1/137\beta)]$ is the real part of the logarithmic derivative of the gamma function evaluated at $1 + i(rZ_1/137\beta)$. It is given by the series (see Jahnke and Emde[69]).

$$\mathrm{Re}\psi\left(1+i\frac{rZ_1}{137\beta}\right)=\sum_{m=1}^{\infty}\left[\frac{1}{m}-\frac{m+1}{(m+1)^2+\left(\frac{rZ_1}{137\beta}\right)^2}\right]. \qquad \text{(C 1)}$$

For m sufficiently large, the series converges like $1/[m(m+1)]$. We take the sum of the first 30 $rZ_1/137\beta$ terms or at least 20 terms, whichever is greater, as the value of the series.

As they are, Eqs. (8) and (11) cannot be used unless inequality (1), $Z_2 \ll 137\beta$, is satisfied. Since this is a severe limitation in the medium-high-specific-energy region for heavy stopping media, we incorporated shell corrections into Eq. (8) by means of the polynomial expression which Barkas and Berger[23] fit to the data by Walske[13, 14] and Bichsel.[36] This polynomial is

$$C_{adj}(I,\eta)=(0.422377\eta^{-2}+0.0304043\eta^{-4}-0.000381060\eta^{-6})10^{-6}I_{adj}^{2}$$

$$+(3.858019\eta^{-2}-0.1667989\eta^{-4}+0.00157955\eta^{-6})10^{-9}I_{adj}^{3}, \qquad (C\,2)$$

where $\eta=\beta/(1-\beta^2)^{1/2}$ and I_{adj} is the average excitation potential adjusted as discussed following Eq. (23) of the text. This polynomial fits the shell corrections of Walske and Bichsel only for specific energies greater than 8 MeV/amu.

The expression which we use to calculate stopping power from Bloch's theory is then

$$\frac{dE}{dR}\left(\frac{MeV}{g/cm^2}\right)=0.3072\frac{(rZ_1)^2}{\beta^2 A_2}B \qquad (C\,3)$$

where

$$B=Z_2\left[\ln\frac{2m_e c^2\beta^2}{I_{adj}}+0.4228-Re\psi\left(1+i\frac{rZ_1}{137\beta}\right)\right.$$

$$\left.-\ln(1-\beta^2)-\beta^2-\frac{C_{adj}}{Z_2}\right] \qquad (C\,4)$$

where $Re\psi[1+i(rZ_1/137\beta)]$ is given by Eq. (C 1), C_{adj} is given by Eq. (C 2), and r is found from experimental Ar ion range data in Al as described in section II B 3. Equations (C 3) and (C 4) can be used only for $\varepsilon \geq 8$ MeV/amu since Eq. (C 2) is valid only for these velocities.

REFERENCES

1. The Omnitron, A Multipurpose Accelerator, UCRL-16828, July 1966.
2. Gerald M. Litton, Penetration of High-Energy Heavy Ions, With the Inclusion of Coulomb, Nuclear, and Other Stochastic Processes (Ph. D. thesis), UCRL-17392, August 1967.
3. Gerald M. Litton, Program BRAGG, A FORTRAN-IV Program For Calculating Bragg Curves and Flux Distributions, UCRL-17391 February 1967.
4. N. K. Aras, M. P. Menon, and G. E. Gordon, Ranges of Fragments From Fission of U^{235} With Thermal Neutrons and the Kinetic Energy Deficit, Nuclear Physics 69, 337 (1965).
5. B. Fastrup, P. Hvelplund, and C. A. Scutter, Stopping Cross Section in Carbon of 0.1-1.0 MeV Atoms With $6 \leq Z_1 \leq 20$, Mat. Fys. Medd. Dan. Vid. Selsk. 35, no. 10 (1966).
6. N. Bohr, On the Theory of the Decrease of Velocity of Moving Electrified Particles on Passing Through Matter, Phil. Mag., 25, 10 (1913).
7. N. Bohr, On the Decrease of Velocity of Swiftly Moving Electrified Particles in Passing Through Matter, Phil. Mag., 30, 581 (1915).
8. H. A. Bethe, Zur Theorie des Durchgangs Schneller Korpuskularstrahlen Durch Materie, Ann. Physik, 5, 325 (1930).
9. H. A. Bethe, Bremsformel fur Elektronen Relativistischer Geschwindigkeit, Z. Physik, 76, 293 (1932).
10. Niels Bohr, The Penetration of Atomic Particles Through Matter, Mat. Fys. Medd. Dan. Vid. Selsk. 18, 8 (1948).
11. N. F. Mott, Proc. Cambridge Phil. Soc., 27, 533 (1931); also see N. F. Mott and H. S. W. Massey, The Theory of Atomic Collisions, (Oxford, Clarendon Press, 1965), page 615.

12. M. S. Livingston and H. A. Bethe, Nuclear Dynamics, Experimental, § 95 The Range-Energy Relation, Rev. Mod. Phys., 9, 261 (1937).

13. M. C. Walske, The Stopping of K-Electrons, Phys. Rev., 88, 1283 (1952).

14. M. C. Walske, Stopping Power of L-Electrons, Phys. Rev., 101, 940 (1956).

15. H. Bichsel, Higher Shell Corrections in Stopping Power, Univ. So. Calif. Report No. 3 (contract AT (04-3)-1367) (1961).

16. F. Bloch, Zur Bremsung Rasch Bewegter Teilchen Beim Durchgang Durch Materie, Ann. Physik, 16, 285 (1933).

17. J. Lindhard and M. Scharff, Energy Dissipation by Ions in the KeV Region, Phys. Rev. 124, 128 (1961).

18. J. Lindhard, M. Scharff, and H. E. Schiott, Range Concepts and Heavy Ion Ranges (Notes on Atomic Collisions, II) Mat. Fys. Medd. Dan. Vid. Selsk., 33, No. 14 (1963).

19. U. Fano, Penetration of Protons, Alpha Particles, and Mesons, in Annual Review of Nuclear Science, vol. 13, p. 1, 1963; also reprinted as Appendix A in reference 24.

20. J. E. Turner, Calculation of Stopping Power of a Heavy Charged Particle in Matter, Health Physics, 13, 1255 (1967).

21. H. A. Bethe and J. Ashkin, Passage of Radiations Through Matter, in Experimental Nuclear Physics edited by E. Segre, vol. 1, p. 166, (John Wiley and Sons, Inc. New York, 1953).

22. Lee C. Northcliffe, Passage of Heavy Ions Through Matter, in Annual Review of Nuclear Science, vol. 13, p. 67, 1963; also reprinted as Appendix B in reference 24.

23. Walter H. Barkas and Martin J. Berger, Tables of Energy Losses and Ranges of Heavy Charged Particles, in Studies in Penetration of Charged Particles in Matter (National Academy of Sciences-National Research Council Publication 1133,

Washington, D. C., 1964), p. 103.

24. Studies in Penetration of Charged Particles in Matter, (National Academy of Sciences-National Research Council Publication 1133, Washington, D. C., 1964).

25. Ward Whaling, The Energy Loss of Charged Particles in Matter, in Encyclopedia of Physics vol. 34, (Springer-Verlag, Berlin, 1958).

26. Earl K. Hyde, The Nuclear Properties of the Heavy Elements, vol. III Fission Phenoma, (Prentice-Hall, Inc., Englewood Cliffs, New Jersey, 1964).

27. Joseph F. Janni, Calculations of Energy Loss, Range, Pathlength, Straggling, Multiple Scattering, and the Probability of Inelastic Nuclear Collisions for 0.1 to 1000-MeV Protons, Technical Report No. AFWL-TR-65-150, September 1966.

28. W. Peter Trower, FORTRAN Subroutine RANGE: Calculating the Range-Energy Relation For Charged Particles in Chemical Elements, UCRL-11647 Rev., September 1966.

29. C. F. Williamson, J. P. Boujot, J. Picard, Tables of Range and Stopping Power of Chemical Elements For Charged Particles of Energy 0.5 to 500 MeV, CEA-R-3042, 1966.

30. Claude Serre, Evaluation of Unitary Energy Losses (i. e. Stopping Power) and Ranges of Charged Particles Traversing a Given Absorbent, CERN-67-05, March 1967, (In French).

31. Hans Bichsel, A FORTRAN Program For The Calculation of Energy Loss of Heavy Charged Particles, UCRL-17538, May 1967.

32. E. V. Benton, Personal Communication, also see R. P. Henke and E. V. Benton, Charged Particle Tracks in Polymers: No. 3-Range and Energy Loss Tables, USNRDL-TR-1102, November 1966.

33. Ya A. Teplova, V. S. Nikolaev, F. S. Dmitriev, and L. N. Fateeva, Slowing Down of Multicharged Ions in Solids and Gases, J. Exptl. Theoret. Phys. (USSR), 42, 44 (1962) [Trans.]: Soviet Phys. JETP, 15, 31 (1962).

34. Peter K. Weyl, The Energy Loss of Hydrogen, Helium, Nitrogen, and Neon Ions in Gases, Phys. Rev., 91, 289 (1953).

35. Samuel K. Allison and C. S. Littlejohn, Stopping Power of Various Gases For Lithium Ions of 100-450 KeV Kinetic Energy, Phys. Rev., 104, 959 (1956).

36. Hans Bichsel, Passage of Charged Particles Through Matter, in American Institute of Physics Handbook section 8 c (McGraw-Hill Book Co., Inc. New York, 1963) p 8-20.

37. J. E. Turner, Values of I and I_{adj} Suggested By the Subcommittee, In Studies in Penetration of Charged Particles in Matter (National Academy of Sciences-National Research Council, Publication 1133, Washington, D. C., 1964) p. 99.

38. J. Kistemaker, F. J. Detteer, J. Sanders, and C. Snook, Energy Deposition in matter by Slow Heavy Particles, in Radiation Research, Proceedings of the Third International Congress of Radiation Research held at Cortina d'Ampezzo, Italy, June-July, 1966 (North Holland Pub. Co., Amsterdam; John Wiley and Sons, Inc., New York, 1967) p. 68.

39. H. Jung, Effects of Elastic Nuclear Collisions on Biomolecules, in Radiation Research, Proceedings of the Third International Congress of Radiation Research held at Cortina d'Ampezzo, Italy, June-July, 1966 (North Holland Pub. Co., Amsterdam; John Wiley and Sons, Inc., New York, 1967), p. 410.

40. J. Knipp and E. Teller, "On the Energy Loss of Heavy Ions," Phys. Rev. 59, 659 (1941).

41. J. Neufeld and W. S. Snyder, Estimates of Energy Dissipation By Heavy Charged Particles in Tissue in Selected Topics in Radiation Dosimetry, International Atomic Energy Agency, Kaerntnerring, Vienna 1, Austria, (1961) p. 35.

42. L. C. Northcliffe, Passage of Heavy Ions Through Matter II. Range-Energy Curves, in Studies in Penetration of Charged Particles in Matter (National Academy of Sciences-National Research Council, Publication 1133, Washington, D. C., 1964), p. 173.

43. Torbjorn Sikkeland, Energy Degradation and Energy Straggling of Argon-40 Ions in Aluminum, UCRL-16453, October 1965.

44. William C. Davidon, Variable Metric Method For Minimization, Argonne National Laboratory, Lemont, Illinois, ANL-5990 (Rev.) November 1959.

45. D. I. Porat and K. Ramavataram, Differential Energy Loss and Ranges of Ne, N, and He Ions, Proc. Phys. Soc. (London), 78, 1135 (1961).

46. D. I. Porat and K. Ravataram, Rate of Energy Loss and Ranges Carbon and Oxygen Ions in Solids, Proc. Phys. Soc. (London) 77, 97 (1961).

47. T. J. Thompson, Effect of Chemical Structure on Stopping Powers For High-Energy Protons (Ph. D. thesis), UCRL-1910, August 1952.

48. Gunnar Aniansson, The Integral Stopping Power of Liquid Hydrocarbons For 5.3 MeV Alpha Particles, Kungl. Tekniska Hogskolans Handlingar, Nr 178 (1961).

49. H. K. Reynolds, D. N. F. Dunbar, W. A. Wenzel, and W. Whaling, The Stopping Cross Section of Gases For Protons, 30-600 KeV, Phys. Rev. 92, 742 (1953).

50. J. H. Ormrod and H. E. Duckworth, Stopping Cross Sections in Carbon For Low-Energy Atoms With $Z \leq 12$, Can. J. Phys. 41, 1424 (1963).

51. J. H. Ormrod, J. R. MacDonald, and H. E. Duckworth, Some Low-Energy Atomic Stopping Cross Sections, Can. J. Phys. 43, 275 (1965).

52. Jacob Gilat and John M. Alexander, Stopping of Dysprosium Ions in Gases and Aluminum, Phys. Rev., 136, B1298 (1964), (UCRL-11055).

53. Morton Kaplan and Alan Ewart, Energetics of the Al^{27} (B^{11}, p3n) Cl^{34m} Reaction From Recoil Studies, Phys. Rev. 148, 1123 (1966).

54. N. O. Lassen, The Total Charges of Fission Fragments in Gases and Solid Stopping Media, Dan. Mat. Fys. Medd. 26, 5 (1951).

55. F. Suzor, Tracks in Various Materials of Uranium Fission Fragments, Ann. Phys. (Paris) (Ser. 12) 4, 269 (1949).

56. N. K. Aras, Range of Fragments From Thermal Fission of U^{235}, Ph. D. thesis, Mass. Inst. Tech., 1964.

57. J. M. Alexander and M. F. Guzdik, Recoil Properties of Fission Products, Phys. Rev. 120, 874 (1960).

58. B. Finkle, F. J. Hoaglund, S. Katcoff, and N. Sugarman, Range of Fission-Recoil Fragments of Known Mass Number, papers 45 and 46 in Radiochemical Studies-The Fission Products, NNES IV vol. 9 (McGraw-Hill, New York, 1951).

59. J. B. Niday, Radiochemical Study of the Ranges in Metallic Uranium of the Fragments From Thermal Neutron Fission, Phys. Rev. 121, 1471 (1961).

60. J. C. C. Milton and J. S. Fraser, Time-of-Flight Fission Studies on U^{233}, U^{235}, and Pu^{239}, Can. J. Phys. 40, 1626 (1962).

61. J. H. M. Brunings, J. K. Knipp, and E. Teller, On the Momentum Loss of Heavy Ions, Phys. Rev. 60, 657 (1941).

62. Bruno Rossi, High-Energy Particles, (Prentice-Hall, Inc.,

Englewood Cliffs, New Jersey, 1952) p. 66.

63. J. Lindhard, V. Nielsen, M. Scharff, and P. V. Thomsen, Integral Equations Governing Radiation Effects (Notes on Atomic Collisions, III), Mat. Fys. Medd. Dan. Vid. Selsk. 33, 10, (1963).

64. Hans E. Schiott, Range-Energy Relations for Low-Energy Ions, Mat. Fys. Medd. Vid. Selsk. 35, 9, (1966).

65. Robley D. Evans, The Atomic Nucleus, (McGraw-Hill Book Company, Inc., New York, 1955), pp. 661-2.

66. Philip Morrison, Application of Energy-Momentum Conservation in Experimental Nuclear Physics vol. II, p 3, edited by E. Segre, (John Wiley and Sons, Inc., New York, 1953).

67. Loren P. Meissner, Lawrence Radiation Laboratory Computer Center, Berkeley, Subroutine D 2 BKY ZAM, November 1965.

68. Anthony Ralston, A First Course in Numerical Analysis, (McGraw-Hill Book Co., New York, 1965), p. 179.

69. Eugene Jahnke and Fritz Emde, Tables and Functions With Formulae and Curves, (Dover Publications, New York, 1945), p. 18.